MerTK inhibition for the treatment of organ fibrosis

Ziyan Pan

A thesis submitted in fulfilment of the requirements for the degree of

Doctor of Philosophy

School of Medicine

The University of Sydney

NSW, Australia

2023

STORR LIVER CENTRE

The Westmead Institute FOR MEDICAL RESEARCH | THE UNIVERSITY OF SYDNEY

Authorship Attribution Statement

In addition to the statements above, in cases where I am not the corresponding author of a published item, permission to include the published material has been granted by the corresponding author.

Ziyan Pan
04/07/2023

As supervisor for the candidature upon which this thesis is based, I can confirm that the authorship attribution statements above are correct.

Mohammed Eslam
04/07/2023

Originality Statement

The research conducted in this thesis was carried out as part of an academic pursuit under the guidance of Professor Mohammed Eslam and Professor Jacob George at the Storr Liver Centre, Westmead Institute for Medical Research, University of Sydney. I thus affirm that, to the farthest extent of my understanding, the substance of this dissertation is the result of my own effort. The present thesis has not been previously submitted for the attainment of any other academic degree or for any other purpose. I thus affirm that the intellectual material included within this thesis is the result of my own work, and that any aid received during its preparation and any sources used have been duly acknowledged.

Ziyan Pan

June 2023

i. Abstract

Background: The evolution of multi-chronic diseases is largely influenced by fibrosis, which acts as a key route. However, effective and low side-effect antifibrotic therapies remains limited. In organ fibrosis, scarring mainly driven by transforming growth factor-β (TGF-β) is a pivotal contributor to disease progression. However, ubiquitously expressed TGF-β is hard to be applied in fibrosis therapy, and identification of refined alternative targets to inhibit TGF-β signalling is needed.

In recent studies, researchers have uncovered new genetic risk variants of myeloid-epithelial reproductive tyrosine kinase (MerTK). Previous studies have shown a significant correlation between these polymorphisms and liver fibrosis progress. This study investigates the potential of MerTK as a new therapeutic target for multiorgan fibrosis, including liver, kidney, and lung, as well as the underlying processes involved in its therapeutic activities.

Methods: MerTK and TGF-β interaction was investigated in vitro. Fibrosis models of liver (bile duct ligation), kidney (unilateral ureteral obstruction) and lung (bleomycin injection) were established by Mertk knockout mice to explore their role in the fibrosis process of each organ. The mechanism of MerTK was explored through RNA-seq, ATAC-seq and Cut&Tag-seq.

Results: I identified MerTK as a TGF-β-inducible nodal effector of organ fibrosis that is upregulated in multiple fibrotic organs in mice. TGF-β elicits a rapid upregulation of MerTK expression in fibroblast. MerTK, on the other hand, can stimulate further production of TGF-β and facilitate the activation of profibrotic TGF-β/SMAD and non-SMAD signaling pathways. This process establishes a profibrotic positive feedback loop that supports the occurrence of fibrosis. Mechanistically, I showed that MerTK is a critical regulator of canonical and noncanonical TGF-β pathways. MerTK regulates the fibrotic gene regulatory transcription

network by regulating chromatin accessibility, RNA polymerase II (pol II) pausing and reprogramming the enhancer landscape. In this study, I used mouse models to investigate the fibrosis in kidney, lung, and liver. Through my research, I was able to show that the fibrogenic signaling loop could be disrupted by the downregulation of MerTK expression. This intervention resulted in a significant reduction in the severity of fibrosis.

Conclusion: The findings combining in vitro, and in vivo investigations have provided evidence that MerTK functions as a novel regulator of fibrosis across several organs by involving shared core pathway. This research proposes that MerTK may serve as a promising therapeutic target for the treatment of multiorgan fibrosis.

ii. Acknowledgements

Ten years have passed since I left home at the age of eighteen and entered Northwest Normal University, which is two thousand kilometres away from home. If I had the chance to go back in time and tell myself ten years ago that one day I would complete PhD in medicine at a top medical research institute, I would never believe my luck. “Zi-Yan” as my parents gave me the meaning of my name – a man with talent and virtue. I believe that studying hard and working hard is very important for me. Now, I feel very lucky and grateful to have the opportunity to write this doctoral thesis.

I would like to express my gratitude to my main supervisor, Professor Mohammed Eslam, for his unwavering support, advice, and motivation over the past three years. He helped me transition from a pure student role to a researcher role, and I feel very lucky to have met him. He showed up early in the office every day to answer my questions, even about the very small details of an experiment. He successfully helped me open the door to my future career and taught me how to think critically about scientific research, the overall design of a project, the conception of experimental plans and the professional writing of articles. I still remember him telling me, near the end of my project experiment, that as a medical researcher, I should not be satisfied with just publishing a paper because a lot of papers are stuck in the translation phase. As a qualified medical scientist, when conducting a research project, I should think about how to contribute the research to clinical development, promote the progress of my medical career and solve real health issues. I do not think I have ever met a better supervisor than Professor Eslam.

Second, I would like to thank Professor Jacob George for welcoming me to the Storr Liver Centre (SLC) and giving me invaluable general advices about my project and my study.

I would also like to express my sincere thanks to Associate Professor Silvana Gaudieri and Winthrop Professor Marc Tennant, my supervisors while I was working on my Master

degree at the University of Western Australia. Without their generous recommendation, I would not have had such a valuable research opportunity at Westmead Institute for Medical Research (WIMR).

Additionally, I would like to thank Dr Olivier, Dr Ali, Dr Jawaher and all the other members of the Functional Genomics Group. When I first came to WIMR, they helped me familiarise myself with various experimental operations quickly. Without them, my studies would not have started so smoothly. I would like to express my gratitude to all the other members of SLC and the other departments of WIMR for their valuable support over the preceding three-year period.

Next, I would like to offer special thanks to my parents. As a child who grew up in a doctor's family, the hospital is the place I am most familiar with besides school. Imperceptibly, it also had a significant impact on my career choice. Ever since I left home for my university studies, I have regretted not being around to take care of my mother during her two operations. However, this is also the main reason why I am committed to basic medical research, as Professor Eslam taught me – to help clinical development, to help doctors solve problems and to benefit more people. I think I'll finally be able to help my parents when they need me.

I would also like to express my special thanks to all the teachers and classmates I met during my student years and all the friends I have met in Lanzhou, Perth and Sydney, especially my previous high school friend with whom I had a reunion once I moved to Sydney. My progress is inseparable from your selfless help, both in study and in life.

I would next like to give special thanks to Ja-Ning. We met at the beginning of my PhD studies. Although COVID-19 has made it rare for her to come to Sydney, she has still given me lots of encouragement, patience, comfort and hope in lots of other ways.

Finally, I would like to thank myself for holding on until now and not giving up after all the setbacks during this decade.

Ziyan Pan

June 2023

iii. Publications

1. **Pan, Z**., J.G. Fan, and M. Eslam, *An update on drug development for the treatment of metabolic (dysfunction) associated fatty liver disease: Progress and opportunities.* Curr Opin Pharmacol, 2021. **60**: p. 170-176.
2. **Pan, Z**., W.K. Chan, and M. Eslam, *The role of B cells in metabolic (dysfunction)-associated fatty liver disease.* Hepatobiliary Surg Nutr, 2021. **10**(6): p. 875-877.
3. **Pan, Z**. and M. Eslam, *Metabolically healthy obese and MAFLD: does weight status alone matter?* Hepatology International, 2022. **16**(6): p. 1253-1255.
4. Alharthi, J., A. Bayoumi, K. Thabet, **Pan.Z**, B. S. Gloss, et al., *A metabolic associated fatty liver disease risk variant in MBOAT7 regulates toll like receptor induced outcomes.* Nat Commun, 2022. **13**(1): p. 7430.
5. **Pan, Z**., S.A. Alqahtani, and M. Eslam, *MAFLD and chronic kidney disease: two sides of the same coin?* Hepatol Int, 2023. **17**(3): p. 519-521.
6. Alharthi, J., **Pan, Z***., B. S. Gloss, D. McLeod, M. Weltman, J. George, and M. Eslam. *Loss of metabolic adaptation in lean MAFLD is driven by endotoxemia leading to epigenetic reprogramming.* Metabolism, 2023. **144**: p. 155583. (* Equally contributed first author).

iv. Contents table

v. Figure list

vi. Tables list

vii. Abbreviations list

Abbreviations	Name
36B4	acidic ribosomal phosphoprotein
AEC2	alveolar epithelial type 2 cell
AFLD	Alcoholic fatty liver disease
Akt	protein kinase B
ALT	Alanine aminotransferase
ATAC-seq	Assay for Transposase-Accessible Chromatin using sequencing
BDL	Bile duct ligation
BLM	Bleomycin
BMP	bone morphogenetic protein
cDNA	Complementary DNA
CKD	Chronic kidney disease
CLD	chronic liver disease
COL1A1	Collagen type I alpha 1
COL1A2	Collagen type I alpha 2
COL3A1	Collagen type III alpha 1
CUT&Tag-seq	Cleavage under targets and tagmentation sequencing
DKK1	Dickkopf-related protein 1
DMEM	Dulbecco's Modified Eagle Medium
DMSO	Dimethyl sulfoxide
ECM	extracellular matrix
EDTA	Ethylenediaminetetraacetic acid
EGF	epidermal growth factor
ERK	extracellular regulatory kinase
FBS	fetal bovine serum
GAPDH	glyceraldehyde 3-phosphate dehydrogenase
GAS6	Growth arrest-specific 6
Gla	glutamic acid
GWAS	genome-wide association study
H&E	Histone and Eosin

HBV	hepatitis B virus
HCC	hepatocellular carcinoma
HCC	hepatocellular carcinoma
HCV	hepatitis C virus
HSC	hepatic stellate cell
IPF	Idiopathic pulmonary fibrosis
JNK	c-jun N-terminal Kinase
LAP	latent association protein
LLC	large latent complex
LPA	lysophosphatidic acid
MAFLD	Metabolic Associated Liver Disease
MAPK	mitogen-activated protein kinase
MCSF	Macrophage colony-stimulating factor
mL	Millilitre
mM	Millimolar
mRNA	Messenger RNA
pA-Tn5	protein A-Tn5
PBS	Phosphate buffered saline
PCR	Polymerase chain reaction
PDGF	platelet-derived growth factor
PVDF	polyvinylidene difluoride
RNA-seq	RNA-sequencing
SEC	sinusoidal endothelial cell
SFRP1	secreted frizzled-related protein 1
TGF-b	Transforming growth factor beta
T_H2 cell-M2	T helper 2 cell-M2 macrophage
TβRI	TGF-β receptor I
TβRII	TGF-β receptor II
UIP	usual interstitial pneumonia
UUO	Unilateral ureteral obstruction
α-SMA	alpha-smooth muscle actin
µl	Microliter

Chapter 1: Introduction and Literature Review

1.1 Organ fibrosis

Organ fibrosis is a debilitating condition that lacks effective therapies and accounts for more than 50% of all mortalities in affluent countries [1]. In this pathological state, the physiological integrity of cells and tissue structures is substituted by scar tissue that is abundant in collagen, primarily seen in epithelial organs, such as the liver, lungs, kidneys and skin; this could lead to the gradual loss of function and the final failure of organs as a result of structural distortion from scar retraction [2].

The excessive production of scar tissue, also known as fibrosis, is a characteristic ultimate outcome of most chronic diseases. Various factors can contribute to the development of fibrosis, such as idiopathic pulmonary fibrosis (IPF) and radiation-induced fibrosis in the lungs, viral hepatitis, alcoholic liver disease, metabolic associated liver disease (MAFLD) leading to liver fibrosis, diabetic nephropathy and hypertensive nephrosclerosis resulting in renal fibrosis [2].

Notably, pathological fibrosis in several organs may exhibit shared underlying features, including chronic damage to epithelial cells, which stimulates the overproduction of cytokines and growth factors. This, in turn, promotes the recruitment and activation of mesenchymal cell precursors, leading to their differentiation into myoblasts. Myofibroblasts release extracellular matrix (ECM) proteins and cytokines that promote fibrosis, therefore impeding the regular processes of repair and degradation and extending the duration of fibrotic progression. Consequently, this leads to the accumulation of excessive scar tissue and the subsequent malfunction of the affected organ **(Figure 1.1)** [2].

Although significant progress in characterising the pathophysiology of fibrosis has been achieved in recent decades, an in-depth understanding of its detailed underlying processes remains elusive. Moreover, other challenges must be addressed to facilitate the translation of

these discoveries into efficient anti-fibrotic drugs [3]. For instance, there is a dearth of suitable animal models and in vitro primary human tissue culture methods that can accurately replicate the whole range of fibrosis seen in humans [4]. Moreover, the considerable variability among individuals with fibrotic disorders and the gradual nature of fibrosis progression provide challenges to the progress of targeted medication development for fibrosis [4].

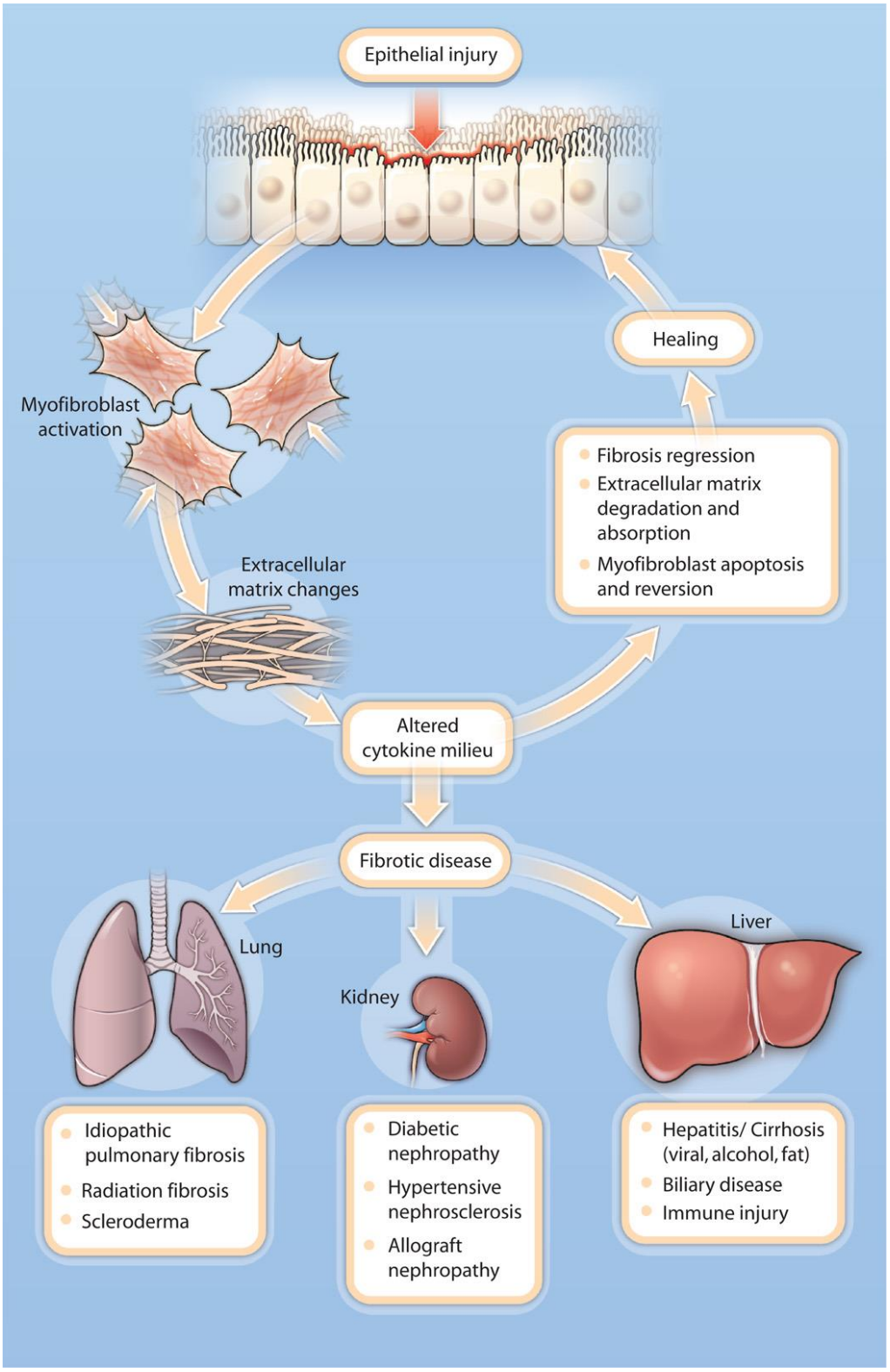

Figure 1.1 Typical events in the development and remission of fibrosis in various tissues [2]

1.1.1 Liver fibrosis

Liver fibrosis is the ultimate consequence of almost all liver diseases and is considered the most reliable indicator of morbidity and mortality linked to hepatic conditions [5]. Globally, the number of persons with chronic liver disease (CLD) is estimated to be over 844 million, and the condition is responsible for over two million deaths annually [6]. As the leading cause of people's loss of their capacity to work, CLD has steadily eclipsed other prevalent chronic conditions, including arthritis, asthma and diabetes [7].

In Australia, where there are over six million people with CLD, more than 7,000 individuals die each year, with a typical mid-50s age of death [8]. By 2030, there will probably be more than eight million people with CLD. Individuals, families and healthcare systems are obviously heavily burdened by this alarming trend [8]. In addition, hepatocellular carcinoma (HCC), a significant adverse consequence of liver cirrhosis, is the sixth-deadliest malignancy in males [9]. Currently, liver transplantation is the only authorised therapy for end-stage cirrhosis because no anti-fibrotic medications exist. As a result, the clinical need for liver fibrosis therapy is enormous [10].

Multiple liver diseases, such as MAFLD, alcoholic fatty liver disease and hepatitis B and C virus infections, may lead to hepatic fibrosis that progresses through the buildup of fibrous scar [9].

1.1.1.1 Hepatic stellate cells (HSCs): the primary effector cells in liver fibrosis

Hepatic stellate cells are a distinct population of non-parenchymal cells that constitute approximately 5%–8% of the overall liver cell population; they are situated in the Disse space, which lies between sinusoidal endothelial cells and hepatocytes [11].

At the cellular level, HSCs are the primary cells responsible for the development of fibrous scarring in hepatic fibrosis. The four distinct phenotypes of HSCs, namely, quiescent, activated, inactivated and senescent, each contribute significantly to the development and resolution of hepatic fibrosis.

HSCs in a healthy liver are often found in a quiescent state and possess a substantial quantity of lipid droplets containing vitamin A, and they are crucial to the maintenance of liver homeostasis in addition to the processes of repair and renewal; these cells are also involved in regulating retinoid metabolism [12]. These lipid droplets serve as the primary vitamin A reservoir inside the human body [12].

However, once the liver undergoes injury, HSCs pass into an active state. The activation of HSCs occurs mechanistically as a consequence of sustained liver injury [10]. This activated state is distinguished by the processes of proliferation, elasticity and chemotaxis [13]. The concentration of vitamin A in the liver that has suffered injury will progressively diminish [14]. With the continuous and repetitive activation of HSCs in individuals with sustained liver disease, HSCs produce collagen, which ultimately leads to fibrosis [15]. Additionally, by secreting transforming growth factor beta (TGF-β) and other agonists, this can induce a cross-talk with immune cells, especially macrophages, which play a crucial function in the initiation of HSCs activation and fibrosis progression [16]. By contrast, activated HSCs possess the capacity to undergo apoptosis or transition back to a deactivated phenotype [10].

Therefore, it is not surprising that reversing the activation of HSCs—reverting them to a resting state—is the focus of ongoing research on anti-fibrotic drugs [12].

1.1.2 Kidney fibrosis

Chronic kidney disease (CKD) is defined as an anatomical or functioning abnormality of the kidney that lasts longer than three months [17]. Because of the lack of visible symptoms in the initial phases, it can be challenging to quantify the true incidence of CKD, but it is thought to affect 10%–14% of the population worldwide and has a detrimental impact on health [18]. In clinics, there are currently few effective treatments for CKD, such as those for fibrosis, which merely serve to slow the course of the disease [19].

Renal fibrosis is a commonly seen clinical characteristic and final manifestation of CKD, characterised by many morphological aspects, including glomerular sclerosis, tubular atrophy, persistent interstitial inflammation and fibrosis, and a sparse distribution of blood vessels [20]. Local fibroblasts and pericytes are stimulated in response to kidney damage, increasing their ability to contract force, secrete mediators of inflammatory processes and produce ECM, all of which aid in the healing process. Nevertheless, suppose a kidney injury is left untreated or suffers significant damage; in this case, the wound healing process becomes dysfunctional [21], demonstrating that ECM proteins, such as fibronectin and collagen, keep on building up in the kidneys and, when combined with oxidative stress and metabolic changes [20], cause kidney dysfunction that eventually leads to failure of the kidneys and end-stage kidney disease [22].

To ameliorate or cure kidney fibrosis, ongoing research for novel therapies has mostly focused on active myofibroblasts, which are the major contributors to collagen, or the enzymes responsible for collagen breakdown [23].

1.1.3 Pulmonary fibrosis

Idiopathic pulmonary fibrosis is a chronic lung condition that currently affects three million individuals globally; the probability of IPF substantially increases with age [24].

Idiopathic pulmonary fibrosis is distinguished by the excessive accumulation of lung scar tissue in the interstitial space, resulting in the formation of a *honeycomb* pattern characterised by subpleural cyst-like spaces with distinct borders. Additionally, IPF is associated with tractive bronchiectasis and progressive thickening of the peripheral alveolar septum [24]. This fibrotic process typically initiates in the lower and surrounding areas of the lungs, eventually spreading to involve the entirety of lung tissue [24].

Tobacco use, stimulation by the environment, persistent infections caused by viruses and comorbidity are all linked with an increased risk [24], with hereditary risk affecting up to 30% of the general population [25].

Mechanistically, the pathogenesis of IPF is the outcome of an intricate multidirectional interplay of epithelial cells, mesenchymal cells and ECMs. Within the affected cell population, growing evidence points to alveolar epithelial cells, particularly alveolar epithelial type 2 cells, as the primary drivers of IPF; lung epithelial cells overproduce fibroblasts as a result of inappropriate stimulation, and they migrate, proliferate and distinguish into active myofibroblasts, secrete significant amounts of ECM and subsequently alter the architecture of lung [26].

Although the lungs have a strong capacity for maintenance upon exposure to various outside harms, repeated alveolar tissue epithelial injury can cause epigenetic alterations that ultimately result in IPF [24]. These alterations include fibrosis, ongoing epithelium ageing, excessive development of profibrotic mediants and ongoing stimulation of mesenchymal cell proliferation [24].

1.1.4 Diagnosis of organ fibrosis

The assessment of organ fibrosis has a crucial role in determining the course, stratification and prognosis of the disease. Therefore, properly identifying fibrosis, particularly in its early stages, is of utmost significance for effectively evaluating the extent of fibrotic development [27-29]. Histological examination is widely regarded as the most reliable and accurate method for diagnosing and determining the severity of fibrosis. Biopsy or surgical procedures are often used to obtain samples for histological analysis, in which precise criteria are utilised to conduct histological scoring across various organs [30].

Nevertheless, the histological evaluation of fibrosis is subject to notable constraints. For instance, the acquisition of histological specimens via subcutaneous biopsy of either the kidney or the liver carries inherent surgical risks, including the potential for haemorrhage [31]. Moreover, biopsy outcomes merely reflect a fraction of the tissue taken from the organ and are inadequate for evaluating the general pattern of fibrosis within the organ [32]. Overcoming variations among and between assessors in identifying the phase of fibrosis proves to be challenging, including obtaining identical histology findings [33]. Consequently, many other non-invasive evaluation techniques have been suggested as supplementary methodologies and have started to be used in clinical settings to some extent. These techniques are detailed in **Table 1**) [30].

Table1: Present techniques and genetic markers used for the diagnosis and grading of fibrosis in organs[30]

	Liver	Kidney	Lung
Gold standard	**Histology (biopsy)**		
Mechanical or functional test	Elastography	Elastography	Body plethysmography
Serum biomarkers (examples)	Composite score (e.g., FIB-4, ELF, Fibrotest, NFS, ADAPT), hyaluronic acid, PIIINP, pro-C3	TGF-β, MCP-1, MMP-2, urinary PIIINP	IL-8, CCL18, MMP-1, MMP-7, IGBPs
Genetic markers (examples)	*PNPLA3, TM6SF2, MBOAT7, GCKR, A1AT, HFE*	*ACE, TGFβ1, PARN*	*MUC5B, TOLLIP, TERT, TERC, FAMI3A. DSP, OBFC1, ATPI1A, DPP9*

1.1.5 Shared pathways of fibrosis across different organs

Organ fibrosis arguably shares common pathways across different organs. Understanding these pathways can pave the way for generic anti-fibrotic drugs or the repurposing of anti-fibrotic drugs for one organ to another, which can accelerate the drug development process.

As indicated above, similar to the typical method of wound repair, many fibrosis diseases affecting organs start off by triggering a sequence of reparative mechanisms inside the injured tissue, with the aim of reinstating the structural integrity of the organ. The occurrence of an initial inflammatory response is a frequent phenomenon, resulting in the infiltration, activation and accumulation of leukocytes in the affected tissue [34]. Although the inflammatory responses involved in fibrosis progression in various organs may exhibit differences, they have a common characteristic. Specifically, they all undergo a transformation into T helper 2 (TH2) cell-M2 macrophages, which subsequently release significant quantities of fibrosis-promoting cytokines and activate downstream myoblasts [34].

Furthermore, myofibroblasts are derived from multiple cellular sources, including epithelial, pericyte, endothelial and bone marrow fibroblasts [35]. Despite their diverse origins, these cells demonstrate common activation pathways, such as TGF-β signalling, Hedgehog and WNT signalling, and platelet-derived growth factor (PDGF) [35]. **Figure 1.2** [35] depicts the manifestation of common and distinct pathways across various phases of fibrosis in diverse organs.

The activation of the Hedgehog and WNT signalling pathways has been identified in various fibrotic diseases and is known to have a pivotal role in the cross-talk with the TGF-β signalling pathway [36-38]. Platelet-derived growth factor is a significant mitogen in mesenchymal cells, known for its ability to induce collagen gel contraction [39]. PDGFRα and PDGFRβ, which are receptor tyrosine kinases for PDGF, are expressed in multiple organs' mesenchymal cells [40]. PDGFRα serves as a reliable indicator for fibroblasts [41], whereas

PDGFRβ has broader expression in mesenchymal cells and pericytes [40]. The activation of mitogen-activated protein kinases (MAPKs) and phosphoinositide 3 kinases occurs via their interaction with PDGF receptors. This interaction also involves tiny RHO family GTPases, which play a role in cell motility, as well as Src and other non-receptor tyrosine kinases, and phospholipase Cγ [42]. Previous research has shown that PDGF is linked to fibrosis progression in multiple organs, such as the liver, bone marrow, heart, kidneys and lungs in murine models [40]. PDGF has synergistic effects with TGF-β via an interaction process, resulting in enhanced fibrosis [43].

TGF-β is a prominent promoter of fibrosis, playing a central role in this pathological procedure, which will be discussed in more detail in the next section as it pertains to the current thesis.

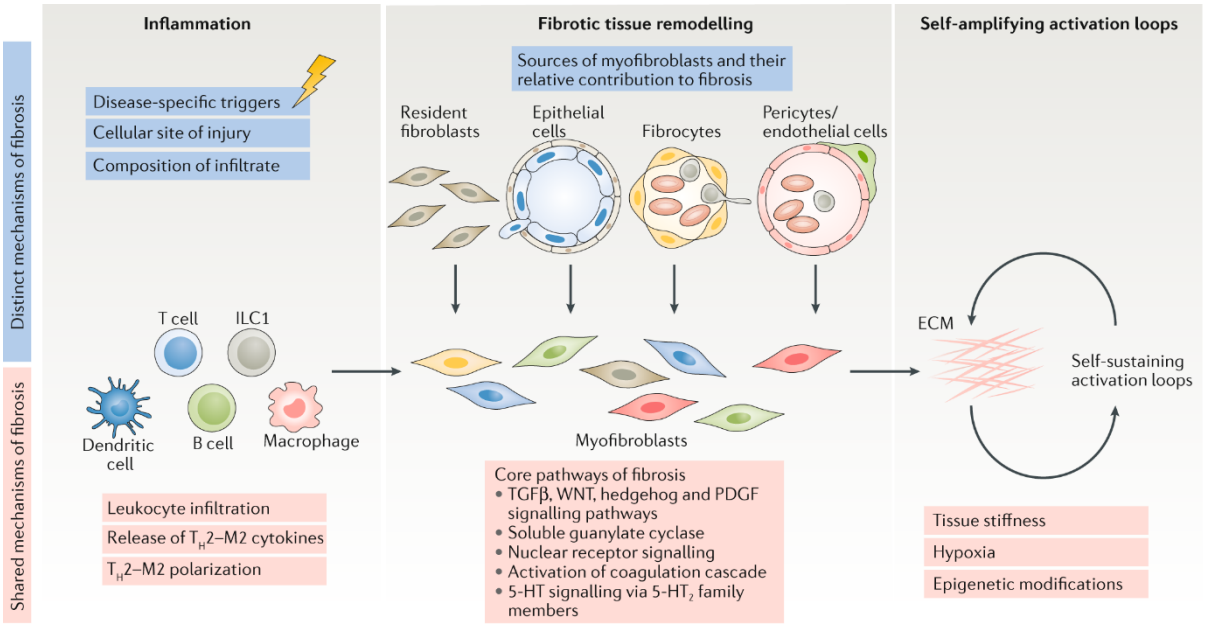

Figure 1.2 The shared and unique processes involved in various phases of fibrotic tissue remodelling [35]. This map illustrates the collaborative and distinct pathways implicated in the initiation and advancement of fibrosis pathology [35][35]. In a general context, leukocyte infiltration and activation, as well as TH2 cell-M2 macrophage polarisation, are influenced by distinct illnesses and various places during the initial phases of the disease. Subsequently, the production of diverse pro-fibrotic cytokines is initiated. Alterations in the surrounding milieu trigger the activation of fibroblasts inside it, leading to their conversion into myofibroblasts. This differentiation process involves fibroblasts originating from different cell types, such as epithelial, pericyte, endothelial and bone marrow fibroblasts. Throughout the course of illness development, the activation of the fibrotic pathway is sustained by tissue remodelling, which is triggered by either the stiffness of the tissue or hypoxia. This sustained activation enables myofibroblasts to retain an active phenotype in fibrotic diseases [35].

1.1.6 TGF-β signalling in fibroblasts

The TGF-β family, including TGF-βs, activins and bone morphogenetic protein, has a total of 33 members [44]. Each member of this family is responsible for mediating distinct signalling pathways [45]. TGF-β has several roles in organisms, such as controlling tissue balance and restoration, modulating immunological and inflammatory reactions, facilitating ECM formation and regulating the differentiation of cells and proliferation [46].

TGF-β is a prominent cytokine that promotes fibrosis, rendering it a key focus for research on anti-fibrotic interventions. Nevertheless, the long-term systemic suppression of TGF-β1 can lead to negative consequences. For instance, studies have shown that TGF-β1 knockout or inhibition mice can hinder tumour suppression and trigger immune reactions throughout the body [2] [47]. These effects are believed to be associated with structural irregularities in mucosal surfaces, particularly in the gut where TGF-β1 is known to regulate tissue haemostasis [48]. This implies that while systemic suppression of TGF-β is anticipated to hinder fibrosis, regulating the extent or time frame of restriction within an appropriate range in applied studies is imperative to prevent associated negative consequences [3], and that approaches for specific targeting of TGF-β signalling are required.

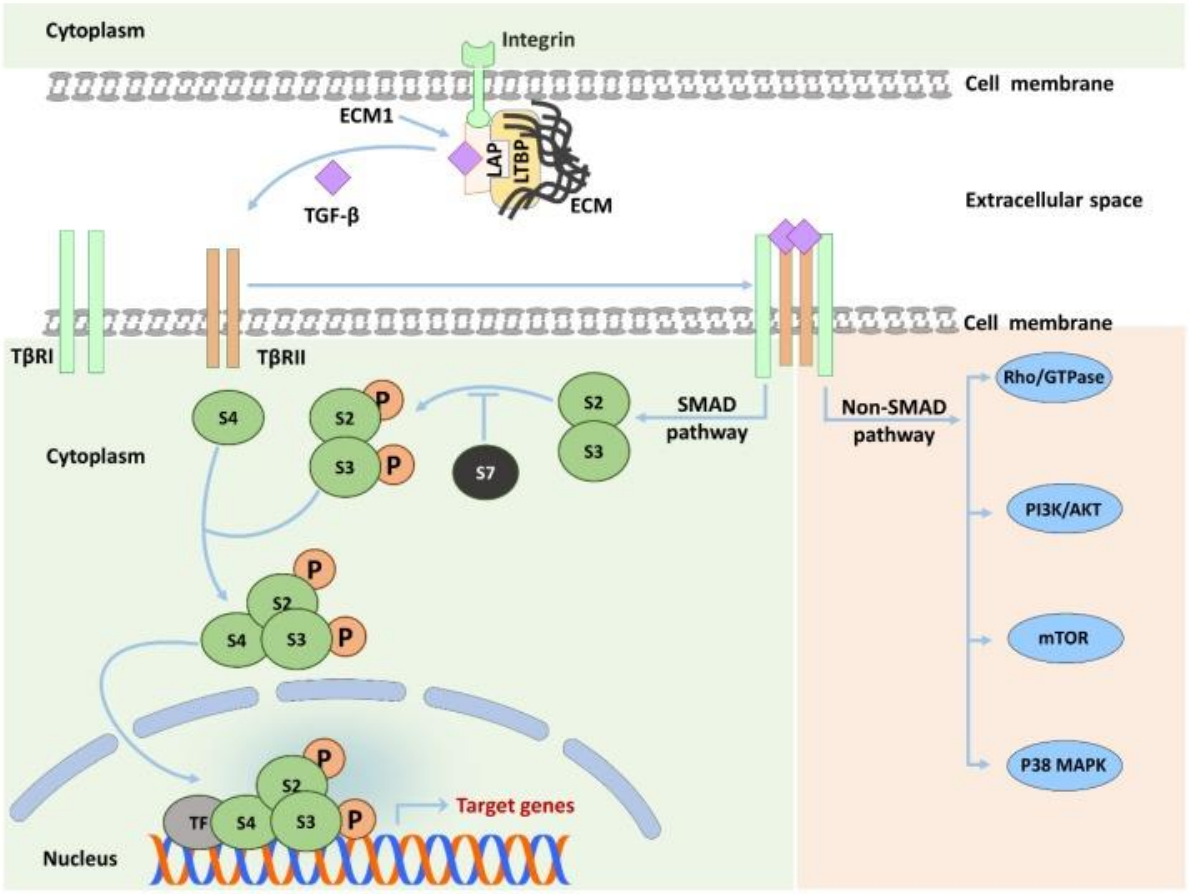

Figure 1.3 Dependence on SMAD and non-SMAD factors [49]. The release of TGF-β occurs initially from the large latent complex (LLC) through an interaction between the integrin and the latent association protein (LAP) [49]. This association leads to the binding of LAP to the TGF-β II receptor (TβRII) and the subsequent formation of a heterotetramer with the TGF-β I receptor (TβRI) [49]. Following this, the regular signalling process is activated mainly through SMAD2 (S2) and SMAD3 (S3) phosphorylation [49]. It has also been shown that SMAD7 can have a negative regulatory effect on the signalling pathway of TGF-β [49]. This is achieved by its competitive interaction with R-SMADs and its binding to TβRI [49].

1.1.6.1 The SMAD-dependent TGF-β signalling pathway

The downstream signalling route of TGF-β may be categorised into two main pathways, the SMAD pathway and the non-SMAD pathway, as depicted in **Figure 1.3** [55]. The activation of TGF-β commences the process of signal transduction through its binding to TβRII and the subsequent recruitment of TβRI. Next, TβRII initiates the phosphorylation of TβRI, inducing a change in its structural arrangement and facilitating its interaction with SMAD2 and SMAD3 proteins, leading to their further phosphorylation [46]. Following phosphorylation, SMAD proteins undergo transformation into pSMAD2 and pSMAD3 [46]. These phosphorylated forms have the ability to combine with SMAD4 to create heterocomplexes, which then migrate to the nucleus, where they bind to DNA [46]. This binding process plays a crucial role in the regulation of transcription for several genes associated with fibrosis [46]. Notably, α-SMA and CTGF are among the target genes that are influenced by this regulatory mechanism [44, 50]. Because of the absence of DNA binding capability in SMAD2 and the relatively low affinity of SMAD3 for DNA, the Smad2/3/4 complex often relies on the recruitment of supplementary transcriptional coactivators to enhance the stability of the activated transcription complex [44, 51].

1.1.6.2 The non-SMAD-dependent TGF-β signalling pathway

TGF-β can activate many signalling pathways, such as the MAPK pathway, which can further activate extracellular regulatory kinase (ERK), P38 and c-jun N-terminal kinase [49]. Some pathways are also independent of SMAD, including c-abl, PI3K/Akt, Rho-associated coiled-coil-containing protein kinases and JAK2/STAT3 [49].

The initiation of MAPK is activated by kinase receptors in response to external stimulation [52]. Following this, the signal is transmitted downstream through phosphorylation [53]. This cascade of events can affect gene transcription [53] and is important in many

physiological processes, including cell proliferation, adhesion and migration. For instance, it is implicated in the induction of hepatic stellate cells during the progression of liver fibrosis [54].

The PI3K/Akt/mTOR signalling pathway is another significant non-SMAD mechanism [55]. Both in vitro and in vivo studies have provided evidence that the suppression of P13K activation may result in the reduction of liver fibrosis [56]. Nevertheless, the implementation of these focused approaches remains constrained by their insufficient specificity and unavoidable adverse reactions.

1.2 Experimental animal models of organ fibrosis

The use of laboratory specimens in the investigation of fibrosis is widely acknowledged as crucial and irreplaceable because of the many benefits they provide in the realm of illness research. First, laboratory animals help researchers thoroughly investigate research questions that cannot be tested immediately on humans. Second, during animal experimentation, it is possible to minimise the range of factors that are challenging to regulate in human studies, such as environmental factors and food [57]. Third, examining fibrosis on a macroscopic organ level is feasible, a capability that is unattainable in an in vitro setting [57]. Finally, the disease may be categorised into several phases of advancement, allowing for the use of additional sampling to facilitate the comprehensive investigation of the characteristics of fibrosis [57].

Nevertheless, acknowledging the existence of some drawbacks associated with animal models is important. Disparities between humans and rodents may be seen in several aspects, such as gene transcription and regulation, metabolic processes and healing responses, which can be attributed to species variations [58]. Moreover, it should be noted that the very complex nature of human organ fibrosis necessitates the recognition that any fibrotic mouse model can only recapitulate a fraction of the multifaceted features shown by human diseases [57]. Hence,

recent suggestions put forward by many journal editors have advocated the use of multiple liver fibrosis models in studies aimed at identifying novel antifibrotic targets in order to ensure the robustness and reproducibility of experimental findings [59].

1.2.1 Liver fibrosis model ------ Bile duct ligation (BDL)

Bile duct ligation treatment is a surgical intervention used to induce hepatic fibrosis. The technique relies on deliberate blockage of the extrahepatic bile duct system in laboratory conditions. This obstruction triggers a cascade of pathological processes, including cholestasis and inflammation, ultimately resulting in a pronounced fibrosis process that originates from the periportal vein region [60].

Hence, the BDL model has emerged as the prevailing standard paradigm for inducing obstructed cholestasis damage and liver fibrosis in rodents and for investigating the underlying pathological process [61]. The BDL model has the capability to induce liver fibrosis in a very short period, leading to the subsequent development of cirrhosis.

1.2.2 Kidney fibrosis model ------ Unilateral ureteral obstruction (UUO)

Renal injury generated by UUO is marked by many pathological alterations, such as tubular dilatation, interstitial dilatation, proximal tubular mass loss, hypertrophy, hydronephrosis, leukocyte infiltration, tubular epithelial cell death and fibroblast deposition [62]. The evolution of kidney fibrosis may be attributed to a combination of haemodynamic alterations resulting from physical stretching, apoptosis of epithelial renal tubules, oxidative damage and inflammation, which are induced by the operation [63-67]. The UUO model is well practiced for its replication of chronic obstructed kidney disease in humans in the study of renal fibrosis [62].

1.2.3 Pulmonary fibrosis model ------ Bleomycin induced pulmonary fibrosis (BLM)

Bleomycin is an antibiotic used for many forms of neoplasm treatments [68]. However, the foremost concern associated with bleomycin usage is its potential to induce pulmonary toxicity, which represents a significant adverse reaction. The administration of bleomycin has been shown to elicit lipid peroxidation, resulting in damage to alveolar cells and subsequent lung inflammation. This inflammatory response is characterised by the presence of interstitial oedema and the infiltration of inflammatory and immunological cells. Ultimately, these pathological processes contribute to the progression of pulmonary fibrosis. This condition is distinguished by an elevated synthesis and accumulation of collagen and other constituents of the ECM [69]. Hence, bleomycin-induced pulmonary fibrosis has emerged as a well-accepted animal model for investigating pulmonary fibrosis. Various intervention techniques for bleomycin delivery, including tracheal injection, abdominal injection and aerosol inhalation, have been used in this context [70].

1.3 Genetics as an avenue for novel approaches to anti-fibrotic drug development

Historically, the predominant approach used to investigate the genetic basis of a disease has been candidate gene studies [71]. This research methodology is characterised by its hypothesis-driven nature, in which preliminary data on specific genes are utilised to formulate hypotheses and assess their validity [72]. Because of the intricate and broad regulatory networks of genes implicated in various diseases, particularly fibrosis, the utility of genetic findings derived from candidate gene investigations is limited. Inconsistencies are also often observed in various studies [72]. Consequently, this approach is deemed inadequate for genetic research pertaining to the majority of complex diseases [72].

Currently, the primary approaches used in genetic research for disorders consist of prospective gene investigations and genome-wide association studies (GWAS) [72]; the latter

are hypothesis-independent strategies utilised to detect genetic variations linked to certain diseases by conducting comprehensive investigations of the whole genome in a substantial cohort of people [73]. The identification of these genetic markers enables a deeper characterisation of the correlation between genes and pathogenicity, leading to the improved development of preventative and treatment measures (**Figure 1.4**) [72-74].

Genetic research offers an exciting opportunity for the advancement of drug development. An examination of pharmaceutical pipelines reveals that targets with a genetic connection with diseases exhibit a greater than twofold likelihood of success in clinical trials and obtaining regulatory approval compared with targets lacking such a genetic association. The next step is to leverage this genetic information to inform the development of new drugs and precision medicine approaches to management.

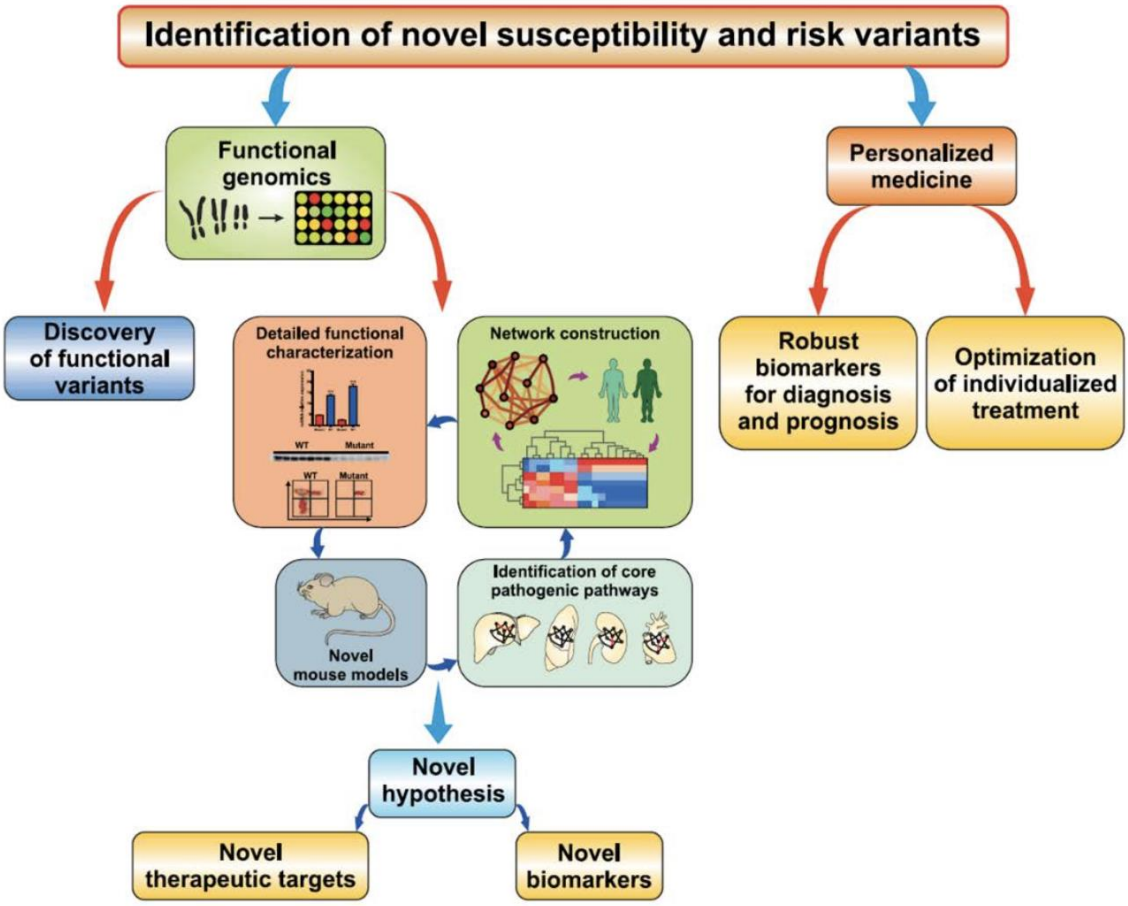

Figure 1.4 Era after the completion of genome-wide association studies (GWAS) [72] Genome-wide studies have the potential to identify a vast majority of the variations in susceptibility to and risks for complex illnesses. The task in the age following GWAS is to investigate the precise functionality of these genetic loci and to elucidate their clinical implications. Functional genomics plays a crucial role in identifying risk modifications and their impacts on transcription, splicing and epigenetic changes. Genome-wide studies enable generating new hypotheses, building genetic networks, identifying key pathogenic mechanisms, generating multiple accurate animal models and exploring complex functional representations, which lead to an enhanced understanding of the mechanisms of diseases and a better identification of potential therapeutic targets [72].

1.3.1 Identification of MERTK as a potential target for fibrosis

A recent GWAS conducted on chronic hepatitis C patients identified multi-genetic loci related to liver fibrosis, and the most significant one was the homozygosity for the non-coding variant of MERTK, specifically the rs4374383 G>A single nucleotide polymorphism (SNP) (**Figure 1.5**) [75]. This discovery has also been confirmed in several liver diseases, such as MAFLD [76, 77].

The genetic data indicated a possible involvement of MERTK in the progression of liver fibrosis. However, the precise functional underpinnings of MERTK and the mechanisms by which it contributes to the evolution of liver fibrosis are not yet fully understood. Additionally, the involvement of MERTK in the advancement of organ fibrosis remains uncertain, as it is unknown whether its role is limited to hepatic fibrosis or extends to fibrosis in other organs as a fundamental mechanism.

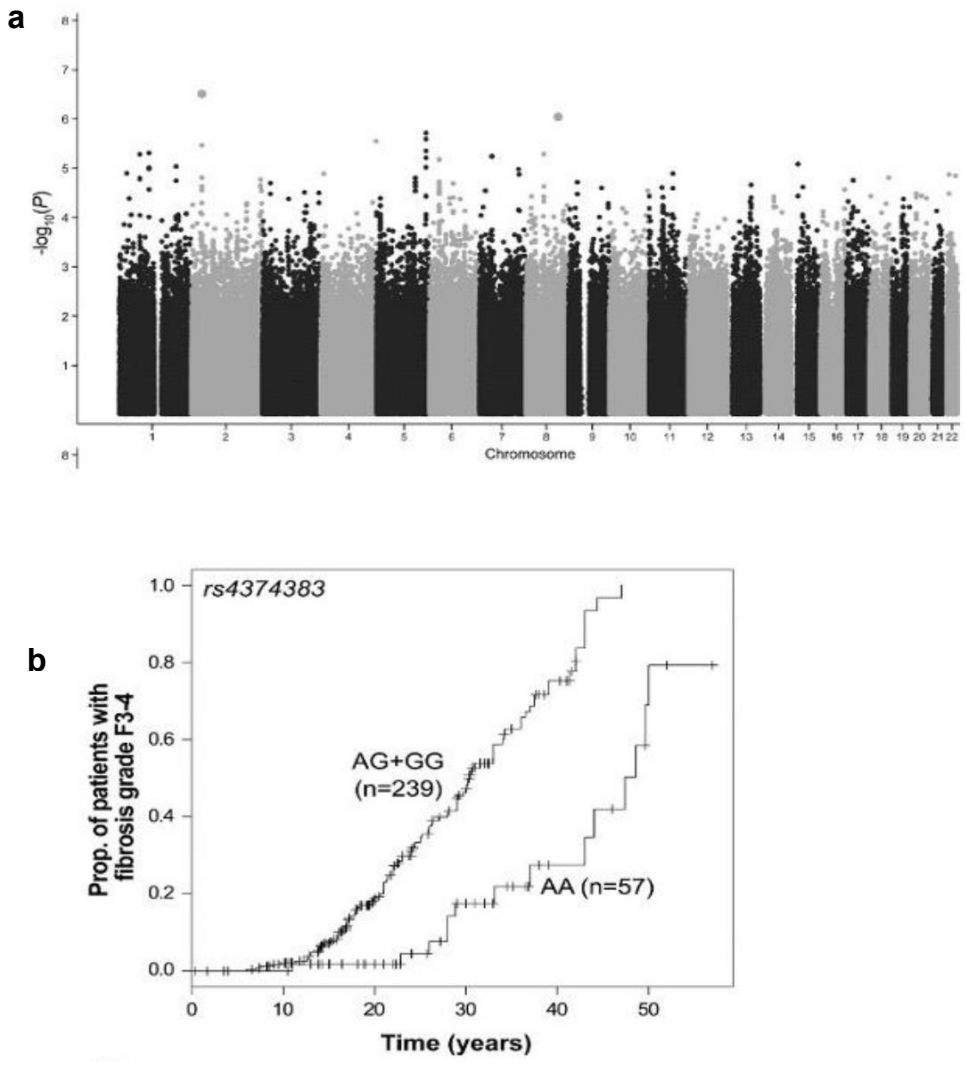

Figure 1.5 The MERTK gene has been identified via GWAS as a newly discovered risk mutation associated with the advancement of liver fibrosis in individuals diagnosed with chronic hepatitis C [75]. **a)** A Manhattan plot was generated via GWAS of liver fibrosis, specifically focusing on a binary phenotype of F0-1/F3-4. The plot displayed large data points to represent single nucleotide polymorphisms (SNPs) with a *p*-value less than 10^-6. **b)** In a subset of patients who had transfusions, the survival curve of SNP rs4374383, which is situated inside the MERTK gene, was assessed using the phenotypic duration of F0-1/F3-4 [75].

1.4 MerTK

1.4.1 Overview of MerTK

MerTK has recently been recognised as a member of the TAM receptor tyrosine kinase family, along with Tyro3 and Axl [78]. Every individual in the TAM family has a distinct extracellular structure (**Figure 1.6**) that links a domain of the transmembrane to a protein kinase located in the cytoplasm [79, 80]. Upon binding to ligands, tyrosine kinases undergo activation [81].

The expression of TAM is seen in several organs, such as the haematological system, neurological system, reproductive system and the liver [82]. MerTK is widely expressed in various cell types, including monocytes/macrophages, dendritic cells, natural killer cells, natural killer T cells, HSCs, megakaryocytes, platelets, epithelial cells and reproductive organ cells [76].

MerTK plays a crucial part in several biological processes, including the facilitation of cell growth and proliferation, the inhibition of cell death [83], the mediation of efferocytosis [84], the regulation of immunological response [85] and the control of inflammation [86]. MerTK serves as the primary phagocytic receptor in macrophages and plays a crucial role in facilitating the clearance of early apoptotic bodies by M2c macrophages [87]. The involvement of MerTK in immunological regulation has been observed, as shown by the findings that MerTK knockout mice experience mortality as a result of septic shock, which may be attributed to a compromised innate immune response [86]. The role of MERTK might differ according to context, cell types and different stages of the disease (acute vs. chronic; early vs. late stage) [88].

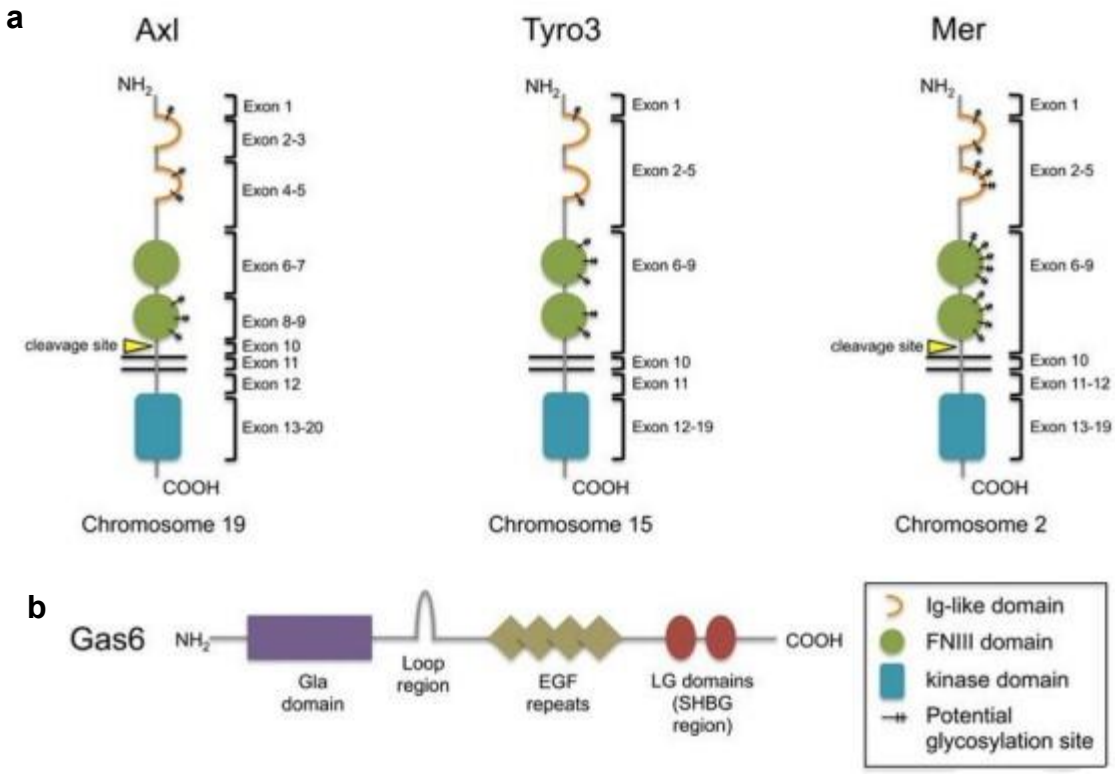

Figure 1.6 Architectural characteristics of TAM receptors and their mutually recognised ligand, Gas6 [80]. **a)** The extracellular architecture of TAM receptor family members is uniform, including two immunoglobulin-like domains responsible for ligand binding, as well as two fibronectin III domains. Both Axl and Mer can generate soluble extracellular components through the occurrence of a proteolytic cleavage beyond the transmembrane domain. However, the same phenomenon has not been observed for Tyro3. Glycosylation sites are seen at many receptor locations, namely, at the following amino acid residues: Axl (43, 157, 198, 339, 345, 401), Tyro3 (63, 191, 230, 240, 293, 366, 380) and Mer (114, 170, 207, 215, 234, 294, 316, 329, 336, 354, 389, 395, 442 [confirmed], 454). **b)** Growth arrest-specific 6 (Gas6) is a protein that relies on vitamin K for its activation and has a higher binding affinity for Axl compared to Tyro3 and Mer. Cell membrane contact may be established via the glutamic acid (Gla) domain, whereas the laminin G (LG) domain can connect to the Ig-like region of the receptor [80].

1.4.2 MerTK binding location

The many ligands of TAM include GAS6, Protein S, Tubby, TULP-1 and Galectin-3 [89-91]. GAS6 and Protein S are ligands that rely on vitamin K for their proper functioning [92]. Both entities have some structural similarities, such as an N-terminal-carboxyl-Gla domain, four consecutive epidermal growth factor-like repeats and a C-terminal region resembling sex hormone-binding globulin that consists of two LG repeats [93]. The activation of these entities requires both dimerisation and γ-carboxylation [93]. Nevertheless, there is a distinction in terms of specificity and affinity between GAS6 and Protein S. GAS6 has the capability to activate all three receptors, namely, MerTK, Axl and Tyro3, while Protein S can only activate MerTK and Tyro3 [79]. Consequently, GAS6 is widely acknowledged as the predominant ligand shared by the TAM family [89].

The role of GAS6 in the advancement of liver fibrosis [94] and myocardial infarction has been demonstrated [95]. Similarly, galactin-3 has been found to be implicated in liver fibrosis [96].

1.4.3 MERTK small molecule inhibitors

Because of the significant involvement of MERTK in different disorders, including cancer, substantial research on the development of small-molecule drugs targeting the MerTK receptor is ongoing. These drugs include UNC569 [97], UNC1062 [98] and UNC1666 [99]. Some of these inhibitors have shown encouraging antitumour efficacy in preclinical application [100].

In particular, UNC569, which is the first documented small-molecule inhibitor of MerTK, has the advantageous attribute of oral administration and exhibits favourable pharmacokinetic properties. Notably, it has shown encouraging preclinical efficacy, both in vitro and in vivo. The chemical composition of UNC569 is depicted in **Figure 1.7** [97, 101]. For the purposes of this investigation, UNC569 was chosen as the pharmacological agent to inhibit MerTK in vivo and in vitro settings.

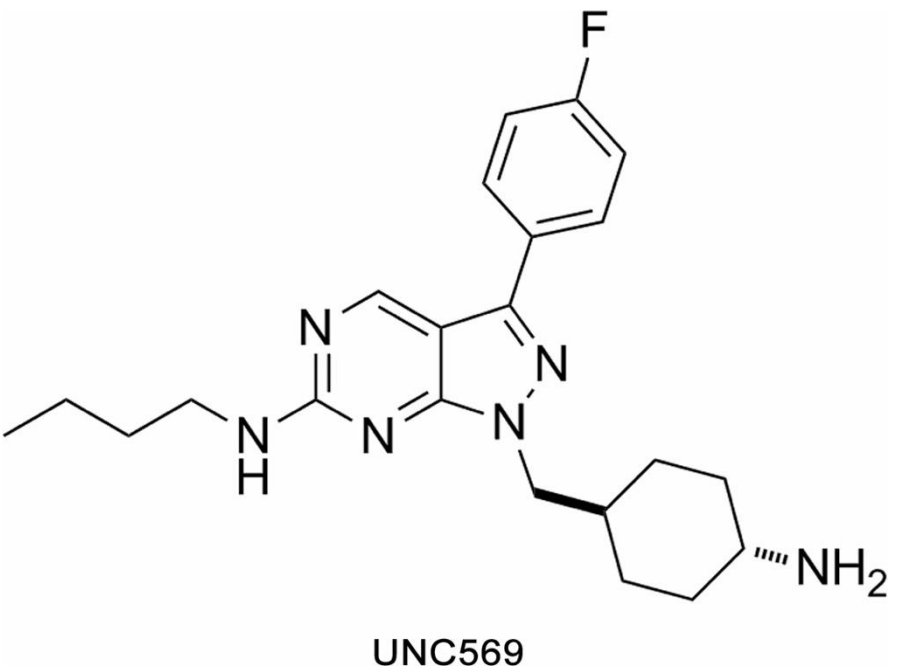

Figure 1.7 Molecular composition of UNC569[97]

1.5 Aims of this research

Previous evidence from our research unit has shown that MerTK plays a significant role in the development of hepatic fibrosis. This finding suggests that MerTK might potentially be targeted therapeutically to address fibrosis. The fibrogenic phenotype was diminished in human and mouse HSCs through the suppression of MerTK, both pharmacologically and genetically [102]. Nevertheless, the precise functional significance of MerTK knockout mice is unknown. Additionally, whether the anti-fibrotic effect of MerTK inhibition is specific to liver fibrosis or extends to other organs is unknown, so clarifying this is pivotal. Finally, the role of macrophage MERK in mediating macrophage–HSC interaction in liver fibrosis has yet to be clarified.

Aims of this research:

Aim1: Explore the role of MERTK in the liver fibrosis **(Chapter 3)**

Aim2: Explore the role of MERTK in the kidney fibrosis **(Chapter 4)**

Aim3: Explore the role of MERTK in the pulmonary fibrosis **(Chapter 4)**

Aim4: Explore the mechanisms of the effect of MERTK activation in signaling pathway in the tissue fibrosis **(Chapter 5-6)**

Chapter 2: Materials and Methods

2.1 Materials

The materials used in this investigation were obtained from the sources listed in **Table 2.1**.

Table 2.1: The origins of the items used in this investigation

REAGENT or RESOURCE	Source / Identifier
Chemicals, Peptides, and Recombinant Proteins	
qScript cDNA SuperMix	Genescript
SYBR Green PCR Master Mix	Invitrogen
RIPA buffer	Sigma Aldrich
Trypsin	Sigma Aldrich
Protease inhibitors	Sigma Aldrich
Dimethyl sulfoxide (DMSO)	Sigma Aldrich
β-mercaptoethanol	Sigma Aldrich
EDTA (Ethylenediaminetetraacetic acid)	Sigma Aldrich
IL-β protein	Thermo fisher (A42508)
Recombinant TGF- beta 1 Protein	R&D systems
IL-4 protein	Sigma Aldrich
UNC569 (MERTK inhibitor)	Axon Medchem
Penicillin	Gibco BRL through Life Technologies
Streptomycin	Gibco BRL through Life Technologies
Lipofectamine RNAi-MAX	Gibco BRL through Life Technologies
Transfection Reagent	Gibco BRL through Life Technologies
Opti-MEM medium	Gibco BRL through Life Technologies
Dulbecco's Modified Eagle Medium (DMEM)	Lonza
RPMI 1640 Medium	Lonza
Phosphate buffered saline (PBS)	Lonza
Recombinant Human M-CSF	Lonza
Recombinant Mouse M-CSF	Lonza
TheraPEAKTM X-VIVOTM-15 Serum-free	Lonza

Critical Commercial Assays	
Detergent Compatible (DC) Protein Assay Kit I	Bio-Rad (5000111)
FavorPrep Tissue Total RNA Purification Mini Kit	Favorgen Biotech Corp (FATRK001-2)
EasySep Human CD14 Positive Selection Kit II	STEMCELL Technologies (17858)
ATAC-Seq Kit	Active Motif (53150)
CUT&Tag-IT™ Assay Kit	Active Motif (53160)
Histone H3K27me3 antibody (pAb)	Active Motif (39055)
Histone H3K4me3 antibody (pAb)	Active Motif (39060)
Histone H3K27ac antibody (pAb)	Active Motif (39034)
Anti-CTCF Antibody (pAb)	EMD Millipore (07-729)
Phospho-Rpb1 CTD (Ser2/Ser5) (D1G3K) (pAb)	Cell Signaling (13546s)
Histone H3K4me1 antibody (pAb)	Abcam (8895)
ALT assay ELISA kit	Abcam (105134)
Hydroxyproline Assay Kit	Sigma Aldrich

2.2 Methods:

2.2.1 Animals

Similarly described previously**[102]**, all animal work in this research are under the guidance of Ethic protocol provided by Australia Government, (Project No. 4302.05.19). The mouse were housed in temperature-controlled tanks inside an animal service facility, where they were subjected to 12-hour alternating light and dark cycles. They were provided with normal mouse food and water for sustenance. The experiment was conducted using male C57Bl/6 background mice that were eight weeks old.

In order to investigate the impact of MerTK abscence on the evolution of fibrosis in numerous organs, three mice models were utilized, specifically:

2.2.1.1 Bile duct ligation (BDL) model

BDL was undertaking as described previously**[102],** briefly, the mice were subjected to gas anesthesia using a 4% concentration of isoflurane (2-chloro-2-(difluoromethoxy)1,1,1-trifluoroethane) in combination with 100% oxygen at 4 liters per minute flow rate. Subsequently, an electric shaver was used to eliminate the fur from the abdominal region of the mice. Following the initiation of anesthesia, the concentration of isoflurane was decreased to a range of 1.5-3.0% in a 100% oxygen environment, while the flow rate was subsequently modified to 1 L/min. Following the application of 70% alcohol disinfectant to the abdominal skin, a 2cm incision was performed along the midline of the abdomen using surgical scissors, therefore exposing the peritoneal cavity.

To facilitate the surgical procedure, a Colibri retractor was used to effectively elongate the peritoneal cavity and achieve complete exposure of the surgical incision. Subsequently, a moistened cotton swab immersed in a solution containing 0.9% sodium chloride (NaCl) was

used to elevate the liver edge, displace the intestine towards the caudal region, and manipulate the duodenum in a downward direction, so facilitating the visualization of common bile duct.

The bile duct was securely fastened using two surgical knots to prevent any potential slippage during the subsequent two-week period. The sternum is then repositioned to its anatomically correct location. The retractor should be carefully extracted from the cavity, followed by a gentle palpation of the abdomen to reposition all organs to their initial anatomical arrangement. Subsequently, the peritoneum, as well as the skin and fascia, were meticulously closed in a sequential manner using an independent 6-0 Mersilk suture.

2.2.1.2 Unilateral ureteral occlusion (UUO) model

The mice were anesthetized with their left side facing up and placed in a lateral decubeus position. They were cut in the middle of the left abdomen to separate abdominal fat and muscle, expose the kidney, and follow the hilum down to find the ureter (like a thin white line). The left ureter was then dissociated using a tweezer and the middle area of the ureter was permanently ligated twice to prevent postoperative slip. After the ligation was completed, the kidney was gently reset and sutured layer by layer. First, the muscle was sutured and then the skin was sutured. Under the premise of solid suture, the thread was shortened as far as possible to prevent the wound cracking caused by the surgical thread falling off after the operation.

For sham operation group, the ureter was exposed but without ligation, and the abdomen was closed directly after the kidney was reset.

2.2.1.3 Bleomycin (BLM)-induced pulmonary fibrosis model

The bleomycin solution was dissolved in saline and thereafter supplied by endotracheal injection at a dosage of 1.5 units per kilogram. The mice were first subjected to anesthesia, followed by immobilization in a headfirst position, and their oral cavities were then opened using tweezers to reveal their tracheas. Introduce a syringe, with its tip removed, into the trachea and provide the administration of bleomycin into the pulmonary system. Subsequently, the mice were maintained in a static posture for a duration of two minutes, so ensuring the uniform distribution of the medication inside the pulmonary system. The control group was injected with saline.

2.2.1.4 Mouse harvesting

Mouse harvesting was previously described**[102]**. Following the completion of the experiment, the mice were subjected to euthanasia. The subjects were assessed for their weight and then exterminated with the administration of ketamine (100 mg/kg) and xylazine (20 mg/kg) through injection. The assessment of sufficient anesthesia in mice was conducted by evaluating the absence of the pain response. The heart was punctured and a sample of entire blood was obtained. Perform a longitudinal incision in the median plane of the abdominal region, afterwards isolating the liver for the purpose of determining its weight. The liver tissue was partitioned into several sections, wherein a portion was promptly frozen in liquid nitrogen, while another portion was treated with 4% paraformaldehyde for further histological investigations. The frozen tissue was maintained at a temperature of -80℃ for further use.

2.2.2 Cell culture and treatments

2.2.2.1 Generation of mouse bone marrow-derived macrophages

Femoral bones were procured from mice aged 8 weeks, namely C57BL/6 and Mertk$^{-/-}$ strains. Following killing, the mice were subjected to a 70% ethanol spray and then underwent dissection using scissors to incise the femur, transect the tibia below the knee, and separate the pelvic bone in proximity to the hip joint. The muscle that is attached is excised, and the femur is afterwards transferred to a culture plate containing sterile phosphate-buffered saline (PBS) and put on ice. The bones were immersed in a 70% ethanol solution for a duration of one minute under a tissue culture mask, followed by a thorough cleansing using sterile RPMI 1640 media. The removal of both epiphyses was conducted with sterilized scissors and tweezers. The bone is carefully inserted into a centrifuge tube and promptly subjected to centrifugation in order to get the bone marrow. The cells were suspended in Dulbecco's Modified Eagle Medium (DMEM) (10% FBS and 50 ng/ml macrophage colony-stimulating factor (MCSF) containing), and afterwards introduced into culture trays. The culture was subjected to incubation at a temperature of 37 °C, with a 5% concentration of carbon dioxide, for a duration of 7 days. On the fourth day, the culture media was replaced in order to eliminate any suspended cells.

2.2.2.2 Culture of cell lines

The protocol was previously described in **[102]**. The Immortarized Human HSCs, LX-2 cells, and immortalized mouse hepatic stellate cells, JS1, used in this research were grown in 10% FBS DMEM media.

2.2.2.3 Tissue culture treatment

The protocol was previously described in **[102]**. Following a period of 16 hours starvation in no serum medium for starvation, the cells were subjected to treatment with a MerTK inhibitor (UNC569) at a concentration of 4 μmol/L, or vehicle control for a duration of 90 minutes. Alternatively, the cells were treated with siRNA for a period of 48 hours, and the transfection procedure used was detailed in section 2.2.3 of the protocol. Following that, TGF-β1 (10 ng/ml) was introduced for a duration of 24-48 hours. In a separate experimental trial, LX2 cells were subjected to treatment with IFN-γ at a concentration of 20 ng/ml, IL-4 at a concentration of 20 ng/ml, or IL-1β at a concentration of 10 ng/ml for a duration of 24 hours.

2.2.3 MERTK knockdown in-vitro

The protocol was previously described in **[102]**. The detailed information of small interfering RNA (siRNA) used in this research are described in **Table 2.2**. The transfection procedure included the use of Lipofectamine RNAiMAX to introduce siRNA into the cells. A concentration of 75 nM was used for both specific siRNA and non-targeted control. The transfection was carried out for a duration of 48 hours, following the instructions provided by the manufacturer.

Table 2.2: List of siRNA used in this investigation

Targeted gene	Company
s8402 human SMAD3 Silencer Select	Thermo fisher (4427037)
s8405 human SMAD4 Silencer Select	Thermo fisher (4427038)
s14079 human TGFBR2 Silencer Select	Thermo fisher (4427038)
ON-TARGET plus Non-targeting siRNA- SMART pool	Dharmacon Cat. No. D-001810-10- 05
ON-TARGET plus Mertk siRNA- SMART pool	Dharmacon Cat. No. L-040357-00- 0005
ON-TARGET plus MERTK siRNA- SMART pool	Dharmacon Cat. No. L-003155-00- 0005

2.2.4 Histology staining

The protocol was previously described in **[102]**. The paraffin sections, with a thickness of 5 μm, underwent a dewaxing process by being immersed in xylene three times for a duration of 3 minutes each immersion. Subsequently, the sections were soaked in 100% alcohol for 3 minutes, followed by a 5-minute immersion in 70% alcohol to replace the xylene inside the sections. Subsequently, immerse the slices in water for a duration of 2 minutes, then proceed with the further coloring procedures as outlined below:

2.2.4.1 Haematoxylin and Eosin Staining

The protocol was previously described in **[102]**. The staining procedure included the application of Harris hematoxylin for a duration of 10 minutes, followed by a subsequent washing step lasting 1 minute. The specimen was thereafter immersed in 0.5% acid alcohol for a duration of 2 to 6 cycles, followed by immersion in Scott's bluing solution for a period of 1 minute, and finally incubated in water for a duration of 2 minutes.

2.2.4.2 Picrosirius Red Staining

The protocol was previously described in **[102]**. This method is used to quantify the accumulation of collagen in different organs and evaluate the degree of subsequent fibrosis. The slide was thereafter incubated in 0.1% solution of Sirius red for a duration of 60 minutes, followed by a 2-minute wash with water.

2.2.4.3 Gomori tricolor Staining

The protocol was previously described in **[102]**. Distilled paraffin sections by water first, then stained nuclei with Celestin Blue for 5 minutes, followed by rinsed in distilled water again. Then stain the sections in haematoxylin for 5 minutes, then washed by running tap water for another 5 minutes. Finally, stained with Gomori's stain buffer for 15 minutes, then rinsed again with distilled water.

2.2.5 Collagen quantification

The protocol was previously described in **[102]**. The quantification of tissue fibrosis was performed by software ImageJ to measure positive area stained by Picrosirius red. The quantitative analysis of hydroxyproline content was conducted using the Sigma-Aldrich kit. The manufacturer's instructions were adhered to, whereby 10mg of tissue was first homogenized in 100uL of water. Subsequently, the homogenized tissue was placed into a pressure-tight polypropylene vial equipped with a cap coated with PTFE. Subsequently, a volume of 100 microliters of hydrochloric acid with a concentration of 12 molar was introduced, followed by incubation at a temperature of 120 degrees Celsius for a duration of 3 hours to ensure thorough hydrolysis. Subsequently, the samples were subjected to remixing and centrifugation with a force of 10,000 times the acceleration due to gravity for a duration of 3 minutes. Transfer a volume of 20 uL of the supernatant to a 96-well plate and afterwards

position it inside a drying apparatus set at 60℃. Subsequently, the reaction mixture was introduced in accordance with the provided instructions and subjected to incubation (60℃, 90 minutes). Subsequently, the measurement of absorbance at a wavelength of 560nm was conducted.

2.2.6 Serum Parameter

The protocol was previously described in **[102]**. The measurement of alanine aminotransferase (ALT) was conducted using the ALT ELISA kit (Abcam) in accordance with the manufacturer instructions.

2.2.7 Immunohistochemistry

The protocol was previously described in **[102]**. The immunohistochemical staining procedure was conducted using the BOND Polymer Refine Detection in order to assure the reliability and consistency of the staining outcomes. The principal reactance implicated is shown in **Table 2.3**.

Table 2. 3: List of primary antibodies information for immunohistochemistry staining

Antibodies	Supplier name/ Catalog number / Clone name / Dilution
anti-p-MERTK	Abcam (ab192649), monoclonal, 1/10000
anti-MERTK	GeneTex [3D07] (GTX53110), monoclonal, 1/7000
anti-αSMA	Sigma (C6198), monoclonal, 1/10000
anti-F4/80	Abcam (ab111101), monoclonal, 1/10000

2.2.8 Gene Expression Studies

2.2.8.1 *Total RNA extraction from tissue and cells*

The protocol was previously described in **[102, 103]**. The extraction of total RNA from frozen mouse tissue or cell samples was performed using the FavorPrep Tissue Total RNA Extraction Mini Kit, following the guidelines provided by the manufacturer. Initially, a solution used here was FARB buffer containing 1% ß-mercaptoethanol. Approximately 20 milligrams of frozen tissue were introduced into a solution consisting of 350 microliters of FARB/ß-mercaptoethanol combination. The resulting mixture was well homogenized and afterwards incubated at room temperature for a duration of 5 minutes. The filter column was carefully inserted into a collecting tube, after which the sample mixture was put into the column. The centrifugation process was then carried out at a force of 16,000 times the acceleration due to gravity (g) for a duration of 2 minutes. The supernatant from the collecting tube was transferred to a fresh centrifugal tube. Subsequently, 350µl of 70% ethanol was added and well mixed. The FARB mini-column was inserted into the collecting tube, and afterwards, the solution containing ethanol was delivered to the FARB mini-column. The collected sample was subjected to centrifugation at a speed of 14,000 revolutions per minute (rpm) for a duration of 1 minute. Following this, the liquid present in the collection tube was discarded. Subsequently, 500 ul of Wash Buffer 1 were added to the FARB mini-column, which was then centrifuged again at 14,000 rpm for 1 minute. The liquid was discarded and 750 µL of Wash Buffer 2 was introduced into the FARB mini-column. The column was then centrifuged at a speed of 14,000 revolutions per minute for a duration of 1 minute. This process was done twice. The material was subjected to centrifugation for an additional duration of three minutes in order to facilitate the drying process. The FARB micro-column was put into a 1.5ml Eppendorf tube. The RNA present in the column was dissolved using 50 µl of RNase-free water. Subsequently, it was incubated for a duration of 1 minute and then subjected to centrifugation at a speed of 14,000

revolutions per minute for a duration of 1 minute. The purity and concentration of the RNA were assessed using a spectrophotometer (NanoDrop) at wavelengths of 260 nm and 280 nm.

2.2.8.2 *cDNA Synthesis*

The protocol was previously described in **[102]**. The synthesis of complementary DNA (cDNA) was performed using 100ng of total RNA and the qScript® cDNA SuperMix (Quanta Biosciences, Gaithersburg, MD). In this experiment, 10µl of RNA samples containing a total of 100 ng of RNA were combined with 2.5µl of qScript Reaction Mix in a 500µl Eppendorf tube. The reaction tube was carefully positioned inside the heat cycler, and the experimental protocol was thereafter configured as shown below: The samples were subjected to a temperature of 25℃ for a duration of 5 minutes, followed by a temperature of 42℃ for a duration of 30 minutes. Subsequently, the samples were exposed to a temperature of 85℃ for 5 minutes. Finally, the samples were stored at a temperature of 4℃. Subsequently, the cDNA was used in the real-time polymerase chain reaction (PCR) analysis.

2.2.8.3 *Real-time Quantitative PCR*

The protocol was previously described in **[102]**. The StepOneTM software applied bioscience equipment was used to conduct real-time PCR. The mRNA levels in mouse samples were standardized by normalizing them to the expression of acidic ribosomal phosphoprotein (36B4), and the mRNA levels in human samples were standardized by normalizing them to glyceraldehyde 3-phosphate dehydrogenase (GAPDH). **Table 2.4** presents the primers used in the experimental procedure.

Table 2.4: List of the sequence of primers involved in this investigation

Gene	Forward	Reverse
m36B4 (mouse)	AATCTCCAGAGGCACCATTG	CCGATCTGCAGACACACACT
TGF-β (mouse)	GTGGGGACTTCTTGGCACT	GAGTGTCCACGACGGTGAG
COL1A1 (mouse)	AGGAGAACCAGGTGACGAAG	CCCCAGCTTCTCCTTTCTCT
COL1A2 (mouse)	GGAACAAATGGGCTCACTGG	CAAGTCCTCTGGCACCTGTA
COL3A1 (mouse)	CCCAACCCAGAGATCCCATT	GGTCACCATTTCTCCCAGGA
αSMA (mouse)	CTCTCTTCCAGCCATCTTTCAT	TATAGGTGGTTTCGTGGATGC
Mertk (mouse)	GTGGCAGTGAAGACCATGAAGTTG	GAACTCCGG GATAGGGAGTCAT
MERTK(Human)	CCTTCAGCATAACCAGTGTGC	TGACAGGTGAGGTTGAAGGC
GAPDH (Human)	CATGGCACCGTCAAGGCTGA	TGGTGGTGCAGGA
α-SMA (Human)	CTGTTCCAGCCATCCTTCAT	CCGTGATCTCCTTCTGCATT
COL1A1(Human)	ACGCTGAACGATACCAAATG	TGCTATACCTTTACTCTTTATGGTGTA
TGF-β1 (Human)	TGTTCGCGCTCTCGGCAGTG	GCCTCGATGCGCTTCCGCTT

2.2.9 Western blot analysis

The protocol was previously described in [102]. The protein obtained from cellular or tissue samples using RIPA buffer was subjected to separation using SDS-PAGE and then deposited onto polyvinylidene difluoride (PVDF) membranes following the guidelines provided by the manufacturer (Bio-Rad, Hercules, CA). Following the transfer process, the membrane was subjected to a blocking step at ambient temperature for a duration of 1 hour. This blocking step included the use of TBST buffer containing 5% skim milk. Subsequently, the membrane underwent two washes with TBST solution. It was then subjected to incubation with a primary antibody diluted in 5% skim milk/TBST solution, and put on a shaker at a temperature of 4°C for an extended period of time. Following the incubation period, the membranes underwent three consecutive washes with TBST solution for a duration of 10 minutes each wash. Subsequently, a secondary antibody, which had been appropriately diluted in a solution of 5% skim milk and TBST, was applied to the membranes. This step was carried out at room temperature and the membranes were incubated for a duration of 1 hour, while being shielded from light. Following the incubation period, the membranes underwent three further washes with TBST. The ChemiDoc Touch Imaging System was used to scan the membranes. **Table 2.5** presents the principal antibodies used in the experimental procedure.

Table 2.5: A compilation of primary antibodies and conditions used in the study

Primary antibodies used in Western blot	
Antibodies	Supplier name/ Catalog number / Clone name / Dilution
anti-GAPDH	Abcam (ab181602), monoclonal, 1/10000
anti-Vinculin	Abcam (ab129002), monoclonal, 1/20000
anti-TGFβ1	Abcam (ab92486), polyclonal, 1/1000
anti-MERTK (human)	Abcam (ab52968), monoclonal, 1/1000
anti-MERTK (mouse)	GeneTex [3D07] (GTX53110), monoclonal, 1/1000
anti-αSMA	Invitrogen (MA5-11547), Monoclonal, 1/1000
anti-Akt	Cell signaling (9272), polyclonal, 1/1000
anti-p-Akt (Ser473)	Cell signaling (4051), monoclonal, 1/1000
anti-Erk1/2	Cell signaling (4695S), monoclonal, 1/1000
anti-p-Erk1/2	Cell signaling (4370S), monoclonal, 1/1000
anti-p-SMAD3 (Ser423+S425)	Abcam (ab52903), monoclonal, 1/1000
anti-SMAD3	Abcam (ab75512), monoclonal, 1/1000
anti-SMAD4	Cell signaling (38454s), monoclonal, 1/1000

2.2.10 RNA-seq

2.2.10.1 Generation of RNA-seq library

As previously described [103-106]. The isolation of total RNA from mouse tissue was performed using a commercially available RNA micro kit manufactured by Qiagen. The confirmation of RNA purity and integrity was conducted using the Agilent Bioanalyzer. The construction of sequencing libraries was conducted using the TrueSeq RNA sample preparation kit v2 (Illumina) with a total RNA input ranging from 100-500ng. In a general sense, the process involves the purification and fragmentation of mRNA, which is then used for the synthesis of cDNA. This is then followed by 3'-end adenylation. The specimens were linked to a distinct adapter and subjected to polymerase chain reaction (PCR) amplification. The libraries underwent validation, standardization, and sequencing procedures using the 2100 BioAnalyzer, a product manufactured by Agilent. A total of three bioreplicated RNA-seq libraries were subjected to sequencing on an Illumina HiSeq 2000 platform. Barcode multiplexing was used, and a read length of 100 base pairs was utilized for each experimental condition. Additionally, four bioreplicates were conducted for each condition.

2.2.10.2 High-throughput sequencing and analysis

As previously described [103-106]. The assessment of library sequencing quality was conducted using FastQC, a software tool developed by Babraham Bioinformatics (www.bioinformatics.babraham.ac.uk/). The process of trimming Illumina adaptor sequences and low-quality reads, wherein read pairs are eliminated if they include less than 20 base pairs, was carried out using Trim Galore, a software tool developed by Babraham Bioinformatics. The STAR aligner[107] was used to map sequencing reads to the mouse genome (GRCm38/mm10) with the assistance of ENSEMBL gene annotations as a reference. The

STAR option --quantMode GeneCounts was used to create read counts data that corresponds to ENSEMBL gene annotations. The studies were conducted using the R Statistical Environment, specifically using the tidyverse package. In this study, the counts data underwent background correction and normalization for library size using the edgeR software. Differential gene expression (DGE) analysis used QLFtest, with a significance threshold of BH MTC adjusted $p < 0.05$ or uncorrected $p < 0.01$. The gene lists underwent functional annotation using GO pathways, utilizing the clusterProfiler program[108], with a significance threshold of adjusted p value <0.05.

2.2.11 ATAC-seq

2.2.11.1 Generation of ATAC-seq library

As previously described in [104-106]. The mouse tissue samples were first homogenized to acquire intact nuclei. Subsequently, these nuclei were subjected to treatment with a highly active Tn5 transposable mutant. This mutant has the ability to concurrently label the target DNA with a sequencing adaptor, so accomplishing the fragmentation of the DNA, often referred to as "tagmentation." The process of labeling and library preparation was conducted using the ATAC-Seq Kit in accordance with the instructions given inside the kit. The nuclei were first enumerated and subjected to centrifugation at a temperature of 4°C and a speed of 500g for a duration of 5 minutes, resulting in the generation of aliquots comprising 50,000 to 100,000 nuclei. The samples were revived by adding 100 µl of ATAC Lysis Buffer, which was kept at a low temperature. To each sample, Tagmentation Master Mix was added 50 µl. The samples were then placed in a thermomixer and incubated at 800 rpm and 37℃ for a duration of 30 minutes. The library was then created by the process of polymerase chain reaction (PCR)

amplification of the labeled DNA, using a unique combination of Illumina's i7/i5 primers that are based on a Nextera adaptor. Ultimately, the library underwent purification by the use of SPRI bead washing. A total of two biological replicates were conducted for each condition.

2.2.12 Cut&Tag-seq

2.2.12.1 Generation of Cut&Tag-seq library

As previously described in [104, 105]. The mouse tissue samples were first subjected to homogenization. Then, aliquots containing around 100,000 cells were produced and treated with wash buffer containing protease inhibitor cocktail. The cells were coalesced with concanavalin A beads and subjected to an overnight incubation with a primary antibody at a temperature of 4℃. Following incubation with the antibody, the chromatin underwent direct cleavage, followed by tagmentation utilizing protein A-Tn5 (pA-Tn5) transposition, and subsequent preparation of NGS libraries. The labelling and library preparation process was conducted using the CUT&Tag-ITTM assay kit (catalog No. 53160, Active Motif), following the instructions provided with the kit. A total of two biological replicates were conducted for each experimental condition.

2.2.12.2 ATAC and Cut&Tag-seq analysis

As previously described in [104, 105]. The NovaSeq PE150 technology, operated by Novogene, was used to do paired-end 100bp sequencing. This process resulted in the generation of 30-40 million paired reads for each sample. Both ATAC-seq and Cut & Tag methodologies use a Nextera transposase sequence. The process of read alignment was conducted with Bowtie2 version 2.2.5[109], employing the GRCm38/mm10 reference sequence. The identification of peaks was carried out using the MACS2 software[110]. Peak

difference analysis was conducted using a Homer software called getDifferentialPeaks, which may be accessed at http://homer.ucsd.edu/homer/. Subsequently, the annotation and enrichment of the identified peaks were done using the Homer program annotatePeaks.pl. The researchers used the Integrated Genomics Viewer (IGV)[111] to effectively visualize the ATAC sequencing (ATAC-seq) data.

2.2.13 Data Analysis and Statistics

As previously described in [102-105]. GraphPad Prism software version 9.0 was used for data analysis. The results were presented as the mean ± standard error of the mean (SEM). The one-way analysis of variance (ANOVA) was used for conducting multi-group study, while the student's t-test was utilized for analyzing two groups. P-values were used to infer the presence of a statistically significant difference. The significance levels were denoted as follows: **** $p \leq 0.0001$, *** $p \leq 0.001$, ** $p \leq 0.01$, * $p \leq 0.05$.

Chapter 3: MerTK suppression mitigate liver fibrosis

3.1 Introduction

The presence of hepatic fibrosis is a major determinant of mortality and adverse liver-related outcomes in virtually all CLDs [112]. Nevertheless, there is currently a lack of approved therapies for fibrosis, which renders liver transplantation the only viable option for those with end-stage liver disease [6, 113]. Identifying novel therapeutic targets that could be translated to clinics and be effectively used for the treatment of fibrosis thus remains an unmet clinical need [114].

Fibrosis is a multifaceted, reversible and orchestrated reaction to persistent damage, including communication between several cell types, such as myofibroblasts and macrophages [115, 116].

At the cellular level, there is unequivocal evidence that HSCs are the major producers of collagen and ECM and are considered the master regulators of the pathogenesis of liver fibrosis [11]. In normal healthy liver, HSCs exhibit a state of quiescence, in which they maintain a dormant state, while concurrently accumulating vitamin A within the liver [117]. The activation of HSCs occurs in response to various growth factors or inflammatory factors when the liver is damaged by viral hepatitis, MAFLD, alcohol addiction and other causative factors. This activation prompts the production of collagen by HSCs, thus contributing to the advancement of fibrosis [118].

The MerTK gene has been identified through GWAS and candidate gene studies as a crucial factor in fibrosis development in various liver diseases, such as MAFLD and viral hepatitis [75, 76, 119]. Despite compelling genetic data, however, the potential therapeutic utility of targeting MerTK in fibrotic disorders of the liver and other organs remains largely unexplored.

In this chapter, an initial investigation was conducted on the reaction of MerTK to TGF-β stimulation, as well as the impact of MerTK deficiency on the intercellular communication

between macrophages and HSCs. This investigation aimed to simulate the cellular-level process of liver fibrosis. It aimed to evaluate the impact of MerTK inhibition on the advancement of hepatic fibrosis after BDL in a mouse model. This investigation included the use of both wild-type (WT) and MerTK$^{-/-}$ animals.

3.2 Method

Tissue culture

Human HSCs (LX-2 cell line), murine HSCs (JS1 cell line), human MDMs, or mouse BMDMs were subjected to treatment with TGF-β1 at a concentration of 10 ng/ml for a duration of 24 hours. This treatment was conducted in the presence or absence of a MerTK pharmacological inhibitor, UNC569, at a concentration of 4 μM, or by the use of human specific MERTK siRNA at a concentration of 75 nM. The treatment duration for human MDMs was also 24 hours.

In order to confirm whether MERTK expression can be reversed by TGF-β related pathway inhibition, LX2 cells were subjected to several treatments. One treatment included the use of a TGF-β inhibitor called LY21097612 (10μM/ml), which was administered 2 hours before stimulated by TGFβ1. Another treatment involved the use of siRNA targeting TGFβR2, SMAD3, SMAD4, or a combination of the three, continuing 24 hours. Following these treatments, the cells were exposed to TGF-β1 for an additional 24 hours.

In order to confirm whether the expression of MERTK is specifically altered by TGF-β signaling, in the particular MerTK modification experiment, LX-2 cells were subjected to treatment with IFN-γ at a concentration of 20 ng/ml, IL-1β at a concentration of 10 ng/ml, or IL-4 at a concentration of 20 ng/ml. **Figure 3.1** presents a brief summary of the design layout related to the in vitro investigation.

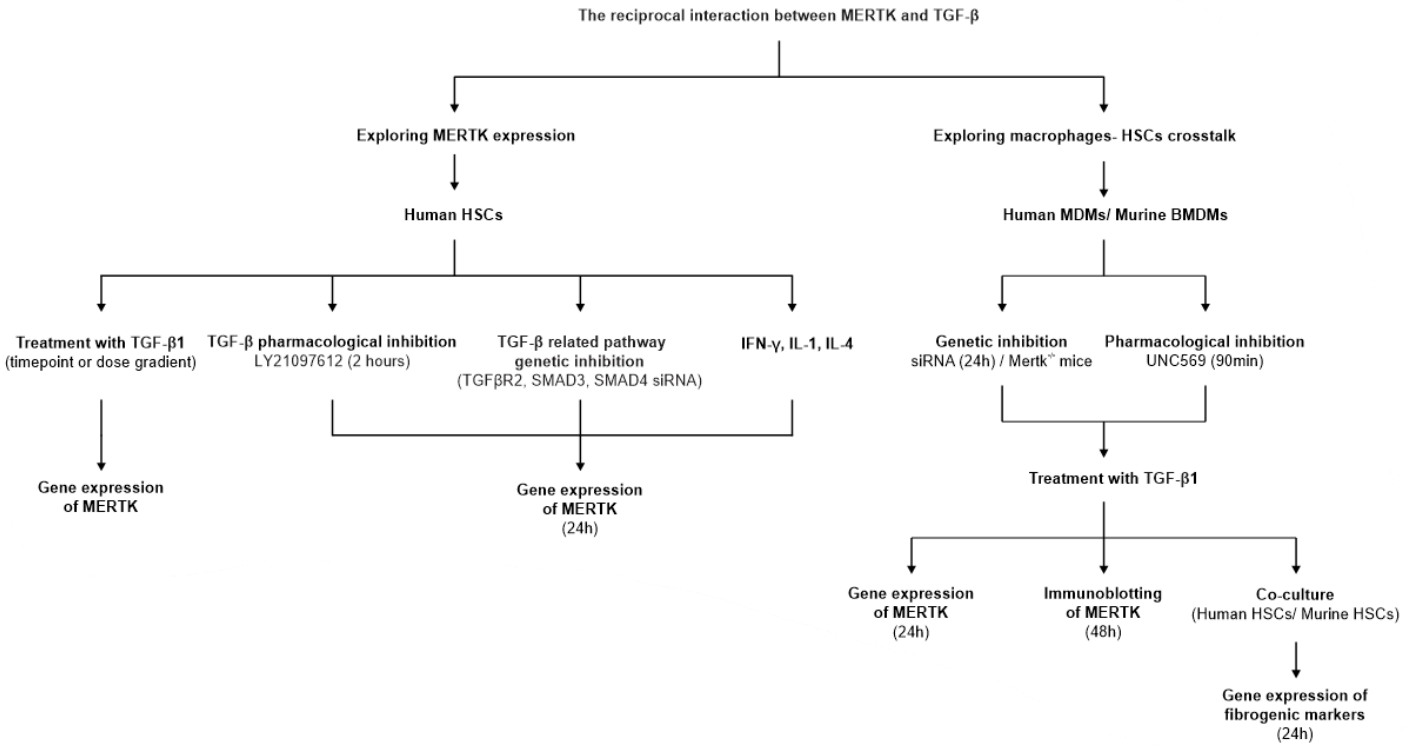

Figure 3.1 In vitro experimental design scheme involved in this chapter

Mouse studies

In order to investigate the potential of MerTK inhibition as a therapeutic strategy for fibrosis, mice with intact MerTK (wild-type) or mice lacking MerTK (Mertk$^{-/-}$) were subjected to either BDL or sham surgery for a duration of 14 days. Then, after an euthanasia, a collection of serum which was then frozen at a temperature of -80 degree was undertaken. Additionally, the livers were subjected to fixation in a 4% paraformaldehyde solution, or alternatively, they were frozen using liquid nitrogen. The schematic representation of the animal model is shown in **Figure 3.2**.

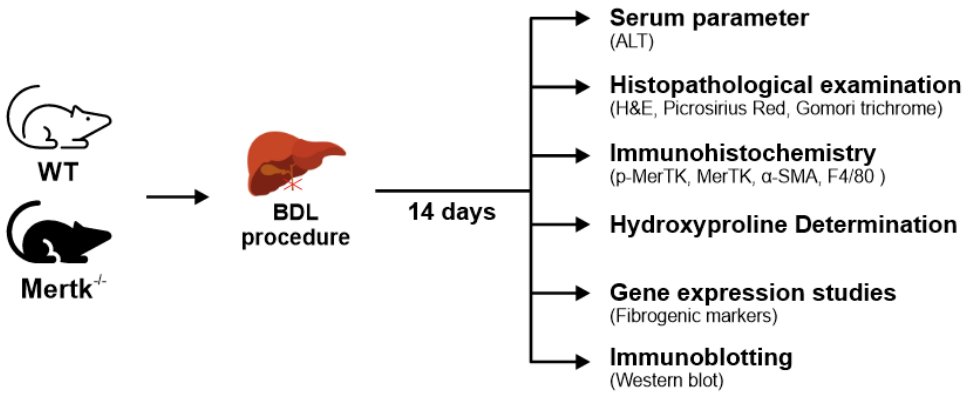

Figure 3.2 Animal experimental design scheme involved in this chapter

As described previously[102], a set of standardized readout to mesaure fibrosis was undertaken to assess the impact of MerTK inhibition on fibrosis phenotypes, encompassing:

A) ***Histopathological examination****:* The paraffin sections underwent staining using H&E for the purpose of examining morphology and inflammation. Additionally, Picrosirius Red staining was performed to assess collagen deposition, while Gomori Trichome staining was used specifically for the staining of type 1 collagen. The quantification of Picrosirius Red staining was performed using the ImageJ.

B) ***Immunohistochemistry staining:*** p-MerTK, MerTK, α-SMA and F4/80

C) ***Hydroxyproline determination:*** The quantification of collagen content was conducted by measuring the hydroxyproline content in the specific kit provided by Sigma.

D) ***Gene expression studies****:* The extraction of total RNA was conducted, followed by the synthesis of cDNA, and afterwards, RT-PCR was used to assess alterations in the expression levels of fibrogenic markers, namely Acta2, Col1a1, Col1a2, and Col3a1.

E) ***Western blot:*** Tissue lysates were prepared and then tested by Western blot to examine alterations of the protein expression, including α-SMA, p-Akt, Akt, p-Erk1/2, and Erk1/2.

Ethics: Similarly described previously**[102]**, all animal work in this research are under the guidance of Ethic protocol provided by Australia Government, (Project No. 4302.05.19).

Statistical analysis: As previously described in [102-105]. GraphPad Prism software version 9.0 was used for data analysis. The results were presented as the mean ± standard error of the mean (SEM). The one-way analysis of variance (ANOVA) was used for conducting multi-group study, while the student's t-test was utilized for analyzing two groups. P-values were used to infer the presence of a statistically significant difference. The significance levels were denoted as follows: **** $p \leq 0.0001$, *** $p \leq 0.001$, ** $p \leq 0.01$, * $p \leq 0.05$.

3.3 Results

3.3.1 The reciprocal interaction between MerTK and TGF-β

Given that TGF-β is a prevalent route associated with fibrosis, I endeavored to elucidate the potential favorable interaction between TGF-β and MerTK. Consequently, the LX-2 cells were subjected to treatment with TGF-β1 at various time intervals and dosages, respectively. Subsequently, the expression levels of MerTK transcripts were assessed. The findings of this study demonstrated a significant increase in the expression of MerTK, which was shown to be both time- and dose-dependent, after stimulation with TGF-β1(**Figure 3.3**).

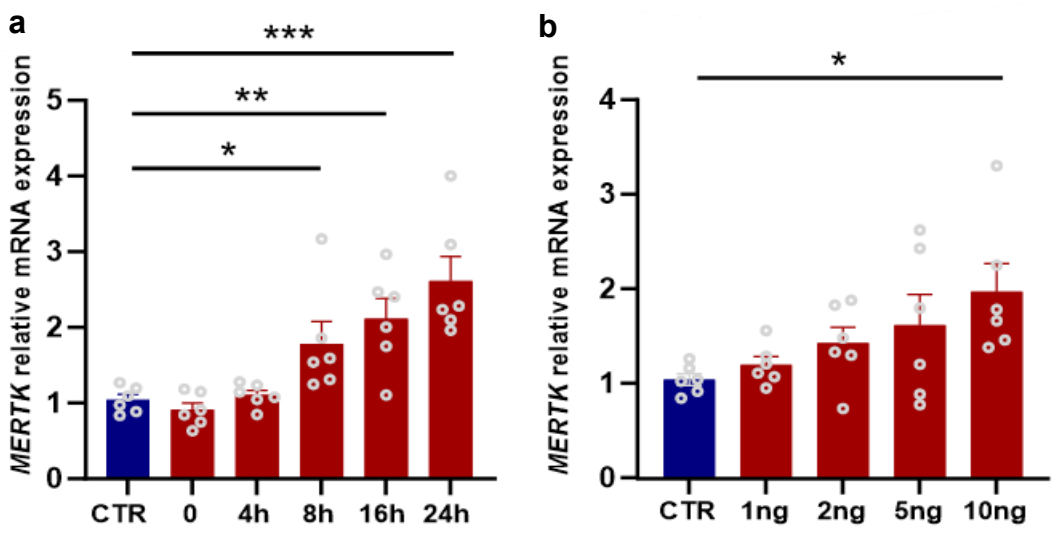

Figure 3.3 The timepoint and dose-dependent MERTK expression through TGF-β treatment a) Human HSC LX2 cells were treated by TGF-β1 (10ng/ml) as a time gradient (0, 4, 8, 16, 24h) and MERTK mRNA expression was assessed by PCR and normalized to untreated LX2 cells and GAPDH **b)** LX2 cells were treated by TGF-β1 for 24h as a concentration gradient (0, 1,2, 5, 10ng/ml) and MERTK relative mRNA expression was assessed by PCR and normalized to untreated LX2 cells and GAPDH. The protocol of statistical analysis is described in **Method**.

The observed augmentation of MERTK, induced by TGF-β1, was entirely counteracted by LY2109761, a specific inhibitor of TGF-β receptor type I/II (**Figure 3.4**).

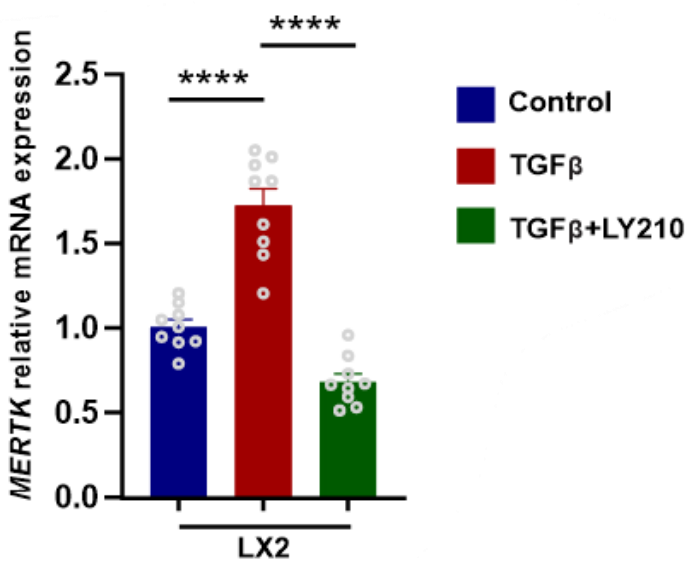

Figure 3.4 MERTK expression is reversed by TGF-β inhibitor The LX2 cells was given treatment with TGF-β1 alone or in combination with the TGF-β inhibitor LY2109761. This treatment was administered 12 hours prior to the addition of TGF-β1 for a duration of 24 hours. Following the treatment, the cells were analyzed for the relative mRNA expression of MERTK using PCR and the results were normalized to the expression of GAPDH. The protocol of statistical analysis is described in **Method**.

To get a deeper understanding of the role of MerTK in the TGF-β framework, an experimental approach was used. LX2 cells were subjected to treatment with several siRNA molecules targeting the TGF-β/SMAD pathway at a concentration of 75 nM for a duration of 24 hours. Subsequently, the cells were stimulated with TGF-β1, and the alterations in MERTK mRNA expression were measured. Similarly, the absence of SMAD3, SMAD4, and TGF-βR2 resulted in a reduction in MERTK mRNA expression, as seen in **Figure 3.5**.

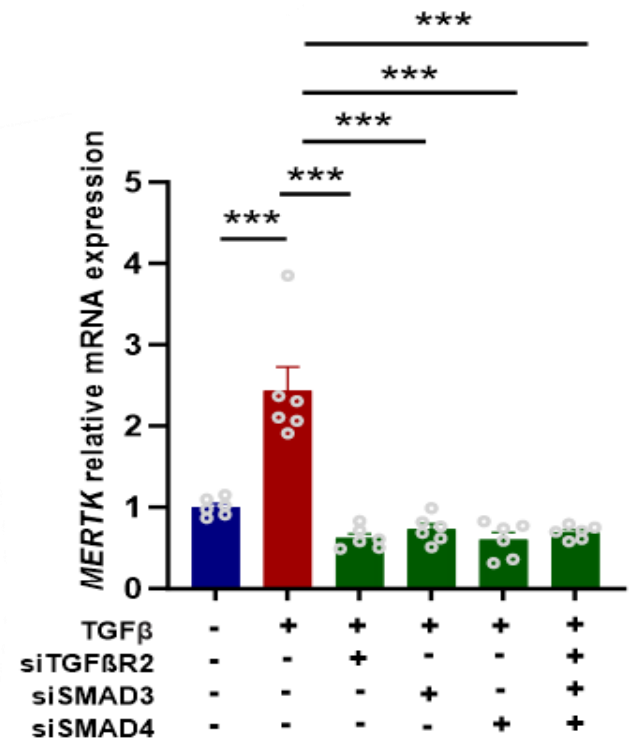

Figure 3.5 MERTK expression reversed by genetic inhibition of TGF-β related pathway

The relative mRNA expression of MERTK was evaluated using PCR and afterwards normalized to the expression of GAPDH. LX2 cells were exposed to transfection with non-coding scramble or TGFβR2, SMAD3, SMAD4 siRNA, or a mixture of the three siRNA for a duration of 48 hours. Following this, the cells were treated with TGF-β1 for a period of 24 hours. The protocol of statistical analysis is described in **Method**.

To investigate the potential impact of TGF-β signaling on the modulation of MERTK expression, LX2 cells were subjected to stimulation with pro-inflammatory cytokines (IFN-γ at a concentration of 20 ng/ml or IL-1β at a concentration of 10 ng/ml), as well as an anti-inflammatory cytokine (IL-4 at a concentration of 20 ng/ml) for a duration of 24 hours. Subsequently, the alterations in MERTK mRNA expression were assessed. The findings demonstrated that the activation of cells with IFN-γ, IL-β, and IL-4 did not have an impact on MERTK expression, suggesting that the modulation of MERTK expression is primarily influenced by TGF-β signaling, as seen in **Figure 3.6**.

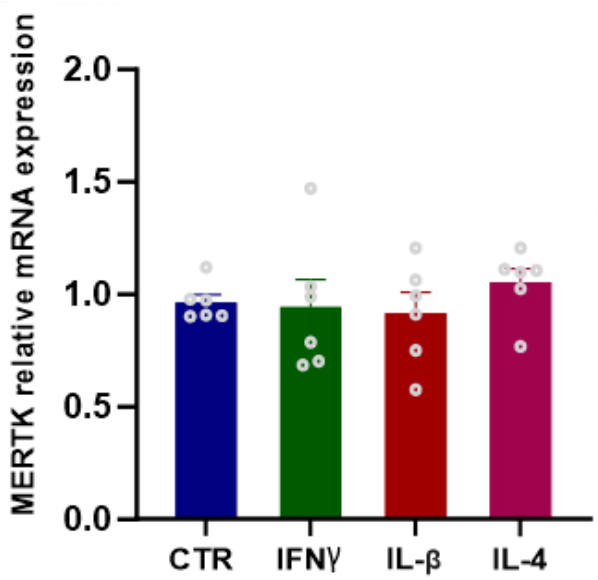

Figure 3.6 Expression of MERTK is specifically altered by TGF-β signaling LX2 cells were exposed to stimulation with IFN-γ, IL-1β, or IL-4 for a duration of 24 hours. Subsequently, the expression of MERTK mRNA was evaluated using PCR and the obtained values were normalized to untreated LX2 cells as well as GAPDH. The protocol of statistical analysis is described in **Method**.

Due to the involvement of many cell types, such as HSCs and macrophages, fibrosis is characterized as a multifaceted biological process in which the expression of MerTK is seen in both cell types. Consequently, an investigation was conducted to examine the impact of MerTK on the intercellular communication between macrophages and HSCs. Initially, human MDM were subjected to treatment with TGF-β1, either in the presence or absence of the MerTK inhibitor UNC569. The findings of this study indicate that the expression levels of MerTK mRNA and protein were dramatically enhanced after stimulation with TGF-β1. Conversely, the use of MerTK inhibitors resulted in a reversal of this effect, as seen in **Figure 3.7**. The findings were replicated in mouse BMDM, as seen in **Figure 3.8**.

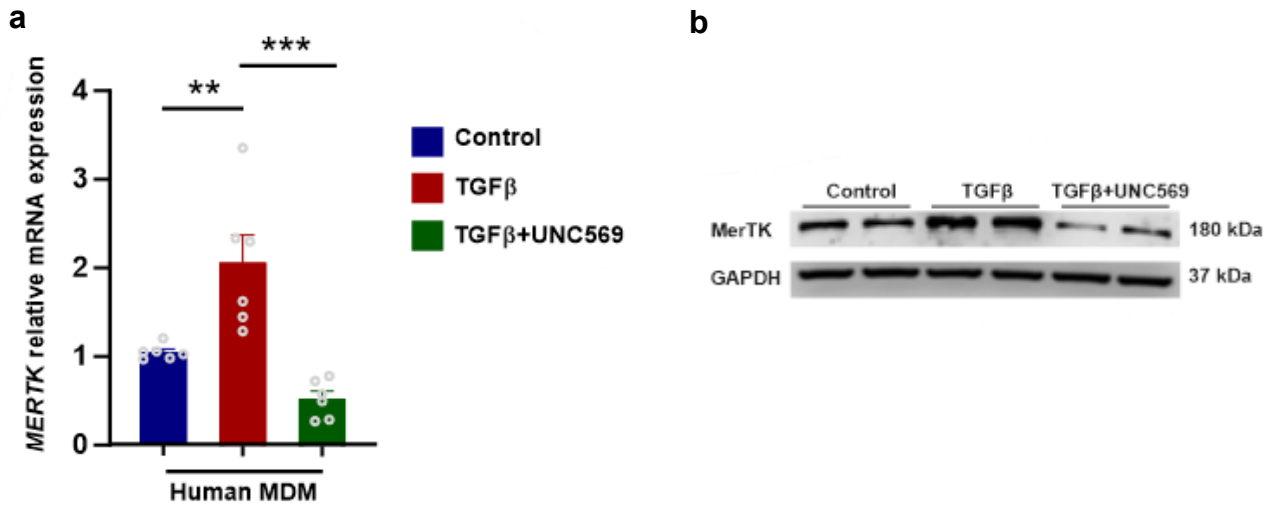

Figure 3.7 A positive reaction between TGF-β and MERTK in human MDM a) Human MDMs were subjected to treatment with TGF-β1 or a combination of TGF-β1 and the MerTK inhibitor (UNC569) for a duration of 24 hours. Subsequently, the MERTK relative mRNA expression was assessed using PCR and normalized to the expression of GAPDH and **b)** using Western blot to confirm the protein expression. The protocol of statistical analysis is described in **Method**.

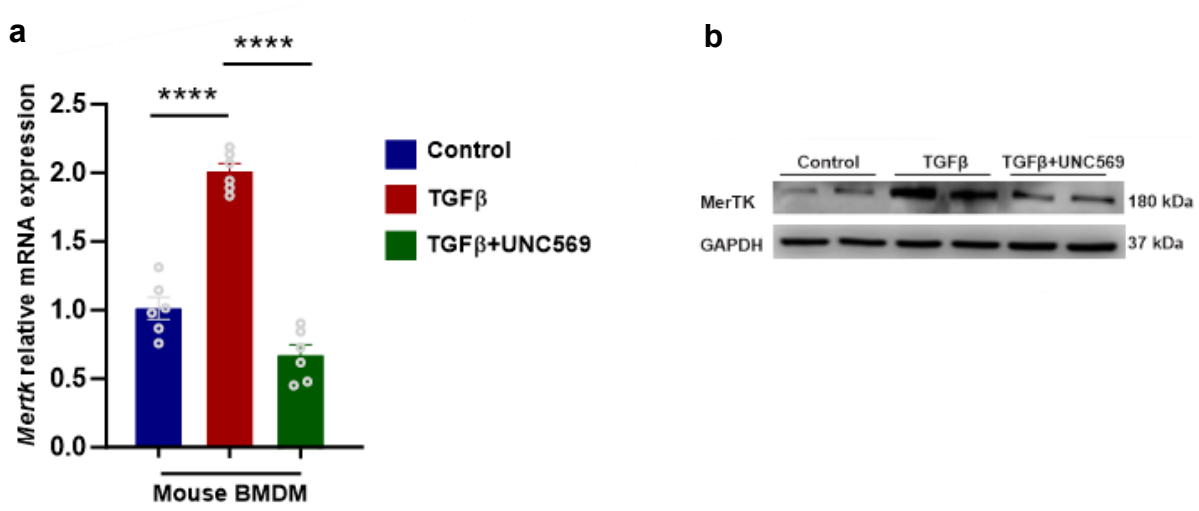

Figure 3.8 A positive reaction between TGF-β and MerTK in Mouse BMDM a) Mouse BMDMs were exposed to TGF-β1 alone or in combination with the MerTK inhibitor (UNC569) for a duration of 24 hours. Subsequently, the Mertk relative mRNA expression was assessed using PCR and normalized to m36B4 and **b)** using Western blot to confirm the protein expression. The protocol of statistical analysis is described in **Method**.

Subsequently, an investigation was conducted to ascertain the potential of inhibiting MerTK in macrophages as a means to mitigate fibrosis in HSCs influenced by their intercellular communication. To investigate the potential inhibitory impact of siRNA on MERTK, a comparison was made between the effects of siRNA and the inhibitor UNC569. Specifically, non-coding scramble or MERTK siRNA was used to stimulate human MDMs, and subsequent analysis was conducted to assess the levels of MERTK expression at both the RNA and protein levels. The findings indicated that, similar to UNC569, the use of MERTK siRNA led to a substantial suppression of MERTK expression (**Figure 3.9**). The co-cultivation of macrophages defective in MerTK (UNC569 and siRNA) with HSCs resulted in a reduction in the expression of fibrotic markers, namely ACTA2 and COL1A1, as seen in **Figure 3.10**. Comparable outcomes were seen for BMDMs obtained from wild-type or Mertk-/- mice, as shown in **Figure 3.11**.

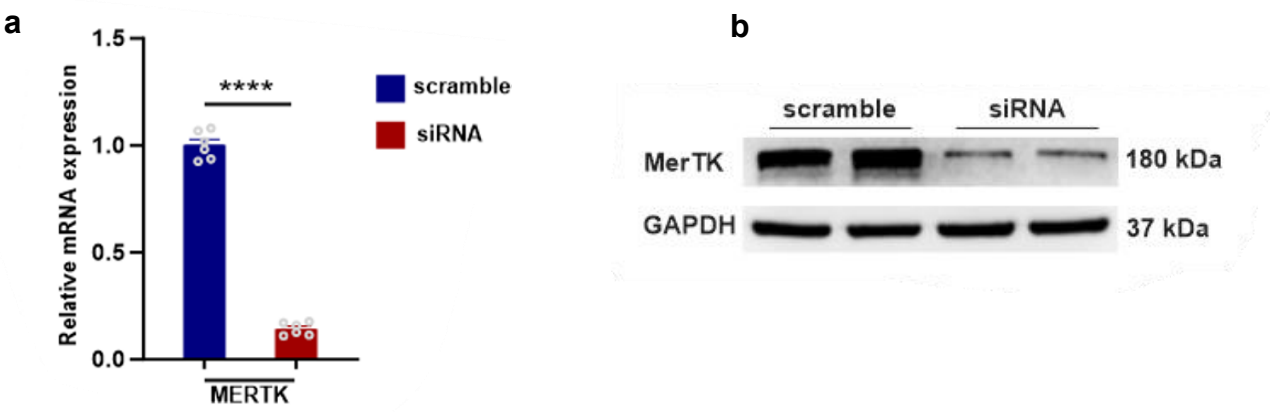

Figure 3.9 Genetic inhibition of MERTK a) Human MDMs were transfected with non-coding scramble or MERTK siRNA for a duration of 48 hours. Subsequently, the MERTK relative mRNA expression was evaluated using PCR, and **b)** protein expression was confirmed by Western blot. The protocol of statistical analysis is described in **Method**.

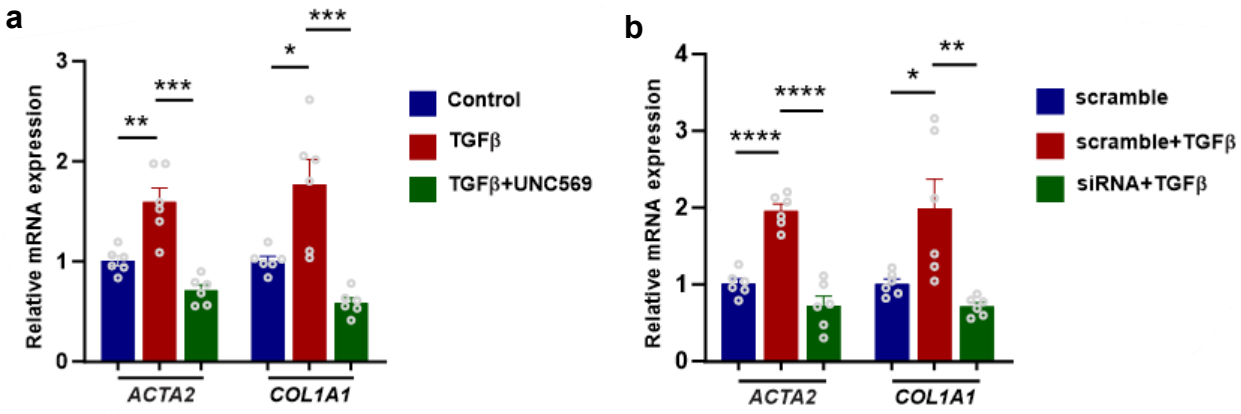

Figure 3.10 MERTK inhibition in Human MDMS attenuates fibrogenic markers in co cultured human HSCs a) Human MDMs were given treatment with TGF-β, either with or without the addition of a MerTK inhibitor (UNC569), for a duration of 24 hours. **b)** Alternatively, MDMs were transfected with non-coding scramble or MERTK siRNA for a period of 48 hours, followed by a 24-hour treatment with TGF-β. During these treatments, MDMs were co-cultured with LX2 cells in trans-well tissue culture plates. The relative expression levels of fibrosis markers were evaluated using PCR and were subsequently normalized to the expression of GAPDH. The protocol of statistical analysis is described in **Method**.

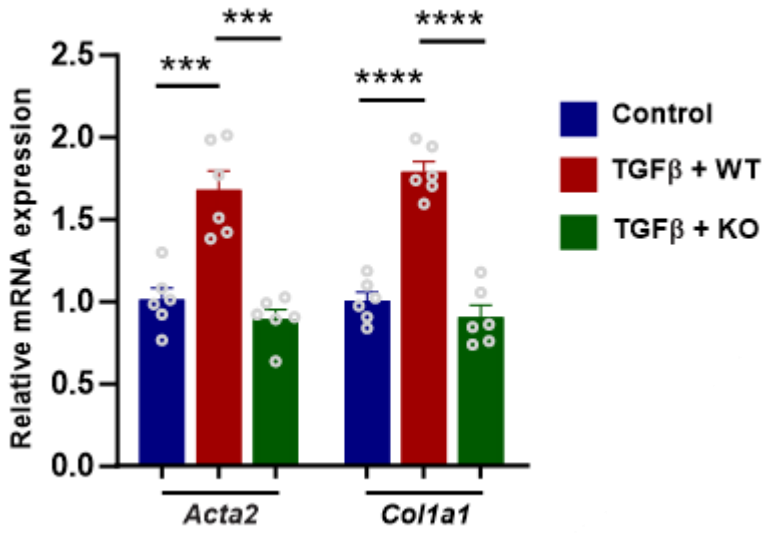

Figure 3.11 MERTK inhibition in Mouse MDMS attenuates fibrogenic markers in co cultured murine HSCs Mouse BMDM lacking the Mertk gene and wild-type (WT) mice were given to a 24-hour treatment with TGF-β1. During this treatment, the cells were co-cultured in trans-well tissue culture plates alongside JS-1 cells. The expression levels of fibrosis markers were evaluated using PCR and were afterwards normalized by m36B4. The protocol of statistical analysis is described in **Method**.

3.3.2 MerTK expression upregulate in liver fibrosis mice

Following the conclusion of the investigation pertaining to the involvement of MerTK in the cellular mechanisms underlying liver fibrosis, an examination was conducted to further elucidate the function of MerTK in hepatic fibrosis. This examination included the utilization of a standard BDL model, using both wide-type mice and $Mertk^{-/-}$ mice.

The first step was evaluating the expression of MerTK in the liver of mice undergoing BDL. The expression of MerTK was found to be low in sham mice liver, but the levels of Mertk mRNA, protein, and p-MerTK were significantly raised in the BDL group, as shown in **Figure 3.12**.

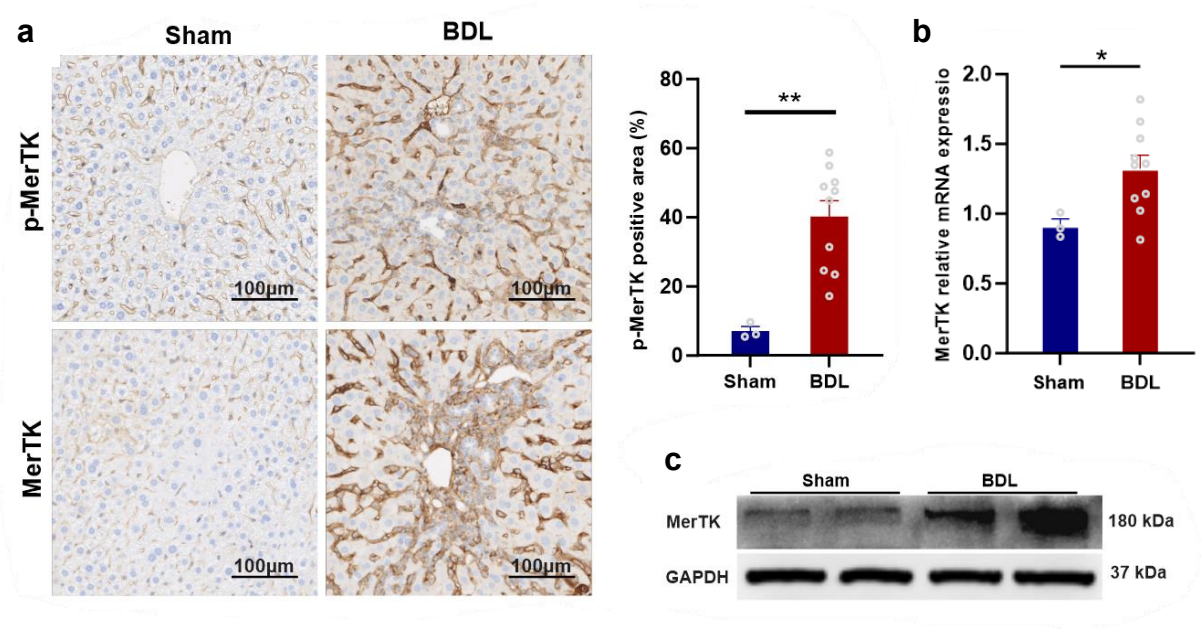

Figure 3.12 The expression of MerTK increased in BDL model liver a) The liver sections were applied to immunohistochemical staining to assess the expression of MerTK (both phosphorylated and total forms). The staining results revealed a significant increase in MerTK expression in the liver sections from the experimental group (right) compared to the control group (left) of sham mice. The scale bar in the images represents a length of 100 μm. Furthermore, the area of p-MerTK positivity was quantified using ImageJ software. **b)** The measurement of Mertk mRNA expression was done using PCR, normalized with m36B4, **c)** and using Western blot to measure the protein expression. The protocol of statistical analysis is described in **Method**.

3.3.3 The effect of MerTK genetic inhibition on ALT levels

In order to investigate the impact of Mertk knockout on liver damage, we conducted an assessment and comparison of serum ALT levels between wild-type and Mertk$^{-/-}$ mice using the BDL paradigm. In comparison to the sham group, the serum ALT level in BDL wild-type mice group exhibited a statistically significant increase when compared to the BDL Mertk$^{-/-}$ group (**Figure 3.13**).

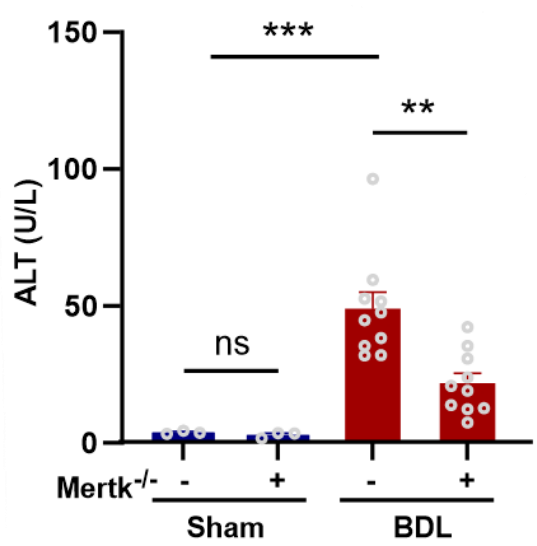

Figure 3.13 The ALT enzyme demonstrated sustained suppression after genetic inhibition of MerTK in BDL model The measurement of ALT as a marker for liver damage was conducted using an ALT ELISA in mice that were either Wide-type or Mertk-/-, after either Sham or BDL treatment, with a duration of 14 days. The protocol of statistical analysis is described in **Method**.

3.3.4 MerTK inhibition improved the liver damage evaluated by histology

In order to get a deeper comprehension of the impact of Mertk knockout on the advancement of liver fibrosis in the BDL model, histological examination using H&E staining was conducted. In comparison to the control group, wild-type BDL mice exhibited notable manifestations of biliary duct hyperplasia, inflammation, and fibrosis. The liver lobules of $Mertk^{-/-}$ BDL mice exhibited little deviation from normal morphology, with no substantial increase seen in bile duct hyperplasia or collagen deposition (**Figure 3.14a**).

The liver slices underwent staining with Picrosirius Red in order to detect and analyze fibrous collagen networks[120]. The presence of fibrous tissue around the proliferating bile ducts was found in BDL wild-type mice, however this phenomenon was not observed in BDL $Mertk^{-/-}$ animals (**Figure 3.14a**). The use of ImageJ enabled the quantification of Picrosirius Red staining, which further substantiated the observation that the absence of MerTK resulted in a notable decrease in collagen accumulation (**Figure 3.14b**).

In a similar vein, the application of Gomori Trichome staining revealed a noteworthy augmentation in the staining of collagen fibers inside the portal vein region of wild-type mice subjected to BDL. On the other hand, there was no statistically significant increase seen in collagen deposition in mice with BDL-induced liver injury lacking the Mertk gene. In general, the absence of Mertk resulted in a decrease in liver damage, collagen accumulation, and fibrosis in the BDL model, as seen in **Figure 3.14a**.

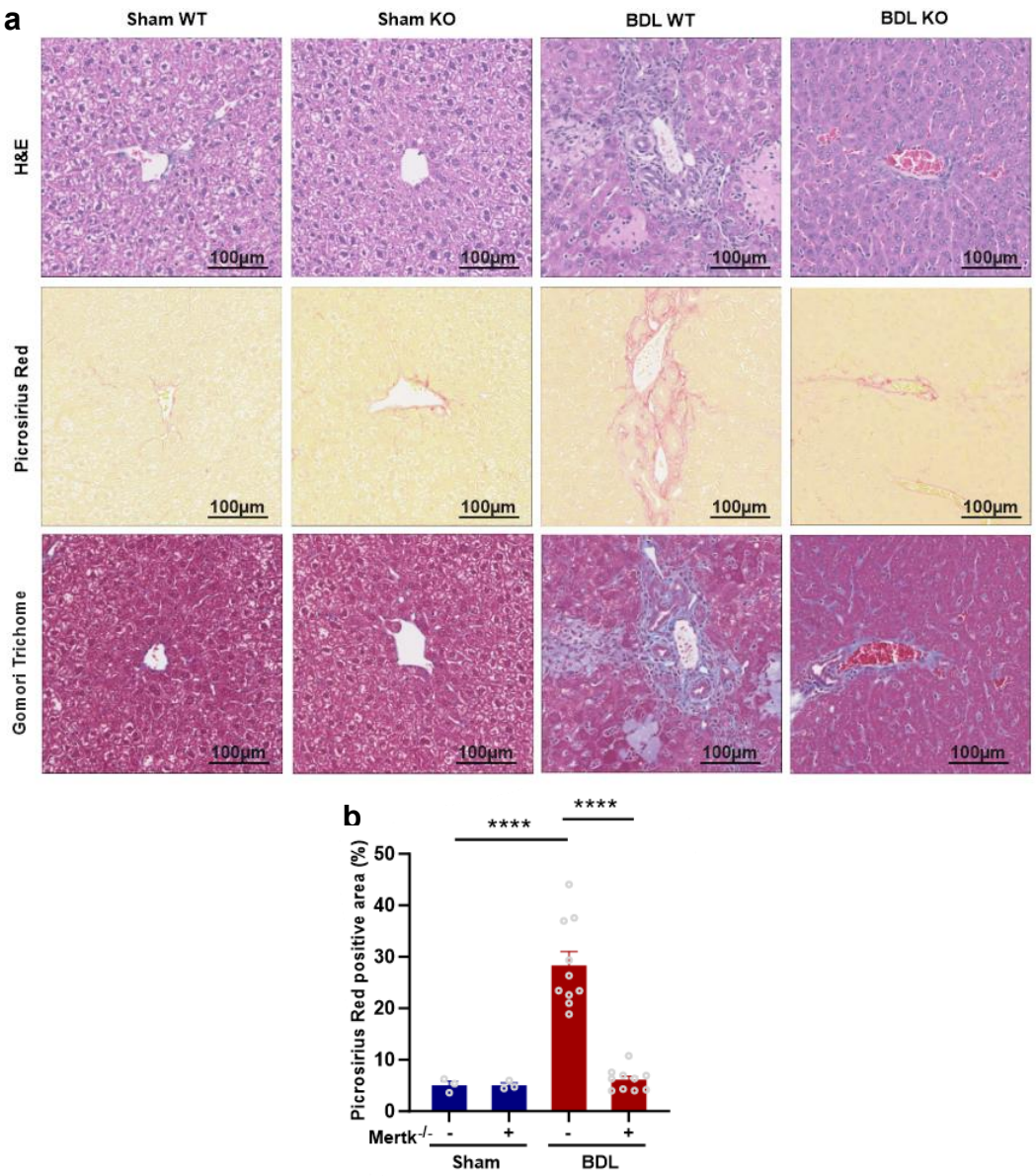

Figure 3.14 The impact of MerTK knockout on liver histology after BDL induction a) Liver slices from Wide-type or Mertk$^{-/-}$ mice, after Sham or BDL administration, were subjected to assessment using H&E staining, Picrosirius Red staining, and Gomori Trichome staining after a 14-day period, **b)** and the quantification of Picrosirius Red positive regions was performed using ImageJ software. The protocol of statistical analysis is described in **Method**.

3.3.5 MerTK inhibition attenuate hydroxyproline content increasing in BDL model liver

To enhance the precision of the quantitative measurement of collagen in the liver, the hydroxyproline concentration in the liver was examined as an indicator of collagen content. In this model, it was observed that the hydroxyproline level of both wild-type mice and Mertk$^{-/-}$ mice in the BDL group exhibited a rise. However, it is noteworthy that the hydroxyproline content in the Mertk$^{-/-}$ mice remained considerably lower compared to that of the wild-type mice (**Figure 3.15**).

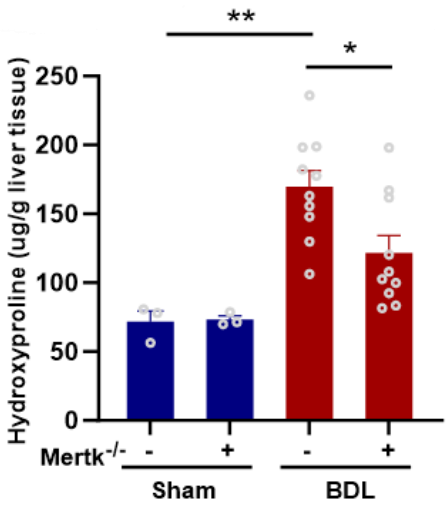

Figure 3.15 Hydroxyproline analysis of liver tissue subsequent to the genetic suppression of MerTK in the BDL model The protocol of statistical analysis is described in **Method**.

3.3.6 MerTK genetic inhibition attenuated fibrogenic markers mRNA expression

To conduct a more extensive examination of the alterations in gene expression associated to fibrosis in the BDL model, four fibrosis indicators were chosen and their mRNA expression changes were quantified using PCR analysis. The findings indicated a considerable decrease in the strength of all markers in the BDL Mertk$^{-/-}$ mice in comparison to the BDL wild-type mice, as seen in **Figure 3.16**.

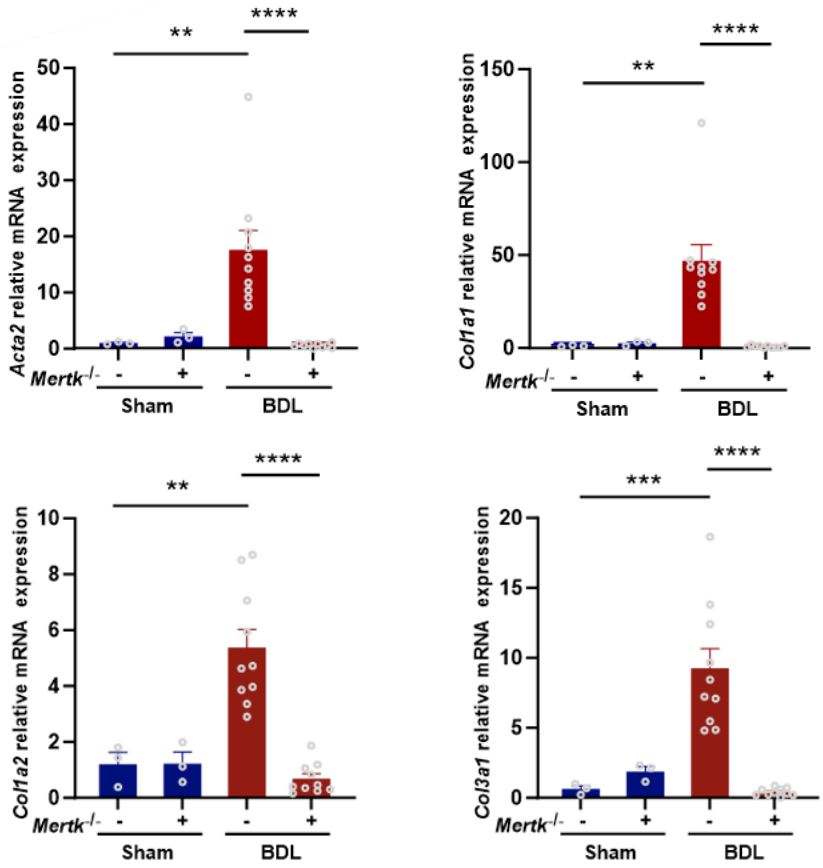

Figure 3.16 Suppression of MerTK results in a reduction of fibrotic markers expression in the BDL model The mRNA expression of fibrosis-related markers (Acta2, Col1a1, Col1a2, Col3a1) was evaluated using PCR in mice with either the Wide-type or Mertk-/- genotype, after either Sham or BDL treatment, at a time point of 14 days. The protocol of statistical analysis is described in **Method**.

3.3.7 Suppression of MerTK resulting reduction of expression of α-SMA in BDL liver

α-Smooth muscle actin (α-SMA) is well recognized as a crucial indicator of fibrosis. Immunohistochemistry and Western blot techniques were used to examine the impact of Mertk deletion on the expression of α-SMA in the liver of mice subjected to BDL. The quantitative analysis of immunohistochemical staining was performed using ImageJ. In accordance with the findings obtained from PCR, the expression of α-SMA protein in the BDL Mertk$^{-/-}$ mice exhibited a statistically significant decrease compared to the BDL wild-type mice, as seen in **Figure 3.17**.

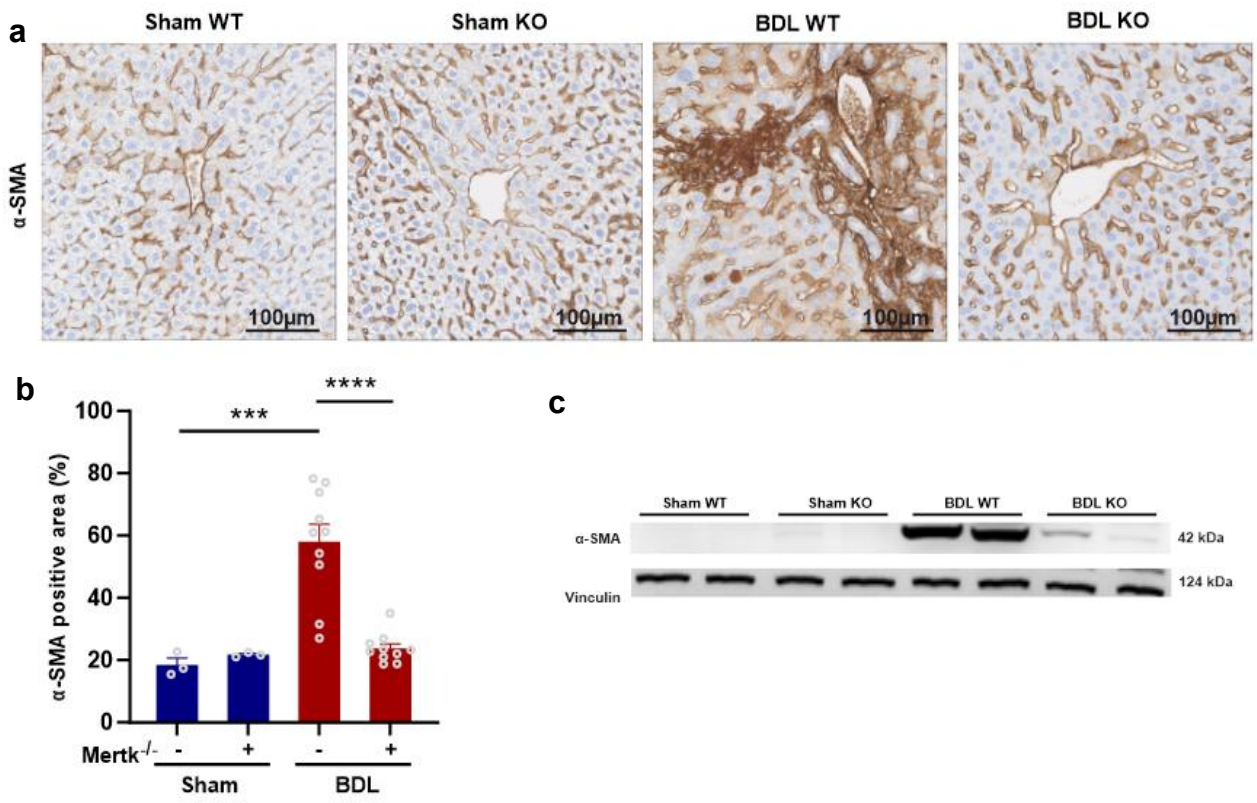

Figure 3.17 The impact of inhibiting MerTK on the expression of α-SMA in the liver of mice subjected to BDL a) liver sections assessed by α-SMA immunohistochemistry staining, and **b)** using ImageJ to assess positive area, and **c)** further confirmed by Western blot. The protocol of statistical analysis is described in **Method**.

3.3.8 Suppression of MerTK inhibits the recruitment of hepatic macrophages

In light of the aforementioned rationale, my prior investigation focused on examining the alterations in MerTK expression inside macrophages and the subsequent impact of co-culturing. It is well-established that hepatic macrophages significantly contribute to the progression of liver fibrosis via the secretion of pro-inflammatory cytokines and chemokines[121]. Consequently, an investigation was conducted to assess the potential impact of Mertk deletion on the infiltration and inflammatory response of macrophages in the liver, using F4/80 immunohistochemical labeling[122]. According to the data shown in **Figure 3.18**, there was a notable decrease in macrophage infiltration in the liver of BDL Mertk$^{-/-}$ mice compared to BDL wild-type mice.

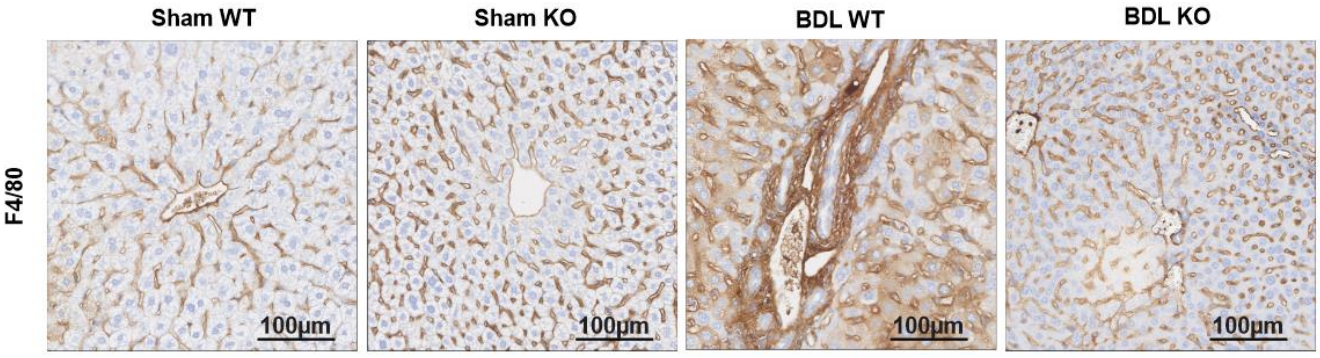

Figure 3.18 The impact of genetic suppression of MerTK on the staining of macrophage F4/80 in the BDL model The evaluation of macrophage infiltration was conducted by performing F4/80 immunohistochemical labeling on liver sections obtained from mice with either the Wide-type or Mertk$^{-/-}$ genotype, after a period of 14 days after undergoing either Sham or BDL therapy.

3.3.9 Inhibition of MerTK resulting the suppression of AKT and ERK phosphorylation

While it has been shown that TGF-β stimulation can lead to the upregulation of MerTK, it is important to note that TGF-β also triggers the activation of other signaling pathways. These pathways include the MAPK pathway and the PI3K/Akt pathway, both of which play crucial roles in intracellular signaling cascades that govern various cellular processes such as cell growth, proliferation, survival, apoptosis and invasion[123-125].

Intriguingly, upon doing an analysis of phosphorylation levels of Akt and Erk in the livers of mice using the BDL model, it was shown by Western blot that the phosphorylation levels of Akt and Erk1/2 were notably reduced in BDL Mertk$^{-/-}$ mice in comparison to BDL wild-type mice (**Figure 3.19**).

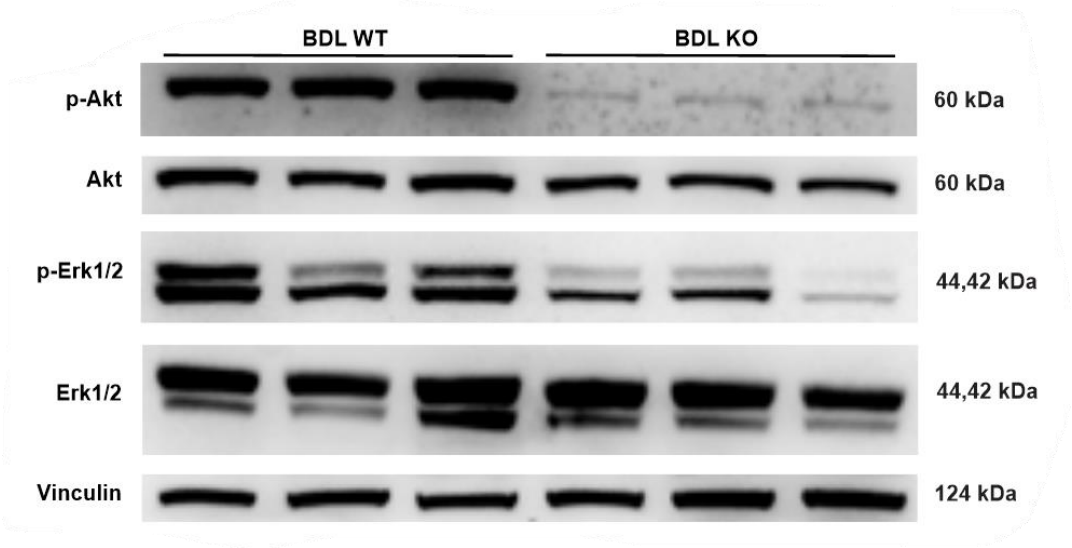

Figure 3.19 The genetic inhibition of MerTK results in the suppression of downstream signaling pathways in the BDL model The protein expression levels of p-Akt, Akt, p-Erk1/2, and Erk1/2 were evaluated by Western blot analysis in both Wide-type mice and Mertk$^{-/-}$ mice, specifically 14 days after BDL.

3.4 Discussion

As elucidated in the present chapter, the first approach included conducting in vitro tests to establish the intimate association between MerTK and TGF-β signalling. This was accomplished using diverse TGF-β stimulus designs specifically tailored to HSCs. Simultaneously, alterations in the expression of MerTK were seen in many cell types, including HSCs and macrophages. The co-culture experiment also provided evidence supporting the extensive involvement of MerTK in multiple phases of the intricate biological process of fibrosis. According to recent research, mice with a particular deletion of MerTK in macrophages exhibited reduced liver fibrosis when subjected to a high-fat diet. This finding suggests that MerTK plays a significant role in the signalling pathways started by macrophages during the development of fibrosis [126].

Subsequently, BDL, a well-accepted liver fibrosis model, was selected to investigate the involvement of MerTK in the progression of hepatic fibrosis. Cholestatic liver disease is a chronic and progressive condition affecting the bile duct, characterised by a diverse spectrum of causes that are both congenital and acquired. These causes include primary biliary cholangitis, primary sclerosing cholangitis and obstructive or pharmaceutical-induced cholestasis [127]. The shared characteristic among these diseases is cholestasis, which arises from compromised bile formation and/or flow. This condition subsequently gives rise to a range of comparable pathological alterations, such as hepatocyte injury, hepatocyte death, inflammatory cell infiltration, bile duct proliferation and fibrosis [128]. Consequently, BDL serves as a suitable model for studying analogous processes occurring in humans.

In this chapter, a comprehensive analysis of the beneficial impact of MerTK knockout on the mitigation of cholestatic liver fibrosis is conducted. This was achieved using many experimental techniques, including the assessment of ALT levels, histological examination, PCR, quantification of collagen and Western blot analysis.

Hepatic fibrosis is a multifaceted biological process that culminates in the development of fibrotic tissue in the liver. This process involves intricate interactions between many cell types, such as macrophages and HSCs. The potential molecular pathways behind the mitigation of fibrosis advancement with MerTK deletion may include the concurrent participation of these two distinct cell types. α-SMA is a prominent indicator of active HSCs [117], while F4/80 is a commonly used marker for monocyte-macrophage in mice [129]. Further analysis of the alterations in the expression levels of these two markers in the BDL model showed that the absence of MerTK resulted in a notable inhibition of HSC activation and a considerable hindrance in the recruitment of macrophages to the liver.

To further investigate the broader downstream pathways regulated by TGF-β, an analysis was conducted to assess the phosphorylation levels of Akt and Erk1/2 in liver tissue obtained from the BDL model. Unexpectedly, the deletion of MerTK hindered the regulation of the MAPK/ERK and PI3K-Akt signalling pathways. This suggests that MerTK can engage in several downstream pathways that are induced by TGF-β, such as the SMAD pathways (as shown by in vitro experiments with SMAD3 and SMAD4 siRNA) and non-SMAD pathways.

In conclusion, the findings presented in this chapter confirm that MerTK is a viable therapeutic target for hepatic fibrosis, as shown by the use of the cholestatic hepatic fibrosis model known as BDL. Considering the prevalence of myoblasts as pathological cell types in almost all fibrotic disorders, the potential therapeutic advantages of targeting profibrosis signals by MerTK inhibition in several organs throughout the fibrosis process are worth exploring. The next chapter thus investigates the impact of MerTK knockout in illness models pertaining to renal and pulmonary fibrosis. The identification of a potential favourable impact of MerTK inhibition on multiorgan fibrosis would constitute a very promising breakthrough.

Chapter4: MerTK inhibition attenuates kidney and lung fibrosis

4.1 Introduction

The liver, lungs and kidneys are among the organs most frequently impacted by fibrosis, which, in aggregate, is responsible for nearly half of all deaths in the developed world. Drugs that target fibrosis are an unmet clinical need. Fibrosis shares common pathways across various organs. Leveraging human genomic information is a viable option for drug discovery, including the identification of the core regulators of tissue fibrosis [130, 131]. Thus, there is ample hope that an understanding of common fibrosis pathways could lead to the development of effective antifibrotic therapies that are effective in all these tissues.

The findings obtained in the in vitro studies and mouse hepatic fibrosis models (BDL) described in the previous chapter were intriguing. While this could implicate major untapped translational and therapeutic potentials, MerTK has not been explored as a therapeutic target in the liver or for fibrotic diseases in other organs.

Thus, as detailed in this chapter, I aimed to expand the scope of my research to explore the inhibitory effects of MerTK in the study of renal and pulmonary fibrosis.

To this end, WT and MerTK$^{-/-}$ mice were further subjected to either unilateral ureteral obstruction (UUO) or BLM injection to study the effects of MerTK inhibition on renal and lung fibrosis, respectively.

Unilateral ureteral obstruction is a popular and reliable model of renal injury disease that simulates human chronic obstructive kidney disease in an accelerated manner [62]. Similarly, the BLM-induced pulmonary fibrosis mouse model is the most widely used experimental model for pulmonary fibrosis [132]. Bleomycin is a chemotherapeutic antibiotic that has been identified as a profibrotic agent when pulmonary fibrosis occurs after the intravenous administration of BLM in lymphoma patients [132]. A recent expansion of what ATS stands for was published in an ATS workshop report confirming the consensus that the endotracheal BLM model is “the most characteristic animal model available for preclinical testing” [133].

4.2 Method

Kidney fibrosis model (UUO): The UUO model was used as a conventional method for inducing kidney fibrosis in order to investigate the potential of MerTK inhibition as a therapeutic target for treating kidney fibrosis. Wild-type or Mertk knockout mice were exposed to either UUO or sham surgery for a duration of 21 days. then, the mice were subjected to euthanasia, following which their kidneys were extracted and then preserved either by fixation in a 4% paraformaldehyde solution or by rapid freezing in liquid nitrogen.

Pulmonary fibrosis model (BLM): The use of bleomycin served as a conventional model for pulmonary fibrosis in order to investigate the potential of MerTK inhibition as a therapeutic target for the treatment of pulmonary fibrosis. Wild-type or Mertk knockout mice were administered intratracheal injections of either bleomycin or saline solution for a duration of 21 days. Subsequently, the mice were subjected to euthanasia, following which their lungs were extracted and preserved either by fixation in a 4% paraformaldehyde solution or by rapid freezing in liquid nitrogen.

Figure 4.1 displays the design diagram of the animal model.

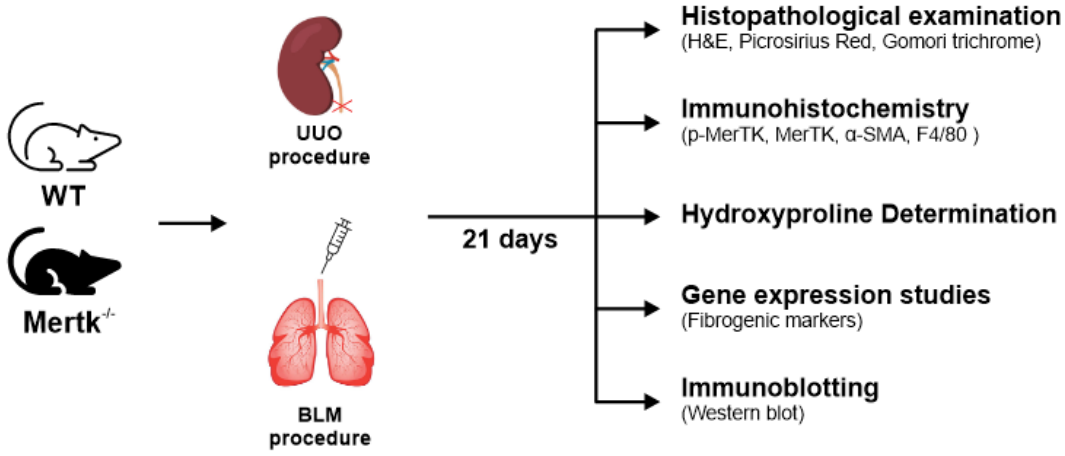

Figure 4.1 Scheme illustrating the animal experimental design

As described previously[102], a set of standardized studies was used to assess the impact of MerTK inhibition on fibrosis phenotypes, encompassing:

A) ***Histopathological examination****:* The paraffin sections underwent staining using H&E for the purpose of examining morphology and inflammation. Additionally, Picrosirius Red staining was performed to assess collagen deposition, while Gomori Trichome staining was used specifically for the staining of type 1 collagen. The quantification of Picrosirius Red staining was performed using the ImageJ.

B) ***Immunohistochemistry staining:*** p-MerTK, MerTK, α-SMA and F4/80

C) ***Hydroxyproline determination:*** The quantification of collagen content was conducted by measuring the hydroxyproline content in the specific kit provided by Sigma.

D) ***Gene expression studies****:* The extraction of total RNA was conducted, followed by the synthesis of cDNA, and afterwards, RT-PCR was used to assess alterations in the expression levels of fibrogenic markers, namely Acta2, Col1a1, Col1a2, and Col3a1.

E) ***Western blot:*** Tissue lysates were prepared and then tested by Western blot to examine alterations of the protein expression, including α-SMA, p-Akt, Akt, p-Erk1/2, and Erk1/2.

Ethics: Similarly described previously**[102]**, all animal work in this research are under the guidance of Ethic protocol provided by Australia Government, (Project No. 4302.05.19).

Statistical analysis: As previously described in [102-105]. GraphPad Prism software version 9.0 was used for data analysis. The results were presented as the mean ± standard error of the mean (SEM). The one-way analysis of variance (ANOVA) was used for conducting multi-group study, while the student's t-test was utilized for analyzing two groups. P-values were used to infer the presence of a statistically significant difference. The significance levels were denoted as follows: **** $p \leq 0.0001$, *** $p \leq 0.001$, ** $p \leq 0.01$, * $p \leq 0.05$.

4.3 Results

4.3.1 MerTK expression upregulate in kidney fibrosis mice

To explore the role of MerTK in renal fibrosis, I first assessed MerTK expression in UUO mouse model kidney. MerTK expression was low in healthy mouse kidney, whereas the expression of Mertk relative mRNA, protein, and p-MerTK increased markedly after UUO surgery **(Figure 4.2).**

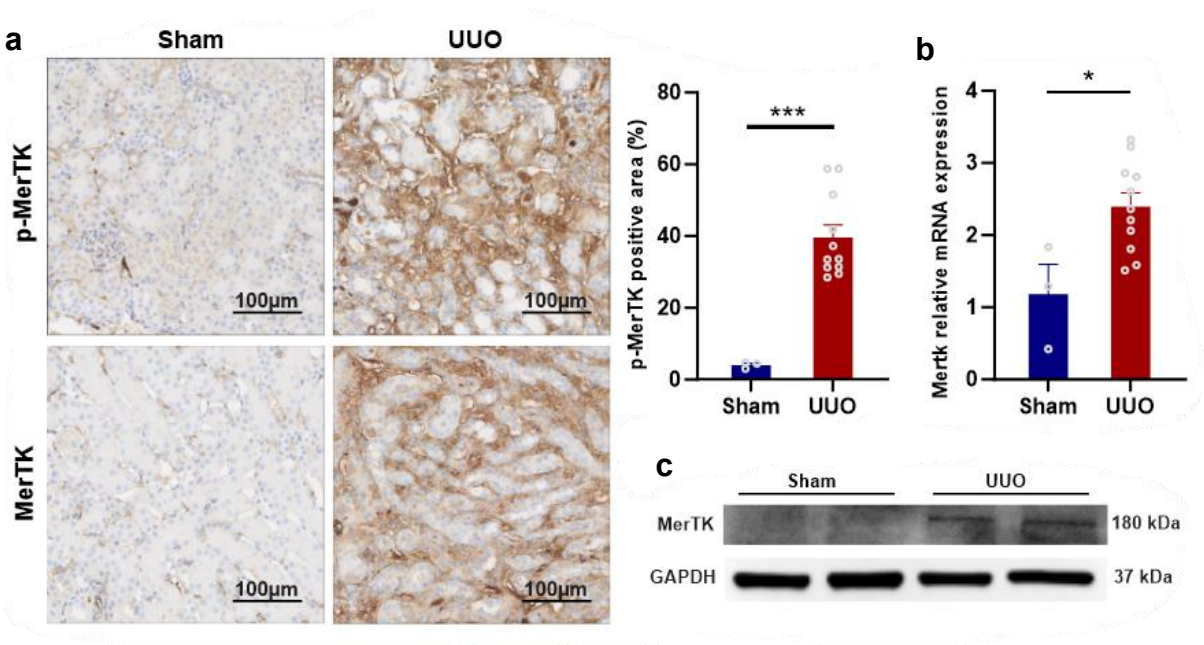

Figure 4.2 MerTK expression is upregulated in kidney fibrosis model UUO mice a) The immunohistochemical staining of kidney sections reveals a notable elevation in the expression of MerTK (both phosphorylated and total forms) on the right side, in comparison to the left side of the kidney sections from sham mice. The scale bar indicates a length of 100 μm, and the area of p-MerTK positivity was measured using ImageJ software. **b)** Mertk mRNA expression measured by real-time PCR normalized to the housekeeper m36B4 and c) protein abundance examined via Western blot. The protocol of statistical analysis is described in **Method**.

4.3.2 MerTK inhibition improved the kidney damage evaluated by histology

H&E staining showed that no pathological changes were observed in the kidney sections of wild-type and Mertk$^{-/-}$ Sham groups, and the renal tubules were intact without atrophy and exfoliation. 21 days after UUO surgery, renal tubules in the wild-type UUO mice showed obvious atrophy, tubule cell shedding, tubule lumen dilation, and interstitial inflammatory cell infiltration, while those lesions in the Mertk$^{-/-}$ UUO mice were not as severe as those in wild-type UUO mice **(Figure 4.3a).**

Picrosirius Red staining and Gomori Trichome staining showed that the basement membrane of renal tubules was intact in both sham groups, and collagen deposition of interstitial fibers was not obvious. 21 days after UUO operation, the basement membrane of renal tubules in the wild-type mice was broken, and the deposition of interstitial collagen and matrix components were significantly increased, showing serious fibrosis. Similarly, the above pathological phenomenon in Mertk$^{-/-}$ mice was less severe than that of wild-type mice **(Figure 4.3a).**

Picrosirius Red staining were applied for quantitative analysis using Image J software. The results showed that after UUO surgery, renal interstitial fibrosis in wild-type mice increased significantly, while after Mertk knockout, fibrosis process was weakened, and fiber deposition was significantly lower than that in WT mice **(Figure 4.3b).**

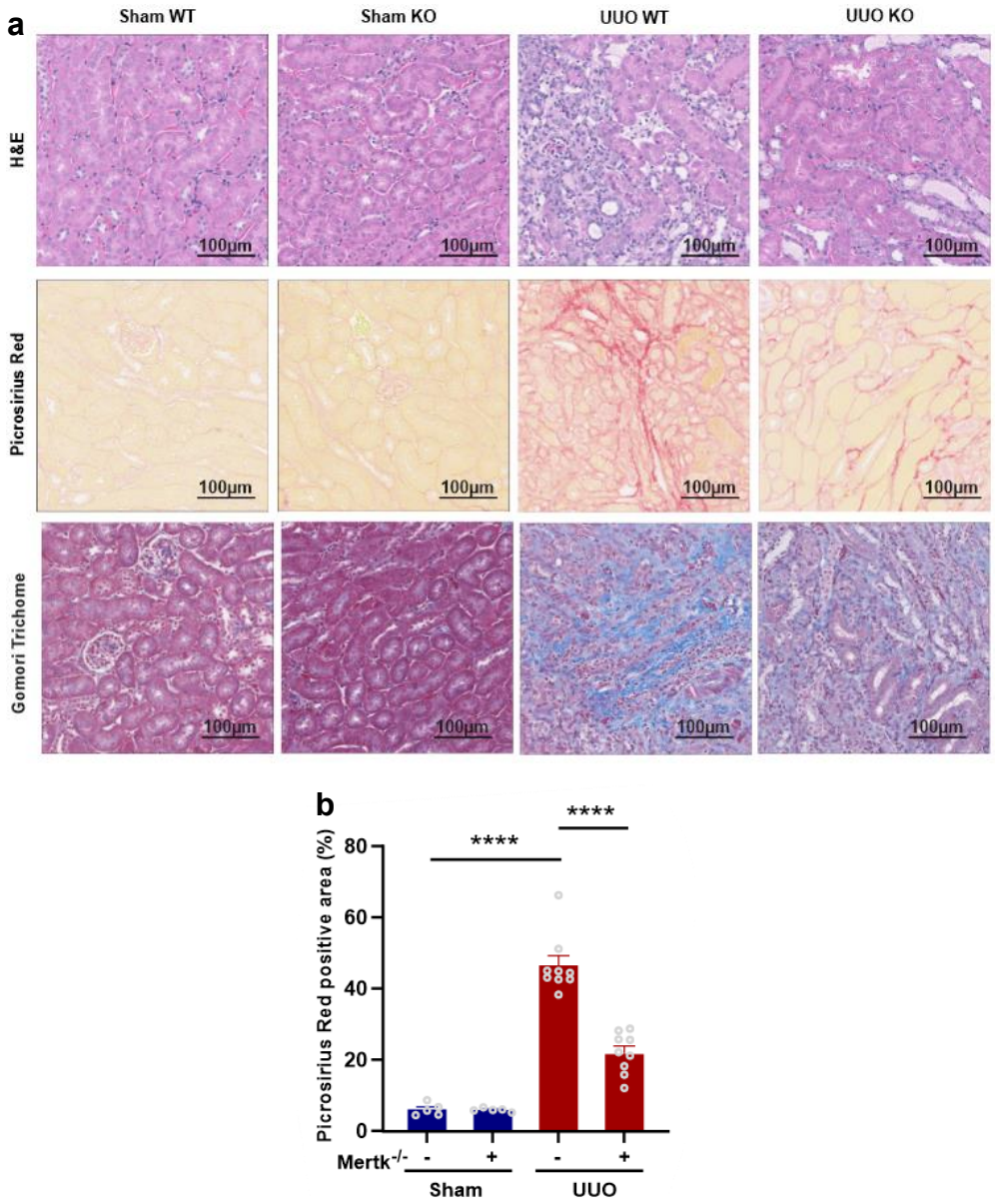

Figure 4.3 The impact of MerTK knockout on kidney histology after UUO induction a) H&E staining, Picrosirius Red staining, Gomori Trichome staining were assessed in kidney sections from Wild-type or Mertk$^{-/-}$ mice 21 days after Sham or UUO treatment and **b)** Picrosirius Red positive areas were quantified by ImageJ. The protocol of statistical analysis is described in **Method**.

4.3.3 MerTK inhibition attenuate hydroxyproline content increasing in UUO kidney

In order to make a more accurate quantitative analysis of collagen in the kidney, I tested the content of hydroxyproline in the kidney as an indicator of collagen content. In the renal fibrosis model, there was no significant difference between the two genotypes mice in the sham group; In the UUO surgery group, although the hydroxyproline content in wild-type mice and Mertk$^{-/-}$ mice was all increased, but the hydroxyproline content of Mertk$^{-/-}$ UUO mice was still significantly lower than that of wild-type UUO mice **(Figure4.4).**

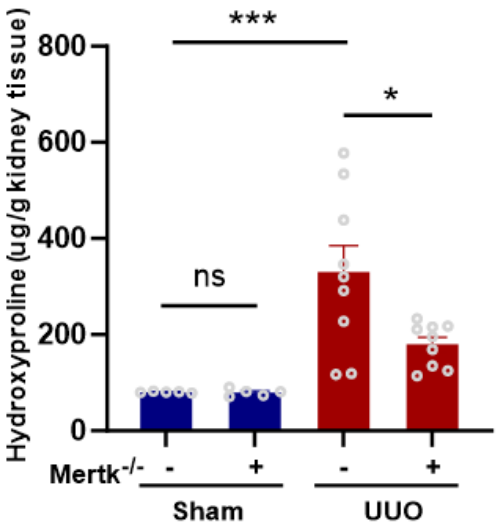

Figure 4.4 Hydroxyproline analysis of kidney tissue subsequent to the genetic suppression of MerTK in the UUO model Hydroxyproline content of kidney were assessed by Hydroxyproline Assay Kit (Sigma) in Wild-type or Mertk$^{-/-}$ mice 21 days after Sham or UUO treatment. The protocol of statistical analysis is described in **Method**.

4.3.4 MerTK genetic inhibition attenuated fibrogenic markers mRNA expression

In order to further comprehensively analyze the expression changes of fibrosis related genes in the UUO model, four fibrosis markers were selected for real-time PCR analysis to quantify their mRNA expression changes. The results showed that compared with wild-type mice, all the markers of UUO Mertk-/- mice were significantly weakened **(Figure 4.5).**

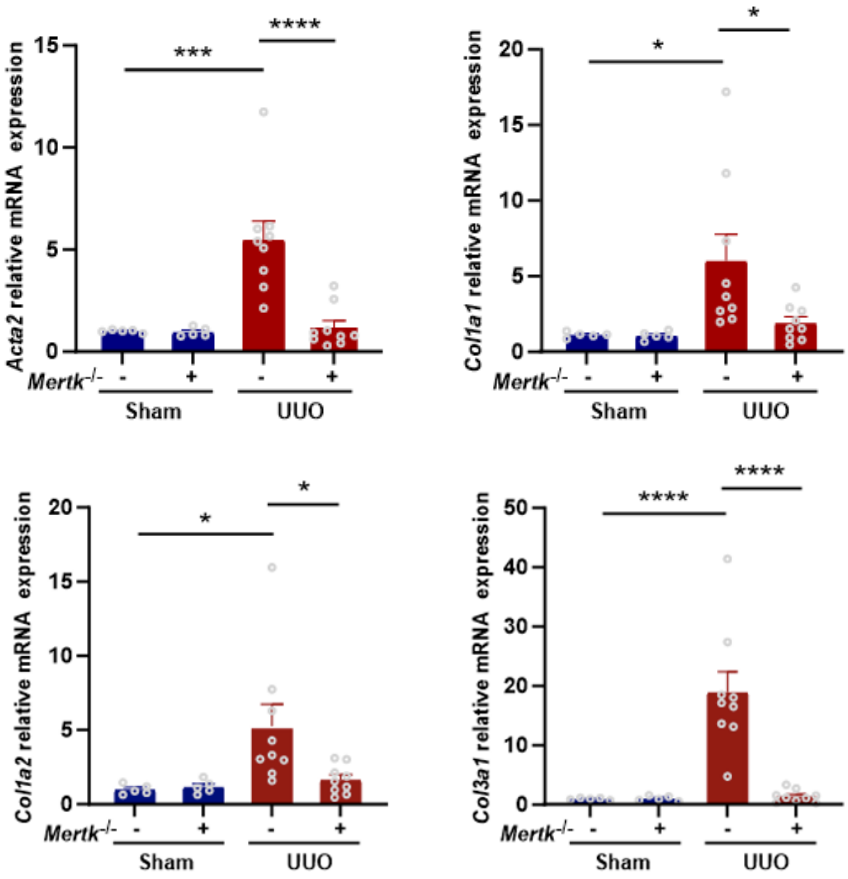

Figure 4.5 Suppression of MerTK results in a reduction of fibrotic markers expression in the UUO model Fibrosis relative markers mRNA (Acta2, Col1a1, Col1a2, Col3a1) expression are assessed by PCR in wild-type and Mertk$^{-/-}$ mice 21 days after Sham or UUO treatment. The protocol of statistical analysis is described in **Method**.

4.3.5 MerTK inhibition decreased the expression of α-SMA in UUO model kidney

α -SMA is one of the most important markers of fibrosis. Therefore, the effect of Mertk knockout on α-SMA expression in UUO mice kidney was detected by immunohistochemistry **(Figure 4.6a)** and Western Blot **(Figure 4.6c)** respectively, and immunohistochemistry staining was quantitatively analyzed by ImageJ software **(Figure 4.6b).** Consistent with the results of RT-PCR, the α-SMA protein expression level in the two genotypes of mice was very low and no significant difference in the sham group, but it was significantly increased in the UUO wild-type mice, while the expression level of the UUO Mertk$^{-/-}$ mice was significantly lower than that of the UUO wild-type mice.

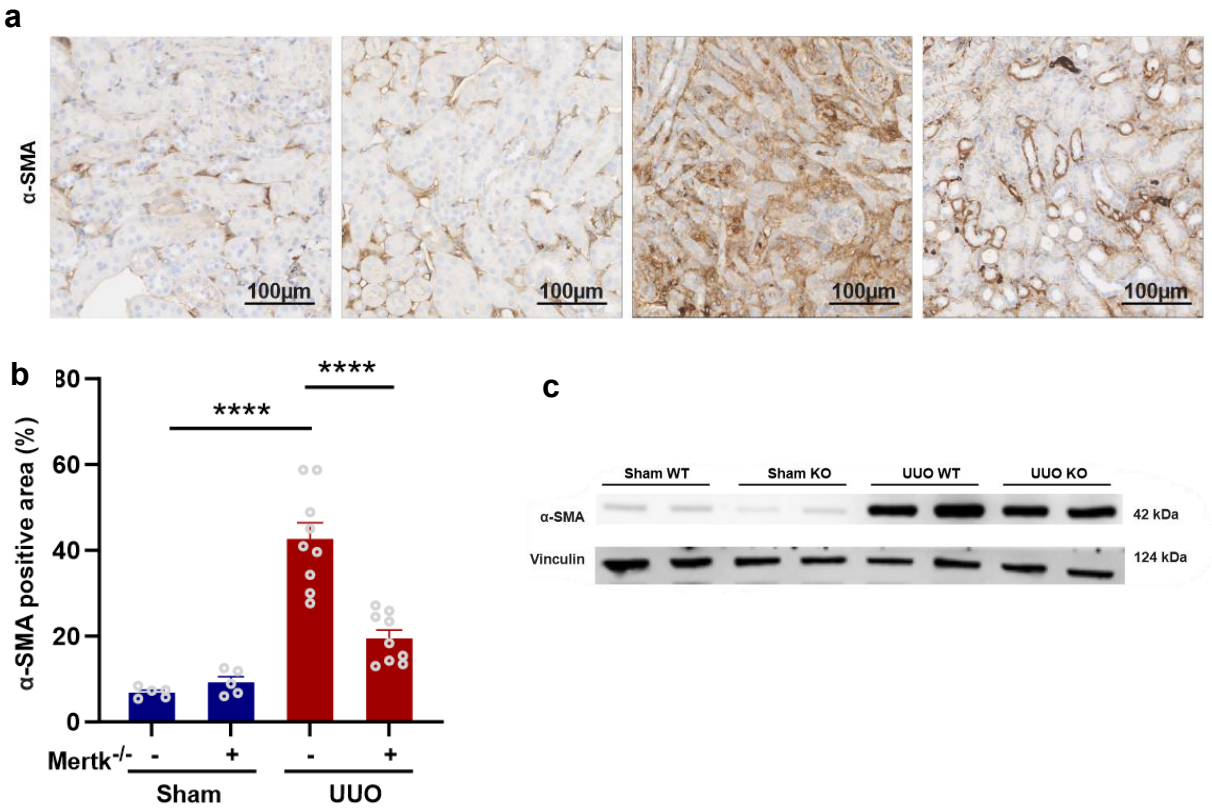

Figure 4.6 The impact of inhibiting MerTK on the expression of α-SMA in the kidney of mice subjected to UUO a) α-SMA immunohistochemistry staining was assessed in kidney sections and **b)** α-SMA positive area was quantified by ImageJ. **c)** Protein expression of α-SMA was assessed by Western blot in wild-type or Mertk$^{-/-}$ mice 21 days after Sham or UUO treatment. The protocol of statistical analysis is described in **Method**.

4.3.6 Suppression of MerTK reduced renal macrophages recruitment in UUO kidney

Macrophages play an important role in the process of liver fibrosis by secreting pro-inflammatory cytokines and chemokines in the liver [121], macrophages are also involved in the process of renal fibrosis [134]. Therefore, I used F4/80 immunohistochemical staining to detect whether Mertk knockout would affect the infiltration and inflammatory response of macrophages in the process of renal fibrosis. As shown in **Figure 4.7**, the amount of macrophage infiltration in the kidney of UUO Mertk-/- mice was significantly lower than that of UUO wild-type mice.

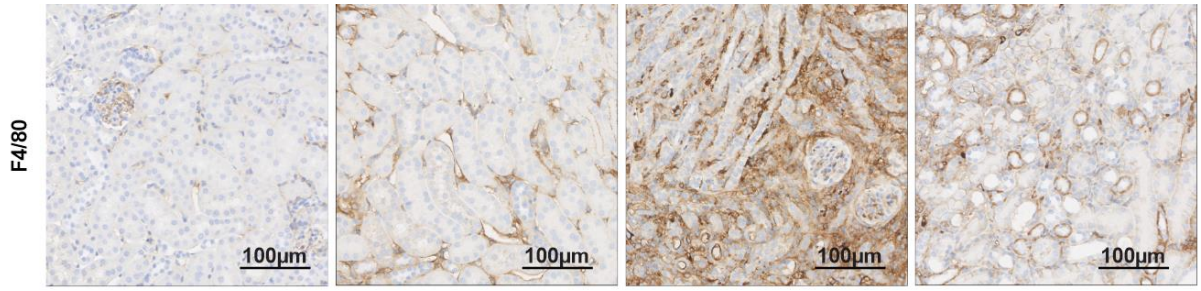

Figure 4.7 The impact of genetic suppression of MerTK on the staining of macrophage F4/80 in the UUO model Macrophage infiltration was assessed by F4/80 immunohistochemistry staining of kidney sections from wild-type or Mertk$^{-/-}$ mice 21 days after Sham or UUO treatment. (n=9 for UUO WT group, n=9 for UUO KO group and n=5 for Sham WT group, n=5 for Sham KO group)

4.3.7 MerTK genetic inhibition silenced AKT and ERK phosphorylation in UUO model

In a hepatic fibrosis model, I have shown that MerTK inhibition blocks the elevated phosphorylation levels of Akt and Erk1/2 proteins. If MerTK is an effective intervention in multi-organ fibrosis, it is likely to act through a similar or even identical pathway.

Therefore, I also used Western Blot to detect the changes in the phosphorylation levels of Akt and Erk1/2 in the UUO model mice kidney. I found that the phosphorylation levels of Akt and Erk1/2 in UUO Mertk$^{-/-}$ mice were also significantly reduced compared with UUO wild-type mice **(Figure 4.8).**

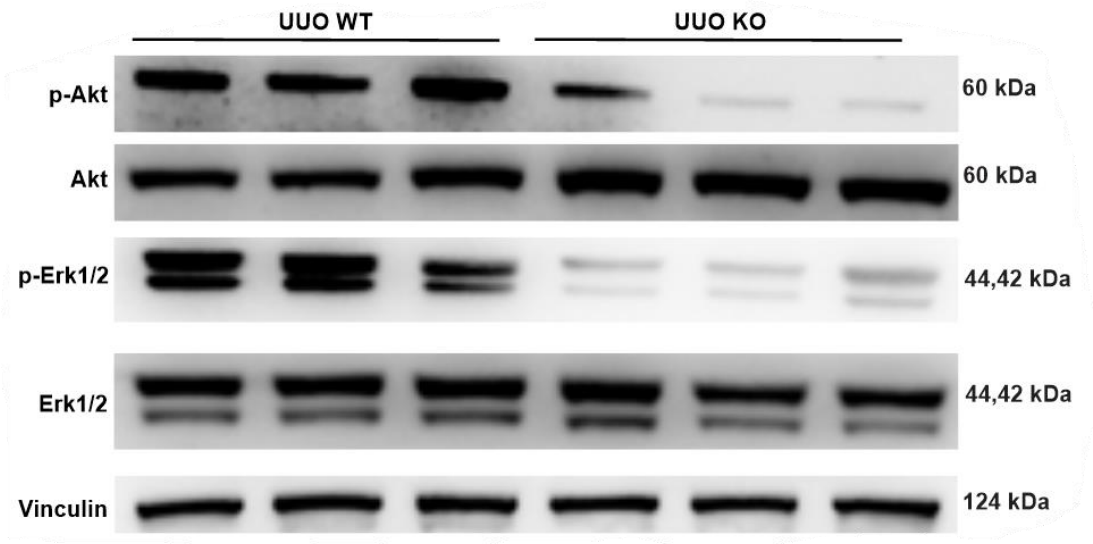

Figure 4.8 The genetic inhibition of MerTK results in the suppression of downstream signaling pathways in the UUO model Protein expression of p-Akt, Akt, p-Erk1/2, Erk1/2 were assessed by Western blot in wild-type mice and Mertk$^{-/-}$ mice 21 days after UUO treatment. (n=9 for UUO WT group, n=9 for UUO KO group and n=5 for Sham WT group, n=5 for Sham KO group)

4.3.8 MerTK expression upregulate in pulmonary fibrosis mice

After verifying the role of MerTK in the process of renal fibrosis, I next opted to investigate the role of MerTK in pulmonary fibrosis.

Initially, I evaluated changes in MerTK expression in mouse lungs in a BLM-mediated pulmonary fibrosis model. As shown in **Figure 4.9**, Mertk mRNA, protein and p-MerTK expression in control mice (saline treatment) were all very low but showed a significant increase in pulmonary fibrosis mice (BLM treatment).

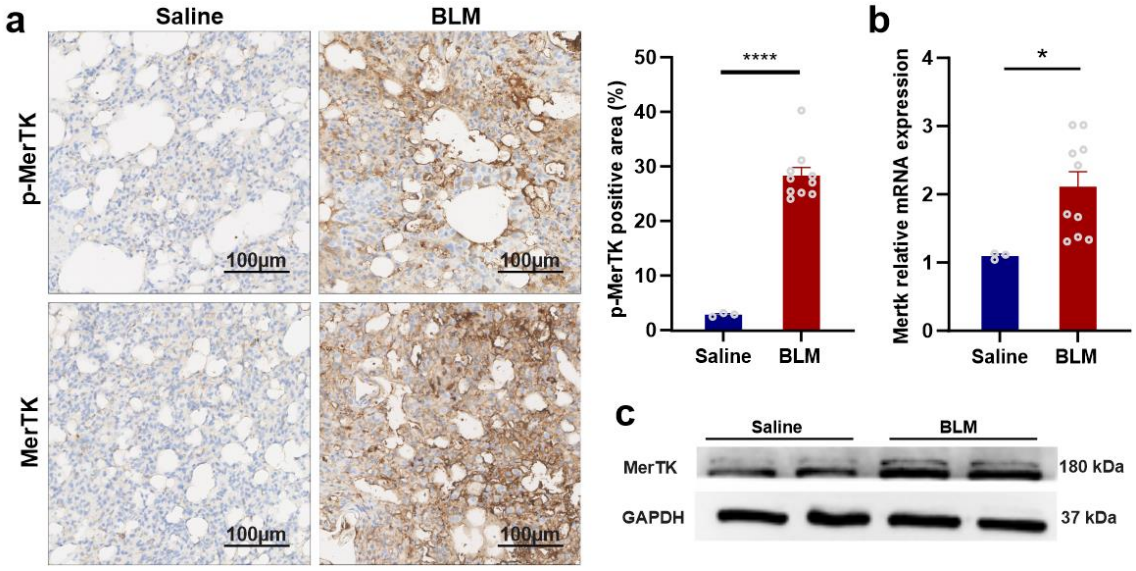

Figure 4.9 MerTK expression is upregulated in pulmonary fibrosis model BLM mice a) The immunohistochemical staining of lung sections reveals a notable upregulation in the expression of MerTK (both phosphorylated and total forms) in the right section, as compared to the left section of sham animals. The scale bar indicates a length of 100 μm, and the positive area of phosphorylated MerTK was quantified using ImageJ software. **b)** Mertk mRNA expression measured by real-time PCR normalized to the housekeeper m36B4 and **c)** protein abundance examined via Western blot. The protocol of statistical analysis is described in **Method**.

4.3.9 MerTK inhibition improved the pulmonary damage evaluated by histology

H&E results showed that the alveolar structure of wild type mice and Mertk-/- mice in saline treatment group was intact and there was no significant difference. The alveolar septum in BLM wild-type group was thickened and there was obvious inflammatory cell infiltration. However, in the BLM Mertk$^{-/-}$ group, the alveolar structure was still maintained, limited alveolar septum thickened and a small amount of alveolar fusion was observed. Compared with the BLM wild-type mice, the inflammation was significantly reduced in BLM Mertk$^{-/-}$ mice **(Figure 4.10a).**

Picrosirius Red staining and Gomori Trichome staining showed that the alveolar structure in both saline groups was complete, and no obvious blue collagen deposition was observed in the alveolar space. Compared with the saline groups, most of the alveolar structures of lungs in the BLM wild-type group were lost, and the lungs were significantly consolidated, with large amounts of blue collagen deposition in the interstitium, and the severity of fibrosis was significantly increased. But a small amount of collagen deposition was observed in the alveolar septum in the BLM Mertk$^{-/-}$ group, and the fibrosis was significantly limited than that in the BLM wild-type group **(Figure 4.10a).**

The quantitative analysis of Picrosirius Red staining was carried out by Image J software. The results showed that the pulmonary fibrosis of wild-type mice was significantly increased after BLM injection, while the fibrosis process was weakened after Mertk knockout, and the fiber deposition was significantly lower than that of wild-type mice **(Figure 4.10b).**

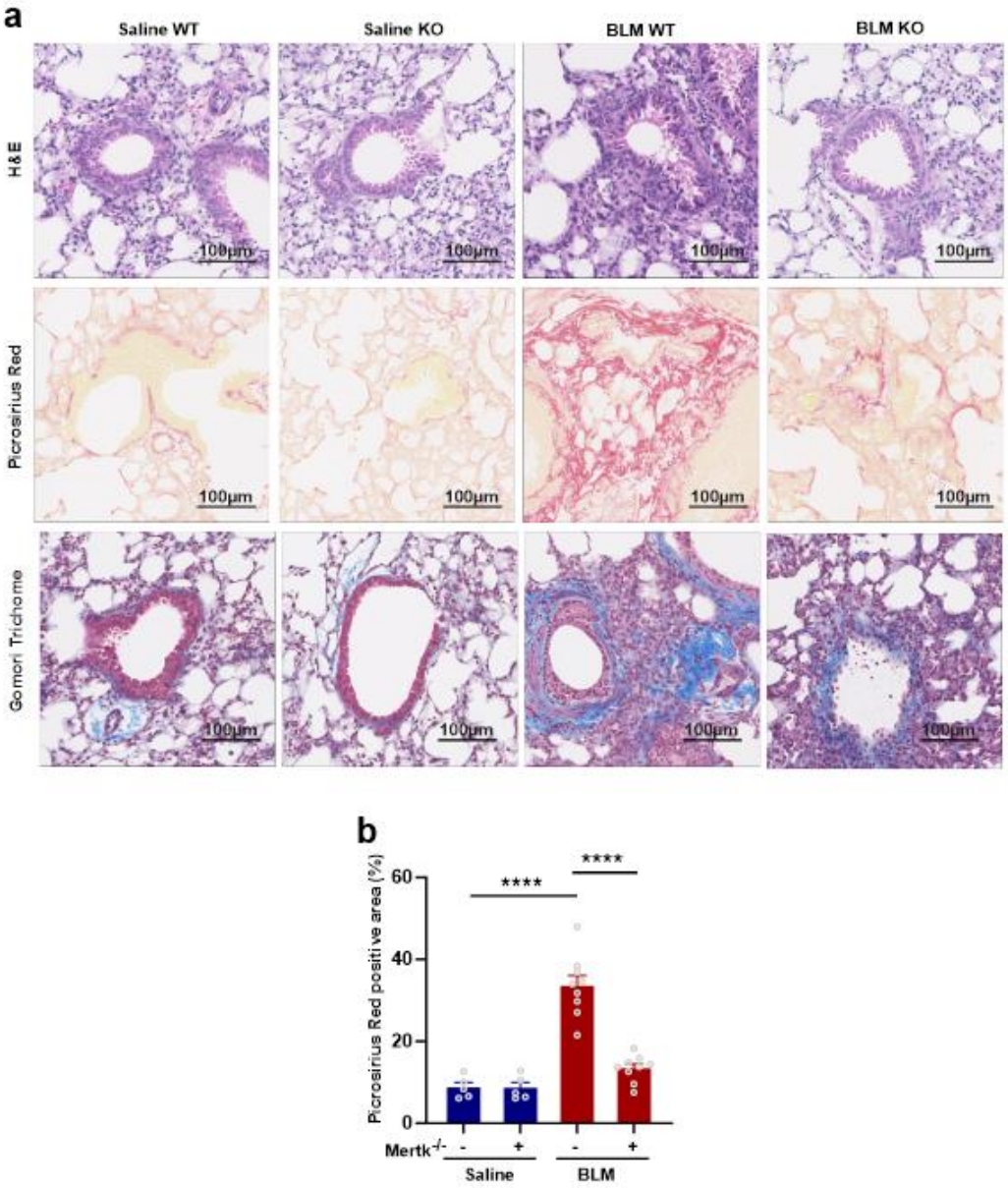

Figure 4.10 The impact of MerTK knockout on lung histology after BLM induction a) H&E staining, Picrosirius Red staining, Gomori Trichome staining were assessed in lung sections from wild-type or Mertk$^{-/-}$ mice 21 days after saline or bleomycin treatment and **b)** Picrosirius Red positive areas were quantified by ImageJ. The protocol of statistical analysis is described in **Method**.

4.3.10 MerTK inhibition attenuate hydroxyproline content increasing in BLM model

As an indicator of collagen content, I also tested the content of hydroxyproline in the lungs to complete a more accurate quantitative analysis of collagen in the lungs. In the pulmonary fibrosis model, there was no significant difference between the two genotypes of mice in the normal saline group. In the BLM group, hydroxyproline content of BLM wild-type mice was significantly increased, but that of Mertk$^{-/-}$ BLM mice was not significantly changed **(Figure 4.11).**

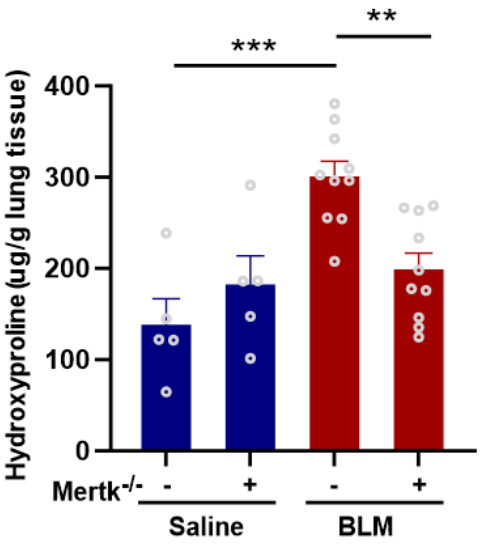

Figure 4.11 Hydroxyproline analysis of lung tissue subsequent to the genetic suppression of MerTK in the BLM model Hydroxyproline contents of lung were assessed by Hydroxyproline Assay Kit (Sigma) in wild-type or Mertk$^{-/-}$ mice 21 days after saline or bleomycin treatment. The protocol of statistical analysis is described in **Method**.

4.3.11 MerTK genetic inhibition attenuated fibrogenic markers expression in BLM

In order to further comprehensively analyze the expression changes of fibrosis-related genes in the BLM model, we continued to use RT-PCR to analyze four fibrosis markers (Acta2, Col1a1, Col1a2, Col3a1) and quantify their mRNA expression changes. The results showed that compared with wild-type mice, all the four markers of BLM Mertk$^{-/-}$ mice were significantly lower than wild-type BLM mice **(Figure 4.12).**

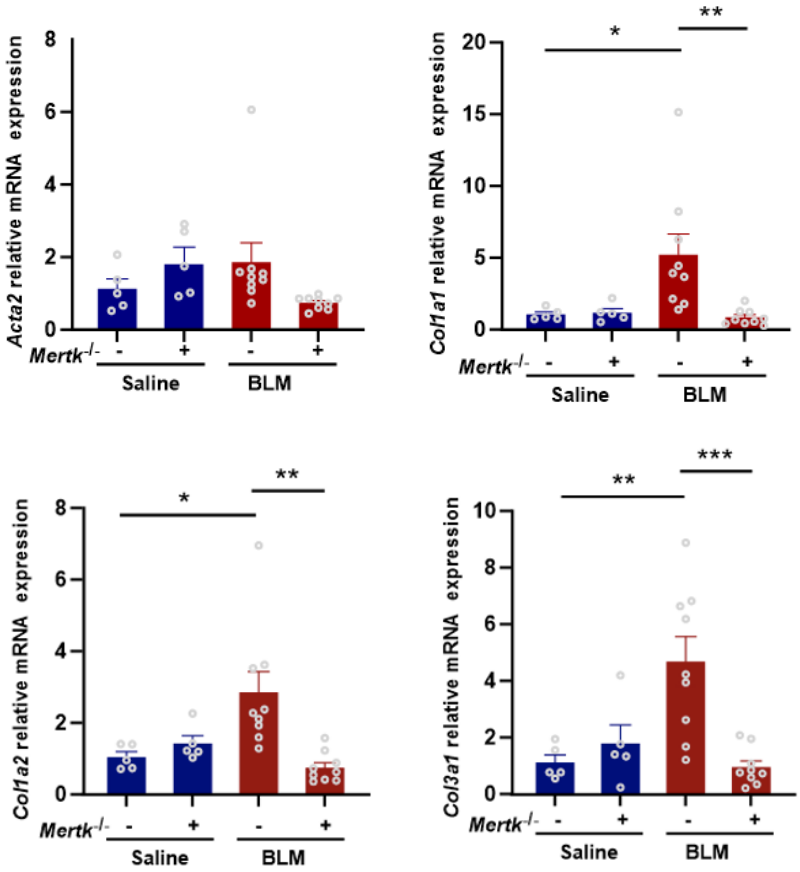

Figure 4.12 Suppression of MerTK results in a reduction of fibrotic markers expression in the BLM model Fibrosis relative markers mRNA (Acta2, Col1a1, Col1a2, Col3a1) expression are assessed by q-PCR in wild-type and Mertk$^{-/-}$ mice 21 days after saline or bleomycin treatment. The protocol of statistical analysis is described in **Method**.

4.3.12 MerTK inhibition decreased the expression of α-SMA in BLM model lung

Since α-SMA is one of the most important markers of fibrosis, it is necessary to analyze the change of α-SMA expression in pulmonary fibrosis. Immunohistochemistry **(Figure 4.13a)** and Western Blot **(Figure 4.13c)** were used to detect the effect of Mertk knockout on α-SMA expression in the lungs of BLM mice, and ImageJ software was used to quantitatively analyze the immunohistochemical staining results **(Figure 4.13b).**

Consistent with RT-PCR results, α-SMA protein had no significant difference between the two genotypes of mice in saline groups, and the expression level was very low. However, the expression in the BLM wild-type mice was significantly increased, while the expression level of BLM Mertk$^{-/-}$ mice was significantly lower than that of BLM wild-type mice.

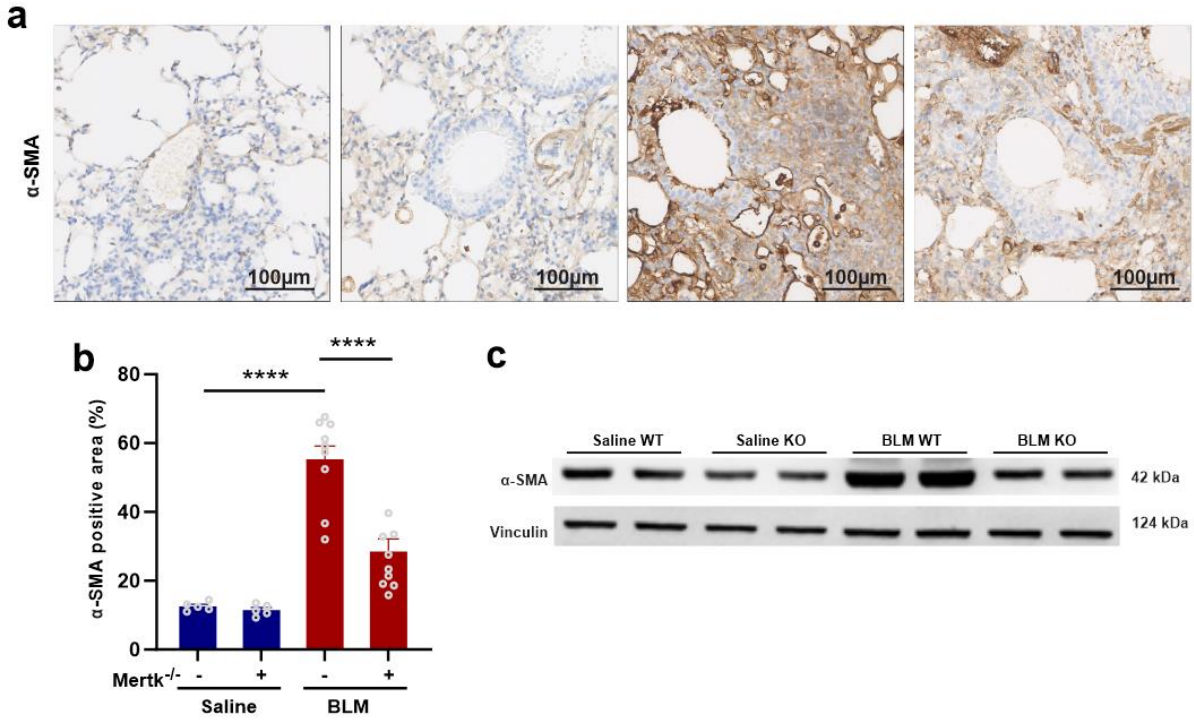

Figure 4.13 The impact of inhibiting MerTK on the expression of α-SMA in the lung of mice subjected to BLM a) α-SMA immunohistochemistry staining was assessed in lung sections and b) α-SMA positive area was quantified by ImageJ. c) Protein expression of α-SMA was assessed by Western blot in wild-type or Mertk$^{-/-}$ mice 21 days after saline or bleomycin treatment. The protocol of statistical analysis is described in **Method**.

4.3.13 MerTK inhibition decreased recruitment of pulmonary macrophages in BLM lung

Previous studies have shown that monocytes can infiltrate into the lung through systemic circulation and mature into macrophages in response to external signals, or can form pulmonary macrophage pools during inflammation or after the disappearance of resident lung macrophages [135, 136]. This activation and filling of macrophages is associated with pulmonary fibrosis [137].

Hence, I also detected the expression changes of F4/80 in the lungs of BLM model mice by immunohistochemistry **(Figure 4.14).**

The results showed that the lungs of BLM wild-type mice showed an obvious increase in inflammation and the aggregation of macrophages. On the contrary, the lung staining of BLM Mertk$^{-/-}$ mice was significantly weaker compared with wild-type mice.

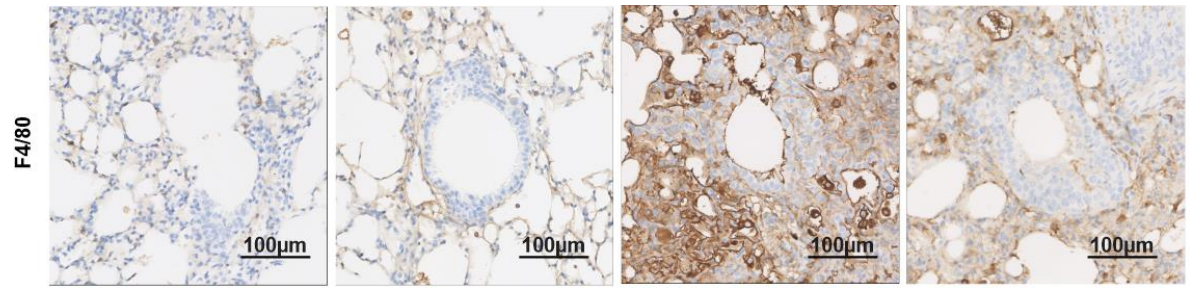

Figure 4.14 The impact of genetic suppression of MerTK on the staining of macrophage F4/80 in the BLM model Macrophage infiltration was assessed by F4/80 immunohistochemistry staining of lung sections from wild-type or Mertk$^{-/-}$ mice 21 days after saline or bleomycin treatment. (n=9 for BLM WT group, n=9 for BLM KO group and n=5 for Saline WT group, n=5 for Saline KO group)

4.3.14 MerTK genetic inhibition silenced AKT and ERK phosphorylation in BLM model

In order to verify whether MerTK mediates fibrosis in different organs by intervening in the same pathways, I also detected the changes in the phosphorylation levels of Akt and Erk1/2 in the lung tissues of BLM model mice by Western Blot. As expected, Mertk knockout significantly inhibited phosphorylation of Akt and Erk1/2 compared to the wild-type.

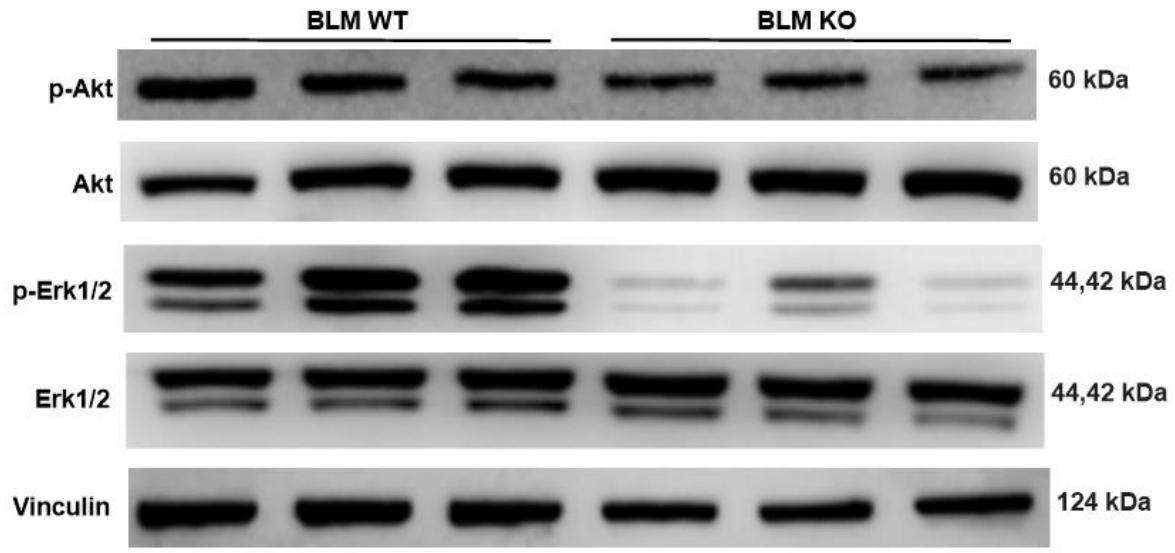

Figure 4.15 The genetic inhibition of MerTK results in the suppression of downstream signaling pathways in the BLM model Protein expression of p-Akt, Akt, p-Erk1/2, Erk1/2 were assessed by Western blot in wild-type mice and Mertk$^{-/-}$ mice 21 days after saline or bleomycin treatment. (n=9 for BLM WT group, n=9 for BLM KO group and n=5 for Saline WT group, n=5 for Saline KO group)

4.4 Discussion

The common final feature of CKD, which affects 10%–14% of the world's population, is renal fibrosis, but detecting it in time is difficult because of the lack of early clinical symptoms [138]. Moreover, there is still a lack of effective clinical treatment for it [17].

As detailed in this chapter, I first used the UUO model for renal fibrosis research. The application of UUO models in rodents is considered an effective means of simulating human chronic obstructive kidney disease in an accelerated manner and has therefore become one of the standard models for renal fibrosis [62].

Idiopathic pulmonary fibrosis is a chronic progressive disease [139] that can lead to loss of lung function, coughing and dyspnoea because of pulmonary fibrosis, thus affecting quality of life [140, 141]. Current IPF therapy can only slow disease progression, but the prognosis is very poor, and lung transplantation is far from meeting the demand [142]. As a result, patients with pulmonary fibrosis are heavily dependent on long-term healthcare services, which leads to a significant socioeconomic burden [143, 144]. All of these factors suggest that further research on pulmonary fibrosis is urgently needed.

As a drug used to treat different types of tumours [68], BLM can cause pulmonary toxicity, its most serious side effect, which can lead to lung remodelling, loss of lung function and, eventually, to death. Intratracheal injection of BLM-induced IPF in mice leads to patellar parenchymal inflammation, epithelial cell injury with reactive hyperplasia, epithelial-mesenchymal transformation, fibroblast activation and differentiation into myofibroblasts, basement membrane and alveolar epithelial injury [145].

As detailed in this chapter, through histology, RT-PCR, collagen quantification and Western blot, I proved that MerTK knockout had a positive effect on alleviating renal fibrosis caused by ureteral ligation and pulmonary fibrosis mediated by BLM.

Organ fibrosis is the end result of a complex biological process involving the interaction of many cell types, including macrophages and fibroblasts. F4/80 and α-SMA are widely used in mice as markers for these two kinds of cells, respectively [117, 129]. In terms of molecular mechanism, the inhibition of the fibrosis process by MerTK knockout may involve the combined action of these two types of cells. I detected the expression changes of these two markers in both the UUO and BLM models and found that knockout of MerTK significantly inhibited not only the activation of fibroblasts but also the recruitment of macrophages to the kidneys and lungs.

In summary, as detailed in this chapter, I used the UUO model and BLM injection model to confirm that MerTK is a promising therapeutic target in renal fibrosis and pulmonary fibrosis.

In the following chapters, I will clarify the mechanism of MerTK inhibition in alleviating organ fibrosis by combining various sequencing and bioinformatics methods.

Chapter5: MerTK regulates the fibrosis process by regulating core transcription and chromatin accessibility

5.1 Introduction

In the previous chapters, I identified MerTK as a novel nodal regulator of tissue fibrosis, yet the molecular mechanisms governing this effect are poorly understood. The etiology of tissue fibrosis is intricate, and recent findings suggest a crucial role for epigenetic factors [130]. Consistently, it has been observed that mice deficient in methyl-CpG-binding protein 2, which serves as a key epigenetic regulator, exhibit reduced fibrosis in various organs, such as the liver, lungs and heart [146, 147]. It has also been established that the epigenetic regulation of transcription plays a pivotal role in governing the fate of fibroblasts, determining whether they become activated or undergo resolution [146, 147].

The ability to physically interact with DNA is facilitated by the dynamic nature of chromatin, which is crucial for creating and preserving cellular identity. The accessibility of this landscape undergoes dynamic alterations in response to external stimuli and developmental cues. Recent evidence indicates that the maintenance of accessibility is regulated in a homeostatic manner, involving a competitive interplay between chromatin-binding factors and nucleosomes [148].

The concept of chromatin accessibility refers to the extent to which nuclear macromolecules may physically interact with DNA that is packaged into chromatin [149]. Chromatin accessibility is a key event in gene regulation [148]. This accessibility is influenced by several variables, including the presence and arrangement of nucleosomes, as well as other chromatin-binding proteins that restrict access to DNA [149].

Additionally, transcriptional regulatory networks provide insight into cellular behaviour by describing the interactions between transcription factors and their gene targets [148]. However, how this transcription remodelling of TGF-β signalling is driven by upstream chromatin landscape patterning remains elusive.

Therefore, defining the impact of MerTK deficiency on accessibility across various organs with fibrosis could provide an understanding of gene regulatory principles. To understand how MerTK regulates TGF-β signalling and, therefore, fibrosis, the experimental approach used in this study included RNA-seq and ATAC-seq to conduct a comparative analysis between the MerTK$^{-/-}$ condition and the WT condition. **Figure 5.1** illustrates the experimental design.

5.2 Method

5.2.1 RNA-seq

A) Generation of RNA-seq library: As previously described [103-106]. The isolation of total RNA from mouse tissue was performed using a commercially available RNA micro kit manufactured by Qiagen. The confirmation of RNA purity and integrity was conducted using the Agilent Bioanalyzer. The construction of sequencing libraries was conducted using the TrueSeq RNA sample preparation kit v2 (Illumina) with a total RNA input ranging from 100-500ng. In a general sense, the process involves the purification and fragmentation of mRNA, which is then used for the synthesis of cDNA. This is then followed by 3'-end adenylation. The specimens were linked to a distinct adapter and subjected to polymerase chain reaction (PCR) amplification. The libraries underwent validation, standardization, and sequencing procedures using the 2100 BioAnalyzer, a product manufactured by Agilent. A total of three bioreplicated RNA-seq libraries were subjected to sequencing on an Illumina HiSeq 2000 platform. Barcode multiplexing was used, and a read length of 100 base pairs was utilized for each experimental condition. Additionally, four bioreplicates were conducted for each condition.

B) High-throughput sequencing and analysis: As previously described [103-106]. The assessment of library sequencing quality was conducted using FastQC, a software tool developed by Babraham Bioinformatics (www.bioinformatics.babraham.ac.uk/). The process of trimming Illumina adaptor sequences and low-quality reads, wherein read pairs are eliminated if they include less than 20 base pairs, was carried out using Trim Galore!, a software tool developed by Babraham Bioinformatics. The STAR aligner[107] was used to map sequencing reads to the mouse genome (GRCm38/mm10) with the assistance of ENSEMBL gene annotations as a reference. The STAR option --quantMode GeneCounts was used to create read counts data that corresponds to ENSEMBL gene annotations. The studies were conducted

using the R Statistical Environment, specifically using the tidyverse package. In this study, the counts data underwent background correction and normalization for library size using the edgeR software. Differential gene expression (DGE) analysis was performed using the QLFtest 5 method, with a significance threshold of BH MTC adjusted $p < 0.05$ or uncorrected $p < 0.01$. The gene lists underwent functional annotation using GO pathways, utilizing the clusterProfiler program[108], with a significance threshold of adjusted p value <0.05.

5.2.2 ATAC seq

A) Generation of ATAC-seq library: As previously described in [104-106]. The mouse tissue samples were first homogenized to acquire intact nuclei. Subsequently, these nuclei were subjected to treatment with a highly active Tn5 transposable mutant. This mutant has the ability to concurrently label the target DNA with a sequencing adaptor, so accomplishing the fragmentation of the DNA, often referred to as "tagmentation." The process of labeling and library preparation was conducted using the ATAC-Seq Kit in accordance with the instructions given inside the kit. The nuclei were first enumerated and subjected to centrifugation at a temperature of 4°C and a speed of 500g for a duration of 5 minutes, resulting in the generation of aliquots comprising 50,000 to 100,000 nuclei. The samples were revived by adding 100 µl of ATAC Lysis Buffer, which was kept at a low temperature. To each sample, Tagmentation Master Mix was added 50 µl. The samples were then placed in a thermomixer and incubated at 800 rpm and 37°C for a duration of 30 minutes. The library was then created by the process of polymerase chain reaction (PCR) amplification of the labeled DNA, using a unique combination of Illumina's i7/i5 primers that are based on a Nextera adaptor. Ultimately, the library underwent purification by the use of SPRI bead washing. A total of two biological replicates were conducted for each condition.

B) ATAC-seq data analysis: As previously described in [104, 105]. The NovaSeq PE150 technology, operated by Novogene, was used to do paired-end 100bp sequencing. This process resulted in the generation of 30-40 million paired reads for each sample. Both ATAC-seq and Cut & Tag methodologies use a Nextera transposase sequence. The process of read alignment was conducted with Bowtie2 version 2.2.5[109], employing the GRCm38/mm10 reference sequence. The identification of peaks was carried out using the MACS2 software[110]. Peak difference analysis was conducted using a Homer software called getDifferentialPeaks, which may be accessed at http://homer.ucsd.edu/homer/. Subsequently, the annotation and enrichment of the identified peaks were done using the Homer program annotatePeaks.pl. The researchers used the Integrated Genomics Viewer (IGV)[111] to effectively visualize the ATAC sequencing (ATAC-seq) data.

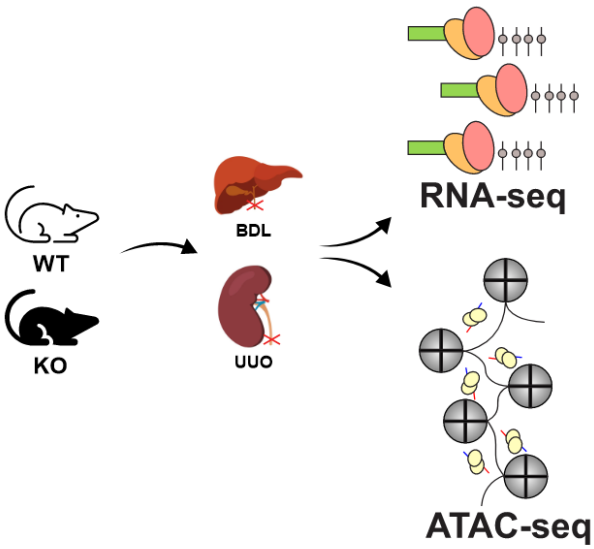

Figure 5.1 Scheme illustrating the experimental design

5.3 Results

5.3.1 MerTK regulates core transcription orchestrates liver fibrosis model

RNA-seq results showed that Mertk knockout resulted in significant transcriptional changes, with up to 3587 genes' expression changed, among which 1828 genes were increased, and 1759 genes were decreased **(Figure 5.2a).** Mertk knockout significantly reduced mRNA expression levels of liver transcription factors and signaling molecules that are important for liver fibrosis, including Col1a1, Col1a2, Acta2 and TGF-β, which expression in the liver of BDL Mertk$^{-/-}$ mice was close to the baseline level **(Figure 5.2b).**

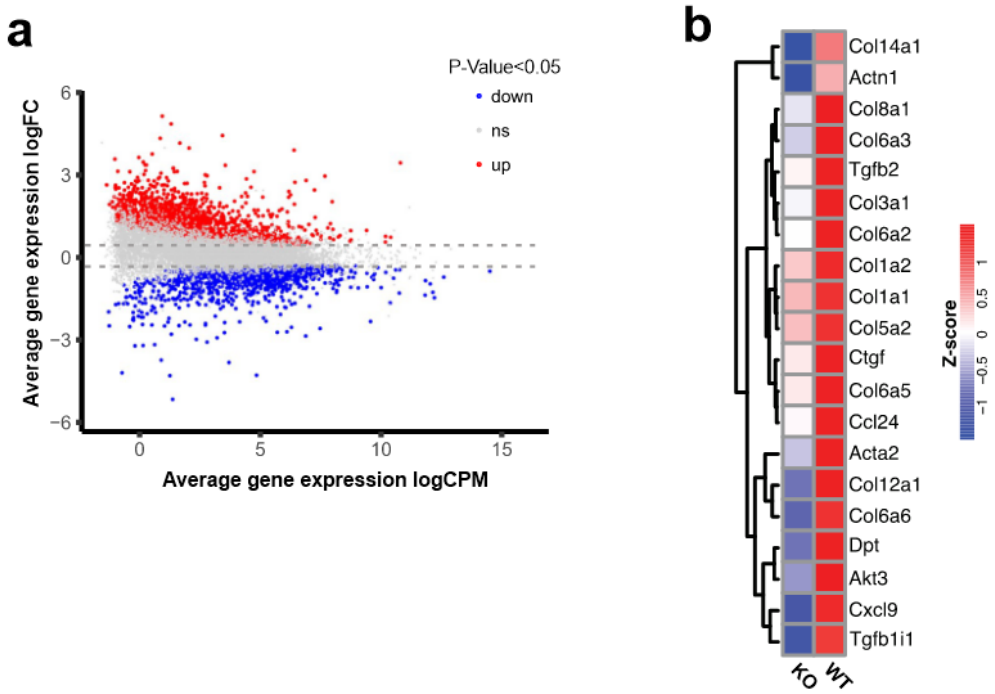

Figure 5.2 RNA-seq shows gene expression differentiation between WT and Mertk$^{-/-}$ mice in BDL model liver a) Volcano plot of the significant DEGs between the WT and MertK$^{-/-}$. **b)** Heatmap showing relative expression of the subset of fibrosis related genes.

5.3.2 MerTK regulates gene set enrichment in liver fibrosis model

Then, by further GSEA analysis of RNA-seq data, I found that, compared with Mertk$^{-/-}$ mice, a wide range of biological processes and cellular components that play a key role in myofibroblast activation and liver fibrosis, including TGF-β/SMAD signaling, the extracellular matrix and collagen generation related genes showed significant enrichment in WT mice.

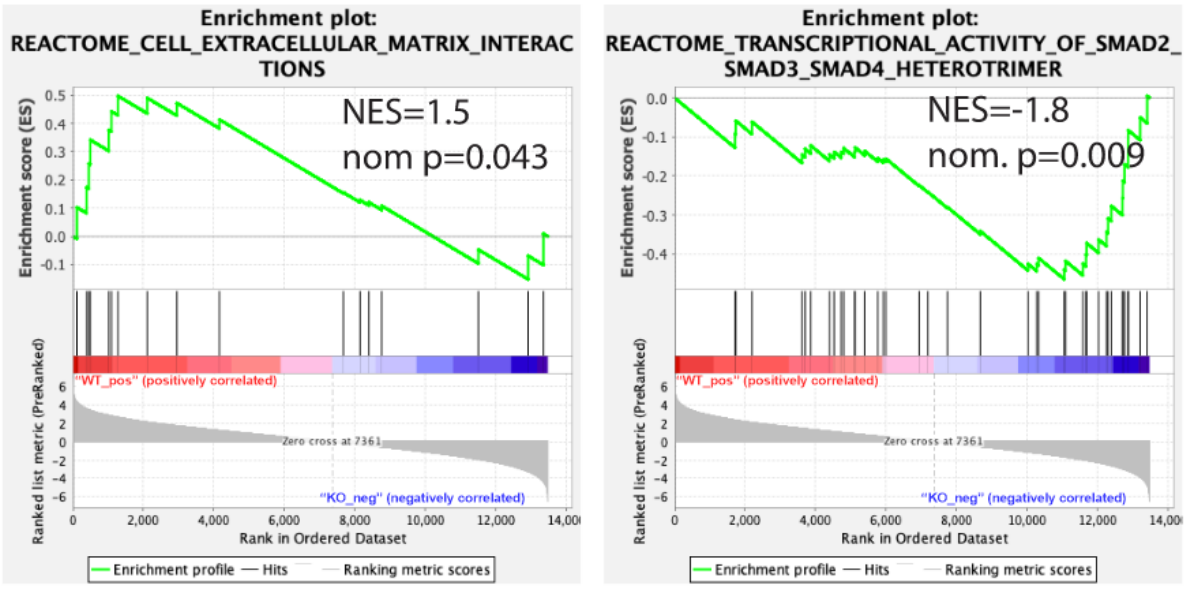

Figure 5.3 GSEA analysis in BDL model liver Gene set enrichment analysis (GSEA) analysis shows over-representation of genes encoding extracellular matrix relative pathway and transcriptional activity of SMAD2, SMAD3, SMAD4 heterotrimer in the WT.

5.3.3 MerTK regulates chromatin accessibility regulatory circuitry in liver fibrosis

In order to assess the impact of MerTK loss of function on the chromatin landscape of fibrosis-related genes, we conducted an investigation into alterations in chromatin accessibility between wild-type and Mertk-/- samples using ATAC-seq in liver tissues obtained from the BDL model. Heatmaps showed that chromatin remodeled after Mertk knockout, the MerTK depletion reduced chromatin accessibility significantly **(Figure 5.4a).**

Then I identified 7,741 regions of chromatin accessibility in all conditions, and I examined and searched for regions of chromatin accessibility that were differentially accessible. The results showed that 6573 chromatin regions were more accessible in Mertk-/- and 1168 chromatin regions were less accessible **(Figure 5.4b).**

Gene Ontology (GO) analysis to examine the annotated genes that are related with the open chromatin areas in the WT mice identified active biological processes implicated in the fibrosis process and TGF-β signalling, such as regulation of cell communication, MAPK kinase, SMAD2/3 and actin and collagen pathways **(Figure 5.4c).**

The analysis of motifs in the ATAC-seq peaks acquired by the wild-type revealed the presence of many members of the AP-1 transcription factor family, including JunB, Fra2, AP-1, Fosl2, and BATF, which were identified as the most prominent motifs. The study revealed a substantial enrichment of SMAD3 **(Figure 5.4d).**

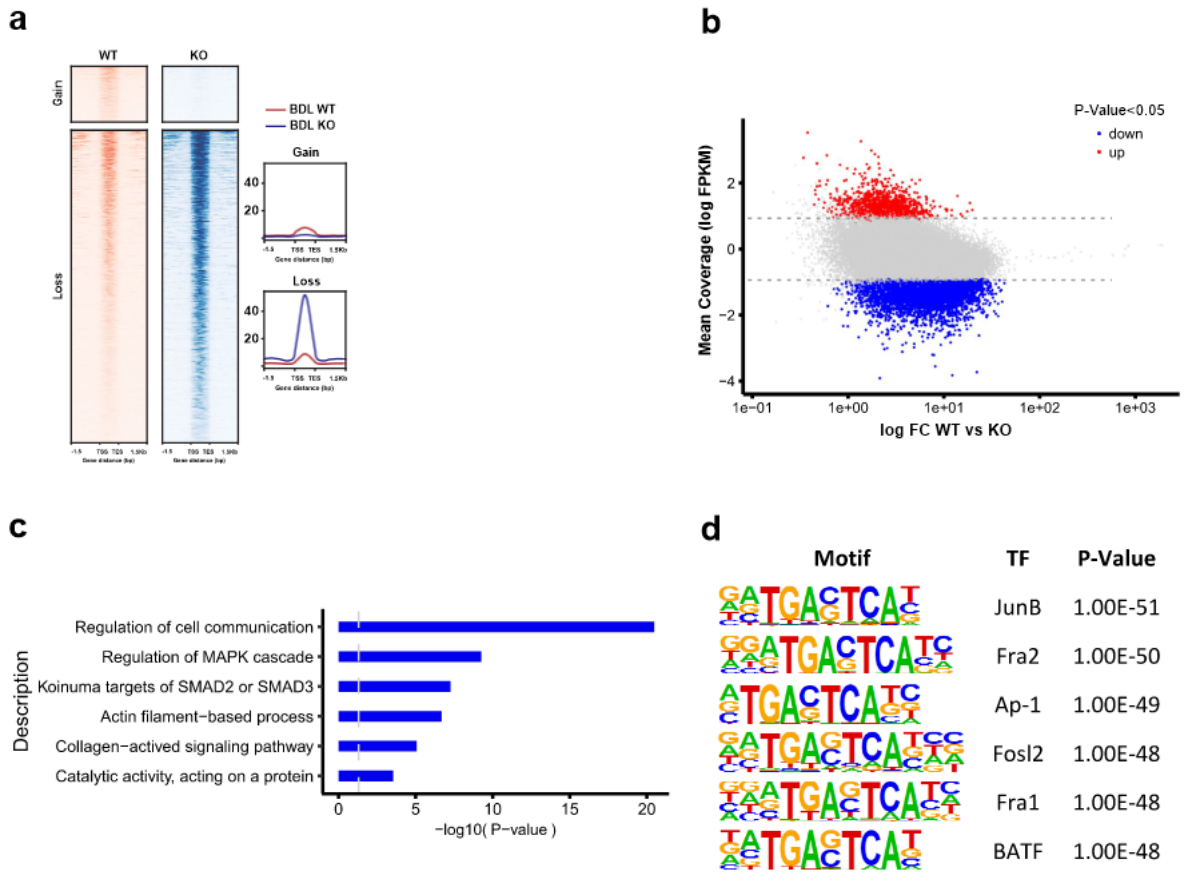

Figure 5.4 ATAC-seq shows the impact of Mertk knockout on the chromatin accessibility in liver fibrosis model a) Heatmap of ATAC-seq (±2 kb from peak center) in the WT and MertK$^{-/-}$. **b)** Volcano plot of the significant differential peaks between the WT and MertK$^{-/-}$. **c)** The subset of differential peaks acquired in the ATAC-seq analysis in the WT samples exhibited enrichment in gene ontology categories. **d)** The chromatin areas exhibiting enhanced accessibility on the wild-type are enriched with transcription factor (TF) motifs.

5.3.4 MerTK regulates transcription and chromatin accessibility correlation in liver fibrosis

I examined if Mertk deficiency mediated changes in gene expression is via chromatin changes. A significant correlation was observed between the group of genes exhibiting variable expression and the group of genes located in close proximity to differently accessible areas, including a total of 770 genes **(Figure 5.5a).** The confirmation of this link was further substantiated by the association of each accessible chromatin region with its proximal genes. From a global standpoint, a noteworthy and measurable correlation was established between the extent of change in mRNA expression and the corresponding alteration in accessibility around each gene locus **(Figure 5.5b).**

Then I applied GO analysis to these 770 shared genes between RNA-Seq and ATAC-Seq and identified key fibrosis related biological pathways including extracellular matrix, integrin cell surface interaction and collagen chain trimerization **(Figure 5.5c).** Considering individual genes, several key genes associated with fibrosis, such as Col1a1, were observed to have down-regulated mRNA expression and decreased accessibility simultaneously in $Mertk^{-/-}$ **(Figure 5.5d).**

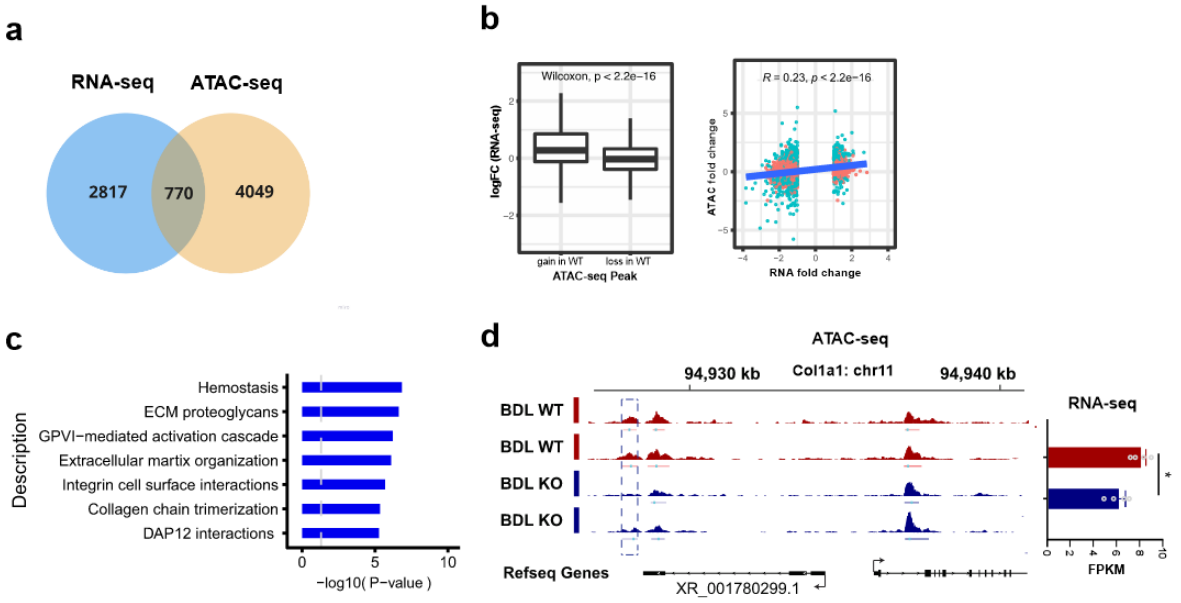

Figure 5.5 Mertk knockout regulates core transcription and chromatin accessibility correlation in liver fibrosis a) Venn Diagram of DEG and differential peaks in the RNA-Seq and ATAC-Seq. **b)** The correlation between accessibility and gene expression level. **c)** Gene ontology categories enriched in the subset of WT- gained shared genes between the RNA-Seq and ATAC-seq. **d)** The browser displays tracks containing ATAC-seq data corresponding to the specified genomic locations. The peaks are visually emphasized by black boxes.

5.3.5 MerTK regulates core transcription orchestrates kidney fibrosis model

Since I have shown that MerTK is an important driver of fibrosis in multiple organs. To explore whether transcription and chromatin effects lacking in MerTK have positive effects against fibrosis in different organs. To this end, we also performed RNA-seq and ATAC-seq in the renal fibrosis model UUO to compare the differences between Mertk$^{-/-}$ and WT mice. Similarly, Mertk knockout significantly reduced mRNA expression levels of kidney transcription factors and signaling molecules that have key role in kidney fibrosis, including Col6a6, Col6a5, Col11a2 which expression in the kidney of UUO Mertk$^{-/-}$ mice was close to the baseline level **(Figure 5.6).**

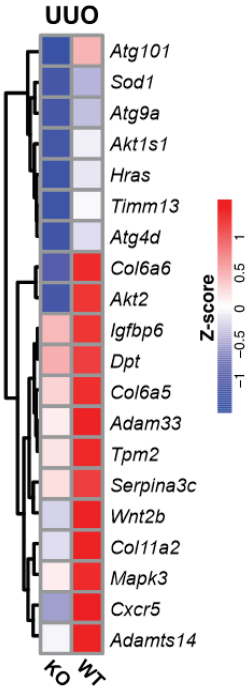

Figure 5.6 RNA-seq shows gene expression differentiation between WT and Mertk$^{-/-}$ mice in UUO model kidney Heatmap showing relative expression of the subset of fibrosis related genes.

5.3.6 MerTK regulates gene set enrichment in kidney fibrosis model

Then, further applying GSEA analysis to RNA-seq data, I found that, compared with Mertk$^{-/-}$ mice, a wide range of biological processes and cellular components that play a key role in myofibroblast activation and kidney fibrosis, including TGF-β/SMAD signaling, the extracellular matrix and collagen generation related genes showed significant decreasing in Mertk$^{-/-}$ compared with WT mice.

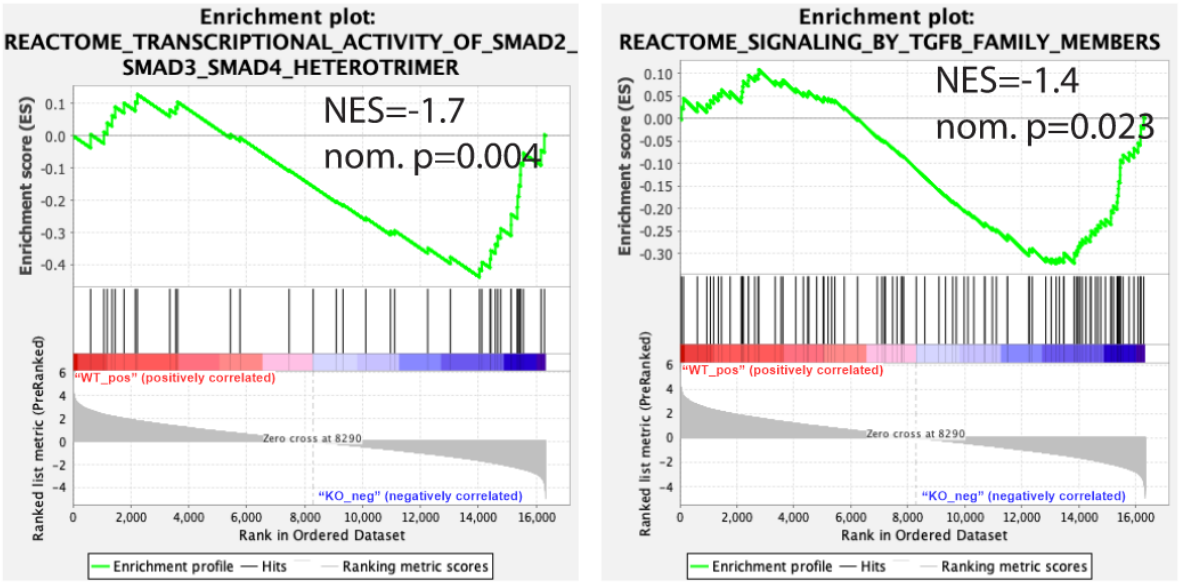

Figure 5.7 GSEA analysis in UUO model kidney Gene set enrichment analysis (GSEA) analysis shows underproportion of genes encoding transcriptional activity of SMAD2, SMAD3, SMAD4 heterotrimer and signaling by TGF-β family members in the Mertk$^{-/-}$ mice.

5.3.7 MerTK regulates chromatin accessibility regulatory circuitry in kidney fibrosis

In order to assess the potential impact of MerTK loss of function on the chromatin landscape of genes associated with fibrosis, we conducted an investigation into alterations in chromatin accessibility between wild-type and $Mertk^{-/-}$ samples using ATAC-seq. This analysis was performed on kidney tissues obtained from the UUO model. Heatmaps showed chromatin remodeled after Mertk knockout, the MerTK depletion reduced chromatin accessibility significantly (**Figure 5.8a**).

GO analysis to investigate the functional characteristics of annotated genes that are linked to the open chromatin areas seen in wild-type mice identified active biological processes implicated in the fibrosis process and TGF-β signalling, such as regulation of cell communication, MAPK kinase, SMAD2/3 and actin and collagen pathways (**Figure 5.8b**).

The browser tracks revealed a significant reduction in chromatin accessibility of the major fibrosis gene, Clo1a2, at the identified loci after MerTK depletion in ATAC-seq data (**Figure 5.8c**).

The analysis of motifs in the ATAC-seq peaks acquired by the wild-type revealed the presence of many members of the AP-1 transcription factor family, including JunB, Fra2, AP-1, Fosl2, and BATF, which were identified as the most prominent motifs. The enrichment of SMAD3 was shown to be statistically significant in the kidney of wild-type mice subjected to UUO (**Figure 5.8d**).

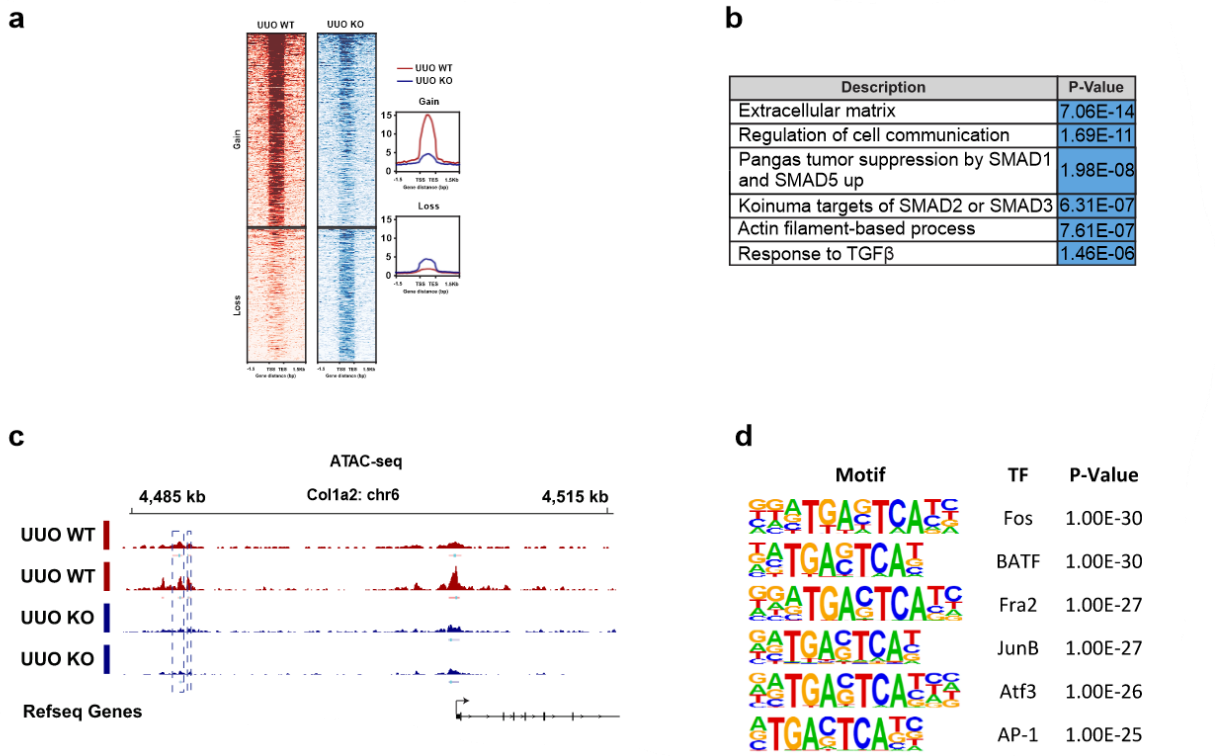

Figure 5.8 ATAC-seq shows the impact of Mertk knockout on the chromatin accessibility in kidney fibrosis model a) A heatmap was generated to visualize the ATAC-seq signal within a ±2 kb region centered around the peak in both the wild-type and MertK$^{-/-}$ samples in the UUO model. **b)** The gene ontology categories that exhibit enrichment in the subset of differentially acquired peaks in the ATAC-seq analysis of wild-type samples. **c)** The browser displays tracks that depict ATAC-seq data at the specified genomic locations. The peaks are visually emphasized by black boxes. **d)** The chromatin areas exhibiting enhanced accessibility on the wild-type display an enrichment of transcription factor (TF) motifs.

5.3.8 MerTK regulates transcription and chromatin accessibility correlation in kidney fibrosis

In the kidney fibrosis model, I have additionally validated the correlation between each accessible chromatin area and its proximal genes. From a global standpoint, a noteworthy and measurable correlation was established between the degree of alteration in mRNA expression and the degree of change in accessibility around each gene locus (**Figure 5.9**).

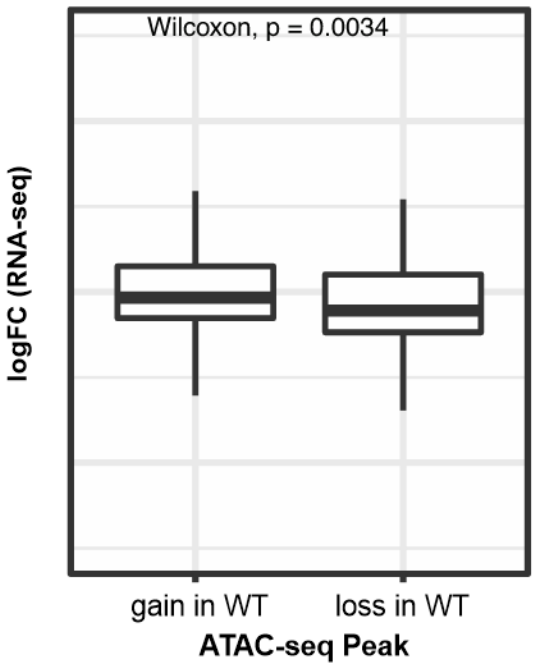

Figure 5.9 Mertk knockout regulates core transcription and chromatin accessibility correlation in liver fibrosis The correlation between accessibility and gene expression level in UUO model.

5.3.9 RNA-seq and ATAC-seq show shared core pathways in multiple organ fibrosis

Lastly, I explored the core transcriptional and chromatin accessibility pathways that are differentially enriched in the comparison of Mertk$^{-/-}$ and WT mice across the two organs (liver (BDL) and kidney (UUO)). Interestingly, this analysis revealed an enrichment of TGF-β signalling and transcriptionally activity of SMAD2/SMAD3 in both the RNA-Seq **(Figure 5.10a)** and ATAC-Seq **(Figure 5.10b).**

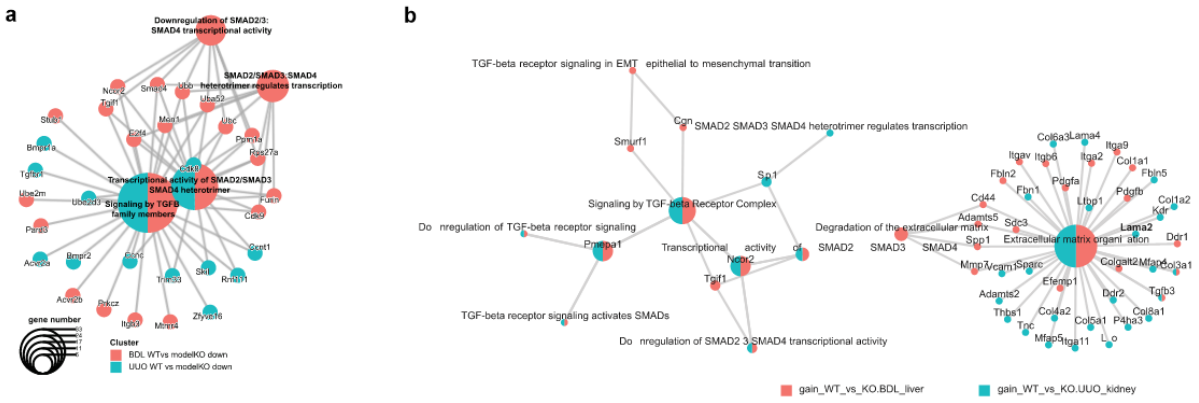

Figure 5.10 Shared core pathway in multiple organ fibrosis generated through RNA-seq and ATAC-seq a) Differential gene expression (DEG) pathways between liver fibrosis (BDL) and kidney fibrosis (UUO) models comparing WT and Mertk$^{-/-}$ showing enrichment of TGF-β/SMAD pathway. **b**) differential peaks pathways between liver fibrosis (BDL) and kidney fibrosis (UUO) models comparing WT and Mertk$^{-/-}$ showing enrichment of TGF-β/SMAD pathway.

5.4 Discussion

Transcriptome sequencing, also known as RNA-seq, is a significant methodology used in transcriptome investigations using high-throughput sequencing systems. This approach enables the quantification of gene expression levels by analysing the sequencing data obtained from each gene [150]. Several recent studies have used RNA-seq to quantify transcriptome alterations associated with illnesses or to differentiate between subtypes. This approach has significantly contributed to the understanding of the molecular pathophysiology of complex diseases at the RNA level [151, 152].

As detailed in this chapter, I first sequenced liver fibrosis and kidney fibrosis tissue using RNA-seq and then compared different conditions in each of the models. The respective mRNA expressions in the liver and kidneys consistently showed significant differences after MerTK knockout. The transcription levels of a series of key genes involved in myofibroblast activation and fibrosis in the respective organs were significantly reduced after MerTK knockout. GSEA analysis also confirmed that the gene sets for a range of biological processes associated with fibrosis were significantly downregulated in both organ fibrosis models of $MerTK^{-/-}$ mice.

ATAC-seq is a technique in molecular biology developed in 2013 to evaluate genome-wide chromatin accessibility [153]; it is a fast and sensitive method for epigenome analysis [154]. ATAC-seq is used to detect DNA sections that are accessible, or open, within the chromatin structure, which is achieved by the utilisation of a hyperactive mutant Tn5 transposase that facilitates the insertion of sequencing adapters into the open portions of the genome [154, 155], followed by DNA fragment purification, PCR amplification and next-generation sequencing techniques to complete the sequencing [156]. Sequencing readings are used to infer areas of increased accessibility and to map areas of transcription factor binding sites and nucleosome locations [154]. At single nucleotide resolution, the number of reads in a region correlates with the degree of chromatin openness [154].

Therefore, in the next step, I used ATAC-seq to examine further the effect of MerTK knockout on transposase-accessible chromatin in these two models. The results also supported that a series of key pathways related to fibrosis, such as cell communication, MAPK kinase, SMAD2/3, and actin and collagen, are suppressed in the fibrosis process of both organs because of MerTK knockout. At the same time, the transcription accessibility of some key genes involved in these biological processes was significantly decreased in MerTK$^{-/-}$ mice.

Interestingly, when I combined the RNA-seq and ATAC-seq data to explore the underlying correlations, I found a high degree of consistency between mRNA expression and transcription accessibility.

The pathway analysis of the two organs showed a significant overlap. Based on RNA-seq and ATAC-seq, respectively, the core sharing pathway network of the two organs in the process of fibrosis was successfully constructed, in which TGF-β signalling and the transcriptional activity of SMAD2/SMAD3 were in the core position. Collectively, these results demonstrated that MerTK regulates TGF-β core transcription regulatory circuitry and orchestrates fibrosis by modulating chromatin accessibility.

Chapter6: MerTK inhibition increases promoter-proximal Pol II pausing and promotes chromatin remodelling

6.1 Introduction

The phenotypic variation of an organism is derived through a cellular network of epigenetic alterations that regulate cell plasticity during cell differentiation [130]. In human disease, including fibrosis, stress-induced signalling converges in the nucleus, leading to chromatin remodelling and altered gene expression, maladaptive cell state transitions and organ dysfunction [157].

Aberrant promoter and enhancer activity has been implicated in fibrosis, and chromatin remodelling can influence neighbouring cells through noncell autonomous mechanisms, fuelling a pathological cross-talk between diverse cellular compartments [158]. Additionally, the transcription of protein-coding genes is a highly regulated process carried out by a large, multicomplex RNA Pol II [159].

Single-cell transcriptomics is a powerful tool for identifying cell types that are particularly vulnerable in disease states and for examining both cell-autonomous and noncell-autonomous changes. Advancements in single-cell RNA sequencing (scRNA-seq) and single-cell assay for transposase-accessible chromatin sequencing (scATAC-seq) techniques have facilitated the examination of transcriptomic and epigenomic chromatin accessibility patterns in a vast quantity of individual cells with high resolution at the single-cell level [160]. ScRNA-seq studies have demonstrated the presence of a substantial variability of gene transcripts within individual cells, thereby offering valuable insights into the expression profile of gene transcripts at the cellular level. On the other hand, scATAC-seq analysis enables the identification of alterations in the accessibility of chromatin, thereby providing valuable insights into the regulation of gene expression at the epigenomic level across the entire genome [160].

The ability to perform simultaneous and integrated analyses of scRNA-seq and scATAC-seq data presents a unique opportunity to gain valuable insights. These insights have the

potential to drive the advancement of therapeutic strategies aimed at specifically inhibiting profibrotic states in specific cell compartments. This approach may prove advantageous in addressing a diverse range of diseases characterised by chronic fibrosis and maladaptive tissue remodelling.

To address this concern, as detailed in this chapter, I performed CUT&Tag for four histone marks that are key to the control and definition of promoters and enhancers, in addition to CTCF and RNA Pol II that control RNA transcription in liver tissue from WT and MerTK$^{-/-}$ mice. **Figure 6.1** illustrates the experimental design. I also complemented these studies by undertaking single-cell multiome sequencing (scRNA-seq and scATAC-seq).

6.2 Method

6.2.1 Generation of CUT&Tag-seq library

As previously described in [104, 105]. The mouse tissue samples were first subjected to homogenization. Then, aliquots containing around 100,000 cells were produced and treated with wash buffer containing protease inhibitor cocktail. The cells were coalesced with concanavalin A beads and subjected to an overnight incubation with a primary antibody at a temperature of 4℃. Following incubation with the antibody, the chromatin underwent direct cleavage, followed by tagmentation utilizing protein A-Tn5 (pA-Tn5) transposition, and subsequent preparation of NGS libraries. The labelling and library preparation process was conducted using the CUT&Tag-ITTM assay kit (catalog No. 53160, Active Motif), following the instructions provided with the kit. A total of two biological replicates were conducted for each experimental condition.

6.2.2 High-throughput CUT&Tag sequencing analysis

As previously described in [104, 105]. The NovaSeq PE150 technology, operated by Novogene, was used to do paired-end 100bp sequencing. This process resulted in the generation of 30-40 million paired reads for each sample. Both ATAC-seq and Cut & Tag methodologies use a Nextera transposase sequence. The process of read alignment was conducted with Bowtie2 version 2.2.5[109], employing the GRCm38/mm10 reference sequence. The identification of peaks was carried out using the MACS2 software[110]. Peak difference analysis was conducted using a Homer software called getDifferentialPeaks, which may be accessed at http://homer.ucsd.edu/homer/. Subsequently, the annotation and enrichment of the identified peaks were done using the Homer program annotatePeaks.pl. The researchers used the Integrated Genomics Viewer (IGV)[111] to effectively visualize the ATAC sequencing (ATAC-seq) and Cut & Tag sequencing (Cut & Tag seq) data.

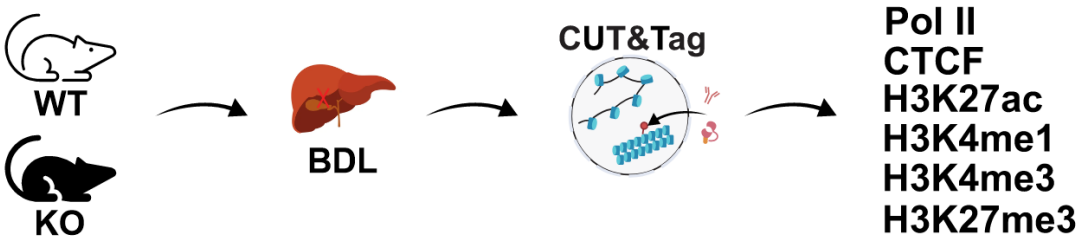

Figure 6.1 Scheme illustrating the experimental design

6.3 Results

6.3.1 Mertk knockout changes the landscape of subset of genes in liver fibrosis model

In order to investigate the potential correlation between the down-regulation of the MerTK-dependent transcriptome and alterations in the RNA Pol II chromatin binding profile, I conducted Pol II CUT&Tag-seq (cleavage under targets and tagmentation sequencing) assays using liver samples from both wild-type and Mertk-/- mice. Interestingly, samples lacking Mertk exhibited elevated levels of Pol II loading at promoters. In order to examine the regulatory role of MerTK in Pol II pausing, an assessment was conducted on the expression levels of established pausing variables. The hepatic expression of Cdk9, components of the NELF complex, and Med26 was shown to be considerably greater in Mertk-/- mice. According to recent research findings, it has been shown that the DNA-binding protein known as CCCTC-binding factor (CTCF) has a role in facilitating the pausing of RNA polymerase II (Pol II) [161]. Consequently, we conducted CTCF CUT&Tag-seq. Consistently, the deletion of Mertk resulted in a significant increase in the CTCF peaks when compared to the wild-type condition (**Figure 6.2**).

The process of Paused Pol II effectively catches enhancer activity and functions as a very effective insulator[162]. Previous studies implicate regulatory enhancers as key genomic mediators of tissue fibrosis [163] and our *in-vitro* data suggested an epigenetic interaction between TGF-β and MerTK pathways. To further investigate whether epigenetic pathways are important for the MerTK profibrotic response, we used CUT&Tag to assess active (H3K27ac, H3K4me3 and H3Kme1) and repressed chromatin (H3K27me3) to generate a comprehensive map of chromatin states in Mertk$^{-/-}$ **(Figure 6.2).** I observed that MerTK deficiency led to widespread alterations affecting the hepatic H3K27ac and H3K4me1 histone marks primed enhancers, but with less impact on H3K4me3 (active promoters) and H3K27me3 (repressive marks) **(Figure 6.2).**

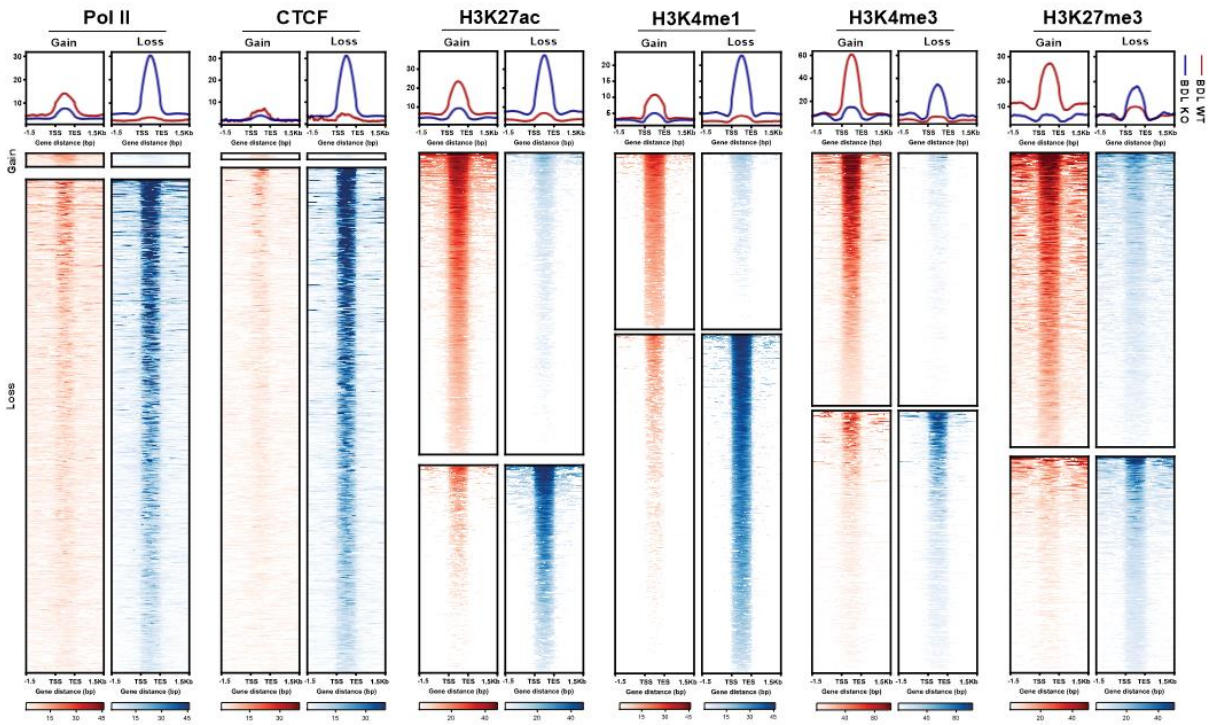

Figure 6.2 The landscape of subset of genes in liver fibrosis model generated by CUT&Tag-seq Heatmaps of CUT&Tag-seq of pol II, CTCF, H3K27ac, H3K4me1, H3K4me3 and H3K27me3 (±1.5 kb from peak center) in WT mice and Mertk$^{-/-}$ mice of BDL model.

6.3.2 Mertk knockout reverses TF binding motifs enrichment in liver fibrosis

The motif studies conducted on the Pol II peaks obtained by the wild-type revealed a group of transcription factor members, including Fra2, PU-1, Fra1, SpiB, AFT3, and JunB, which emerged as the highest-ranking motifs. Motif analyses of the WT-gained CTCF peaks also identified CTCF as the top-ranking motif, demonstrating specificity of the signal **(Figure 6.3).**

Closer examination of the transcription factors binding sites for both H3K27ac, H3K4me1 revealed a overlapping enrichment in motifs for prominent profibrotic transcription factors such as those factors belonging to the ETS family (PU.1, ETS1, SPiB, ETV1) (**Figure 6.3**); SMAD3 was also significantly enriched. Of the ETS members, PU.1 has been strongly implicated as a regulator of fibrosis in multiple organs [164].

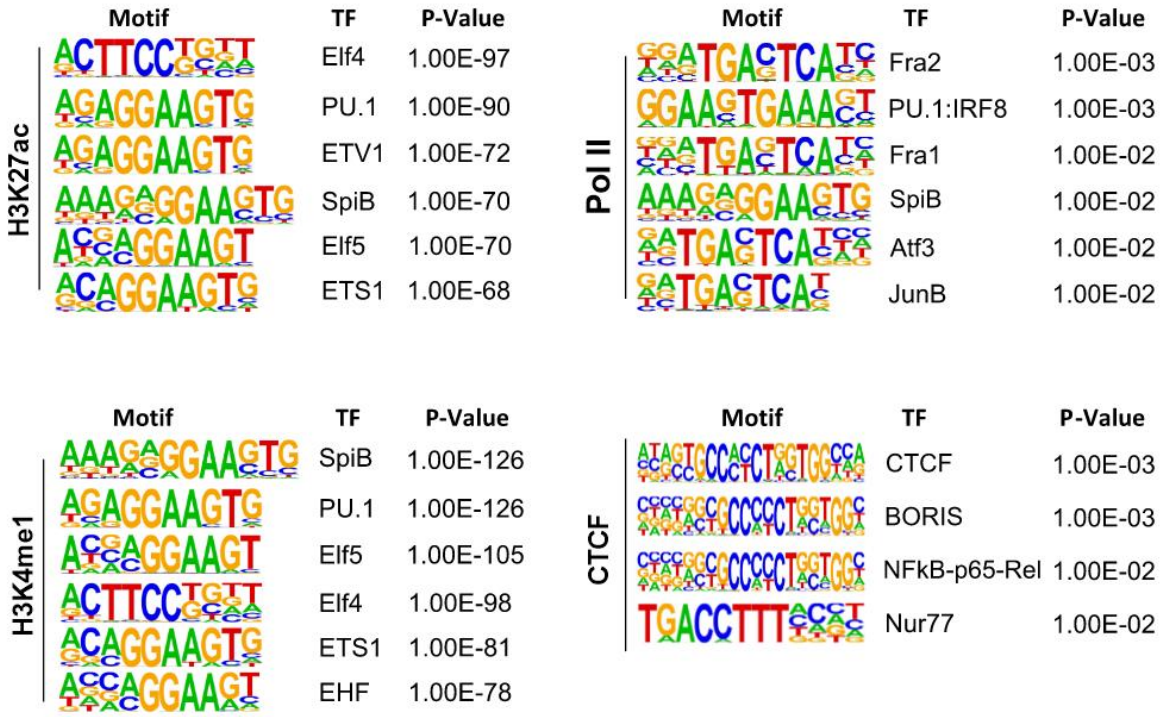

Figure 6.3 The effect of TF binding motifs enrichment caused by Mertk knockout in liver fibrosis TF binding motifs are shown to be significantly enriched in genomic regions where wild-type samples have differential peaks enrichment in histone modifications H3K27ac, H3K4me1, Pol II, and CTCF.

6.3.3 Mertk knockout shows consistent tendency between Pol II CUT&Tag-seq tag density and ATAC-seq tag density

The above results indicate that the observed decrease in transcriptome activity was not a consequence of diminished recruitment of Pol II to promoters or impaired transcription start. Rather, it was associated with an elevation in Pol II pausing in close proximity to the promoters. To determine whether transcribing Pol II contributes to chromatin accessibility, I investigated the global relationship between transcription initiation (via changes in Pol II signal changes) and changes in chromatin accessibility (via ATAC-seq data). I detected a very weak but significant positive correlation between them (R=0.044) **(Figure 6.4).** Thus, MerTK modulates chromatin accessibility, irrespective of Pol II transcription initiation.

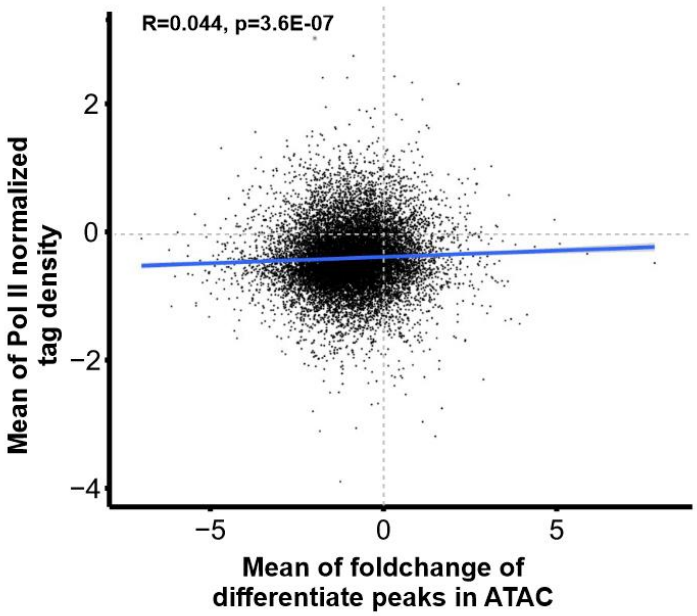

Figure 6.4 Correlation of normalized Pol II CUT&Tag-seq tag density and ATAC-seq tag density The presented data showcases the correlation between the normalized tag density of Pol II CUT&Tag-seq and ATAC-seq in both Mertk-/- and WT samples. Additionally, a linear regression line is shown to illustrate the relationship between ATAC-seq and Pol II.

6.3.4 Mertk knockout enhances genes pausing ratio

In order to validate the impact of Mertk knockout on Pol II pause release, we conducted an analysis to construct the pausing index. This included calculating the ratio of Pol II occupancy at promoters and gene body regions[165]. The present investigation demonstrated that the absence of Mertk resulted in an increased Pol II pausing index, as seen in **Figure 6.5**. The findings supported that the observed decrease in transcription, resulting from MerTK loss in liver fibrosis, can be attributed to an upregulation of promoter-proximal Pol II pausing.

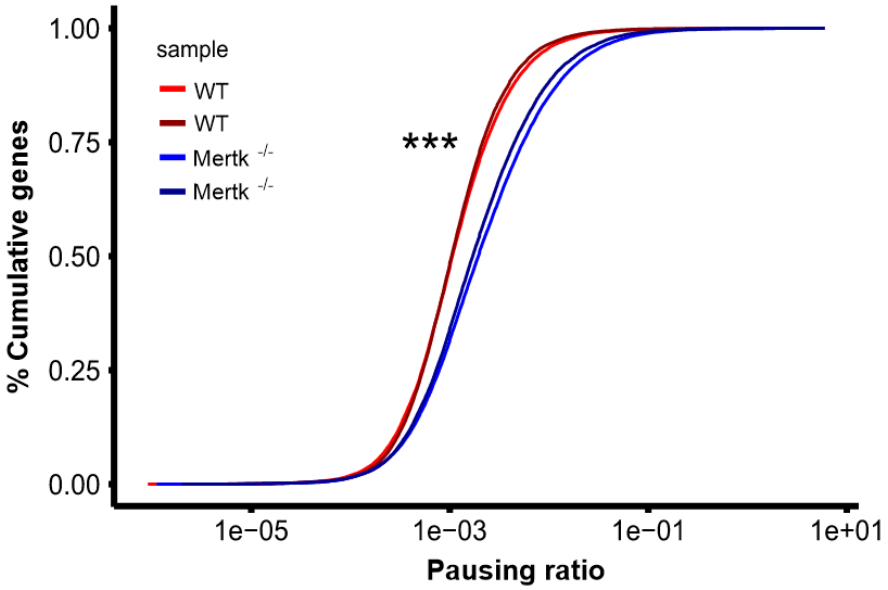

Figure 6.5 Plot representing the pausing index The data presented in the study demonstrates a significant increase in the pausing ratio in the correct direction across all genes in Mertk$^{-/-}$ group as compared to the wild-type group.

6.3.5 Mertk knockout shows consistent tendency between Pol II pausing index and CTCF CUT&Tag-seq tag density

For further confirmation, we examined the correlation between CTCF signal changes and the level of pausing of Pol II. Our data showed that both are positively correlated (R^2= 0.14, $p<2.2x10^{-16}$) **(Figure 6.6).** Thus, deficiency of MerTK regulates Pol II pausing likely via CTCF.

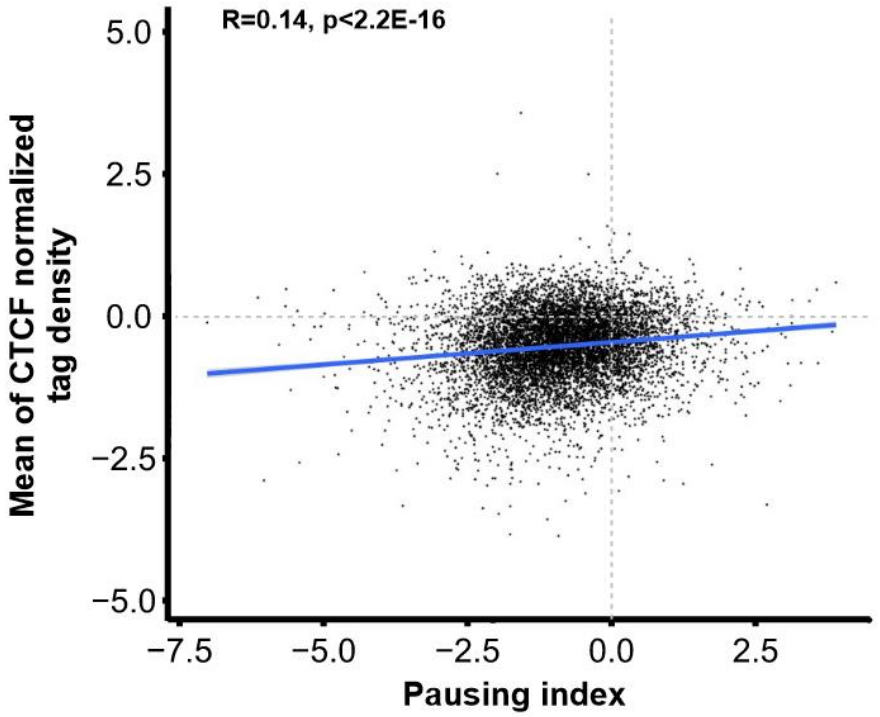

Figure 6.6 Correlation of normalized Pol II pausing index and CTCF CUT&Tag-seq tag density Correlation between normalized Pol II pausing index and CTCF CUT&Tag-seq tag density in the $Mertk^{-/-}$ and WT and the linear regression line between CTCF and Pol II pausing index is shown.

6.3.6 CUT&Tag-seq identified different chromatin states

To further define the impact of MerTK deficiency on the joint chromatin state, We used ChromHMM to define chromatin states with a multivariate hidden Markov model (HMM) [166]. The methodology used in this study involves the assessment of the collective occurrence or non-occurrence of histone modifications in order to develop chromatin state models. I identified 10 chromatin states as active or inactive with combinations of our four histone tags (**Figure 6.7**).

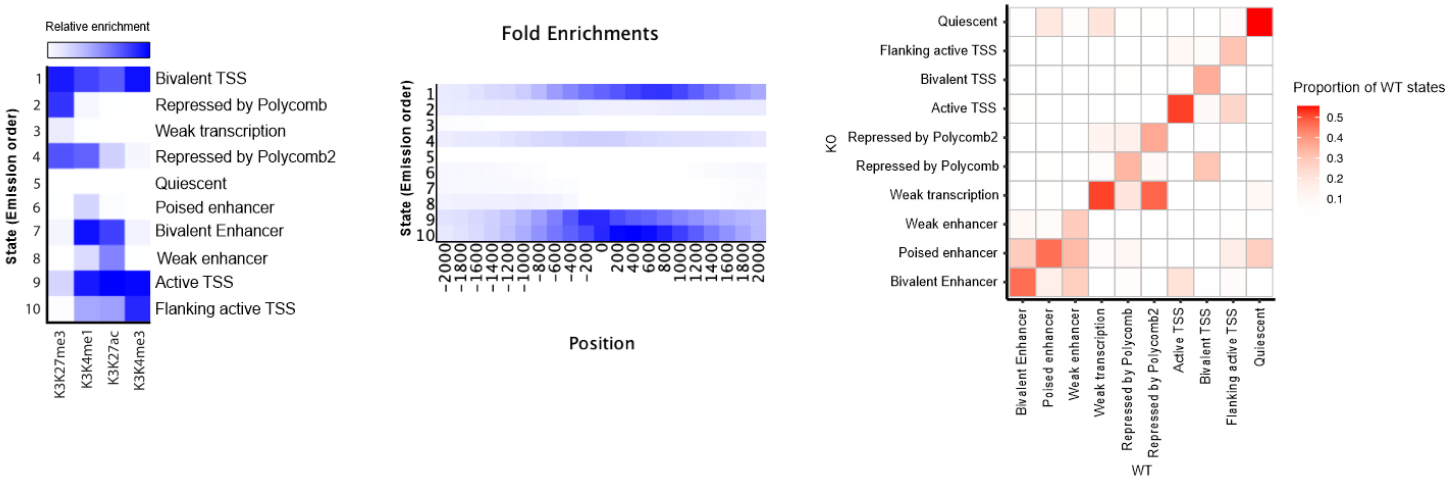

Figure 6.7 Chromatin states identified by ChromHMM The chromatin states are classified as either active or inactive based on the presence or absence of certain combinations of four histone tags (H3K27ac, H3K4me1, H3K4me3, and H3K27me3), using the ChromHMM 10-state model. Heatmaps are visual representations that depict the emission probabilities and transition probabilities of histone marks between different chromatin states. They also illustrate the enrichments of chromatin states for various genomic annotations. Additionally, heatmaps provide insights into the probabilities of chromatin state transitions, which are learned from ChromHMM. These heatmaps effectively demonstrate the proximal genomic locations associated with different chromatin states.

6.3.7 Mertk knockout changes the chromatin states in liver fibrosis model

To examine the dynamics of the chromatin states between WT and Mertk$^{-/-}$ conditions, I surveyed chromatin state switching frequencies across the two conditions. The result showed that Mertk$^{-/-}$ regulates the switching between active and inactive chromatin states. Notably, the candidate enhancers that become inactive or bivalent in Mertk$^{-/-}$ predominately arise from switching between active and inactive chromatin states, rather than being *de novo* (**Figure 6.8**).

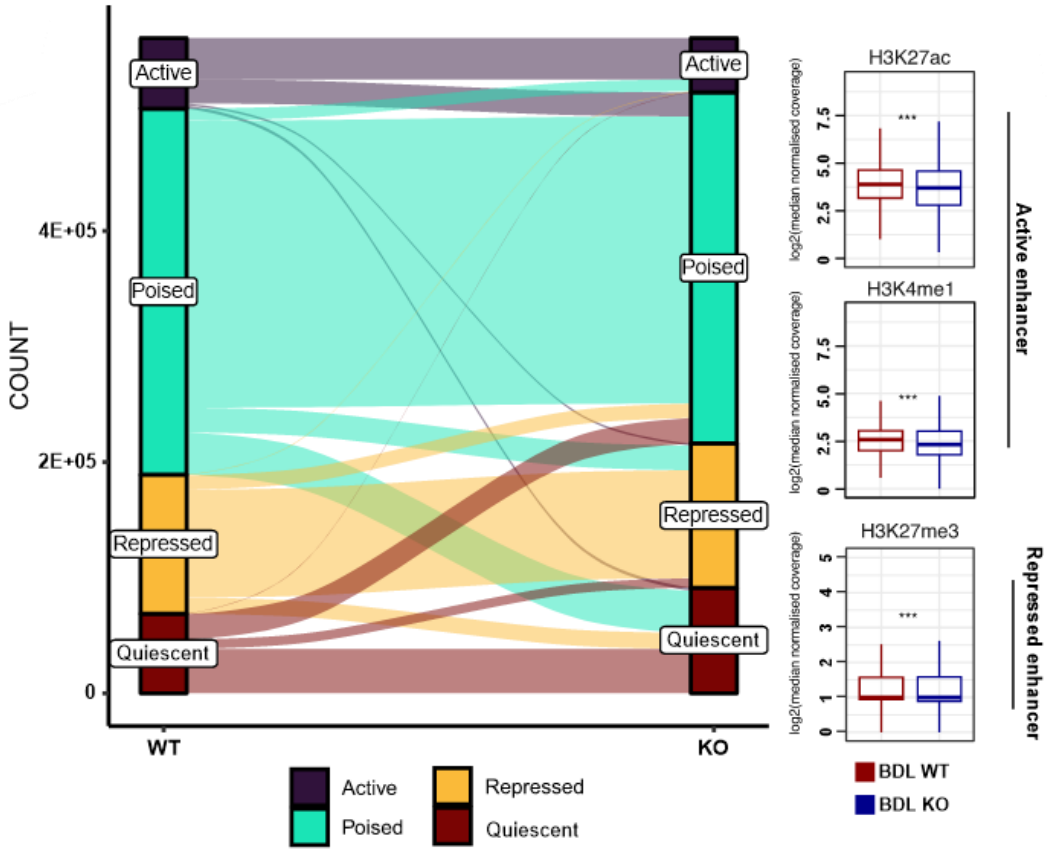

Figure 6.8 Global dynamics of chromatin states change in Mertk knockout River plot showing the global dynamics of active, poised, repressed and quiescent enhancer regions between the WT and Mertk$^{-/-}$ and boxplot showing Representative of these changes.

6.3.8 Mertk knockout reverses the landscape of genome

Mertk knockout significantly altered the inhibitory landscape of gene subsets. Consistently, in Mertk$^{-/-}$ mice, H3K4me1, H3K27ac, H3K4me3, and H3K27me3 were found to be reduced in Col1a1 and SMAD3, key genes in the process of fibrosis **(Figure6.9).**

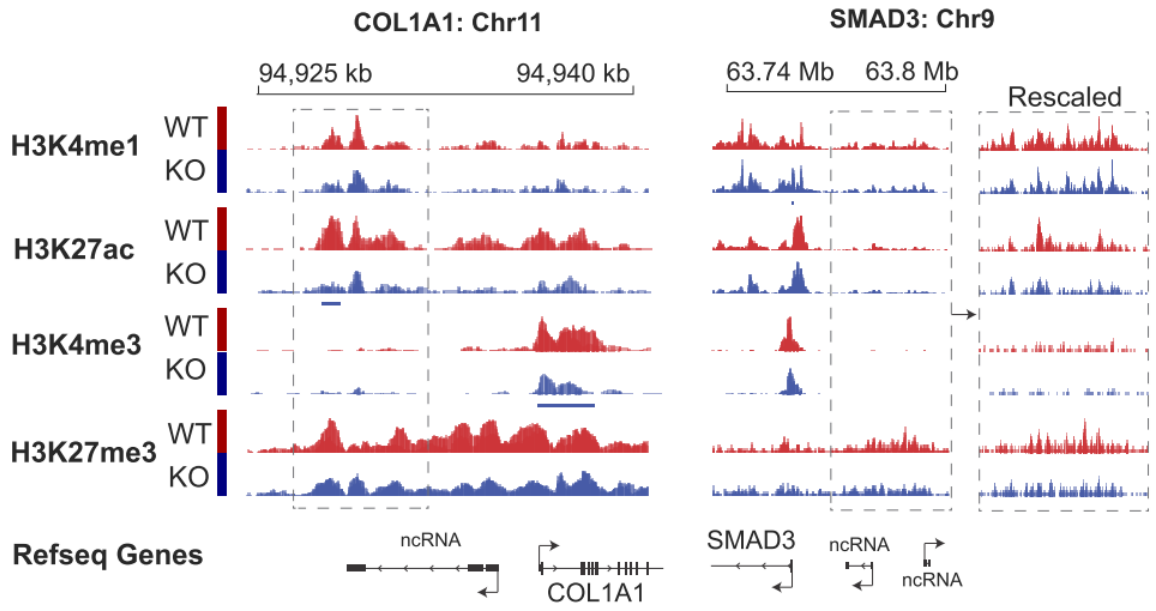

Figure 6.9 The effect of Mertk knockout in genome landscape in liver fibrosis Representative genome browser showing CUT&Tag-seq data at indicated loci. Peaks are highlighted by black boxes.

6.4 Discussion

Based on the results I obtained, as detailed in the previous chapter, I demonstrated that MerTK knockout significantly reduced the expression of fibrosis-related gene sets and the accessibility of corresponding chromatin regions. As detailed in this chapter, I attempted to use CUT&Tag-seq with multihistone antibody to elucidate the mechanism of chromatin accessibility changes caused by MerTK knockout.

CUT&Tag-seq is a method for studying protein–DNA interactions. CUT&Tag-seq combines the cleaved DNA of the antibody-targeted protein A-Tn5 with a large volume of sequencing, enabling precise mapping of the whole DNA binding site of any protein of interest [167].

As detailed in this chapter, RNA Pol II, the key initiation event responsible for the transcription of DNA into mRNA [168], was first examined. It was found that MerTK inhibition showed more peaks in the heatmap, apparently contrary to the global result of reduced chromatin accessibility. This prompted me to further examine CTCF, a DNA-binding protein that promotes Pol II pauses, whose heatmap showed a significant spike in MerTK$^{-/-}$. This suggests that MerTK knockout may inhibit fibrosis progression by enhancing Pol II suspension.

According to the CUT&Tag evaluation of activators H3K27ac, H3K4me3 and H3Kme and suppressor H3K27me3, MerTK knockout generally changed the peaks of these four histones but mainly focused on H3K27ac and H3K4me1. A motif analysis of Pol II peaks identified the top six transcription factor members, namely, Fra2, PU.1, Fra1, SpiB, AFT3 and JunB, which showed a good overlap with the top six transcription factor binding sites of H3K27ac and H3K4me1. The overlapping contents mostly belong to the ETS family, which is a major transcription factor promoting fibrosis, among which PU.1 has proven to be a regulatory factor of multiorgan fibrosis [164]. PU.1 not only activates resting fibroblasts but

also repolarises ECM-degrading inflammatory fibroblasts into an ECM-producing fibrotic phenotype, while the inactivation of PU.1 can reprogramme fibroblasts into resting fibroblasts, leading to fibrosis regression [164]. This suggests that MerTK knockout can significantly inhibit the binding of these transcription factors. Other studies have also confirmed that, in addition to significant functional heterogeneity, fibroblasts exhibit significant plasticity and phenotypic transformation during the progression and regression of fibrosis [169-171].

By studying the global relationship between transcription initiation and changes in chromatin accessibility, the pausing ratio at all genes and the correlation between changes in CTCF signalling and Pol II suspension levels, I found that chromatin accessibility regulation by MerTK was achieved through the increase of promoter-proximal Pol II pausing rather than the direct control of Pol II transcription initiation.

When I compared the chromatin states of the two conditions (WT vs. MerTK$^{-/-}$) dynamically, I found that MerTK knockout could significantly change the original active state to repressed and quiescent states, which can also be observed in the repressed state of MerTK$^{-/-}$ samples in the landscape of specific genes.

In conclusion, as detailed in this chapter, I confirmed that MerTK deficiency increases promoter-proximal Pol II pausing and promotes chromatin remodelling to inactive chromatin states, thereby preventing fibrosis progression.

Chapter7: Comprehensive Discussion

7.1 Findings Summary

Using cell-based and mouse models, I have shown that MerTK, a member of the TAM receptor tyrosine kinase family, is a critical and hitherto overlooked driver of multiple organ fibrosis. Specifically, this study has demonstrated that during persistent injury, MerTK expression increases and is driven by the profibrotic regulator TGF-β. It has been shown that MerTK and TGF-β signalling reciprocally and positively interact, creating a feed-forward loop that facilitates profibrotic TGF-β signalling. Mechanistically, I propose (**Figure 7.1**) that the regulation of fibrotic transcriptional programmes by MerTK is dependent on the context-specific epigenetic regulatory network of TGF-β/SMAD signalling. MerTK is a critical regulator of this fibrotic gene regulatory transcription network by regulating chromatin accessibility and RNA Pol II pausing and by reprogramming the enhancer and transcription factor network that regulates both the canonical and noncanonical TGF-β pathways.

TGF-β is a master regulator of fibrosis through the activation of both canonical (SMAD-based) and noncanonical (non-SMAD-based) signalling. My data suggest the existence of a fibrosis-promoting positive feedback loop between TGF-β and MerTK. Epigenetic mechanisms are established as landmark events in the activation of TGF-β and TGF-β signalling control transcription by regulating enhancer activity [172]. A mechanism delineated by the work presented here is compelling evidence that MerTK modifies the local epigenetic landscape of TGF-β signalling to promote fibrosis. This study also suggests that MerTK can promote cell-restricted enhancer functions to mediate a profibrotic positive feedback loop.

A network of enriched transcription factors controls TGF-β signalling and fibrosis; a direct interaction and transcriptional cooperation between SMAD and the components of the AP-1 and ETS transcription families have been reported [173]. This study has shown that MerTK activates TGF-β noncanonical signalling (ERK and AKT phosphorylation). Extracellular regulatory kinase regulates chromatin opening in several ways, including

transcription factor regulation, such as that of AP-1 and ETS [174]. MerTK also activates TGF-β1-induced SMAD transcriptional activity and reductions in the recruitment of SMAD3 to target gene promoters. These data collectively point to the cooperative effect of MerTK on both SMAD and non-SMAD pathways.

The data indicate that impairment of chromatin accessibility and increased promoter-proximal Pol II pausing are mediated via CTCF as key mechanisms rather than Pol II transcription initiation. Paused Pol II captures enhancer activity and acts as a potent insulator [175]. This study has shown that MerTK regulates this switching between the active and inactive chromatin states. Taken together, these results suggest that cell context-specific transcriptional responses to MerTK are mediated by regulating the epigenetic configuration that controls transcriptional regulation by TGF-β.

Fibrosis is a complex response that involves a dynamic cross-talk between multiple cell types, including myofibroblasts and macrophages. MerTK inhibition provides an opportunity to selectively curtail the cross-talk between these cells to restrain fibrosis. Such a selective approach may avoid interference with other TGF-β-regulated gene networks that are crucial for cell viability.

The only other published report that examined the role of MerTK in fibrosis found antifibrotic effects of macrophage MerTK deficiency in a fatty liver model [126]. By contrast, my data, derived in kidney, lung and multiple liver models, has demonstrated that MerTK is a potent nodal regulator of fibrosis.

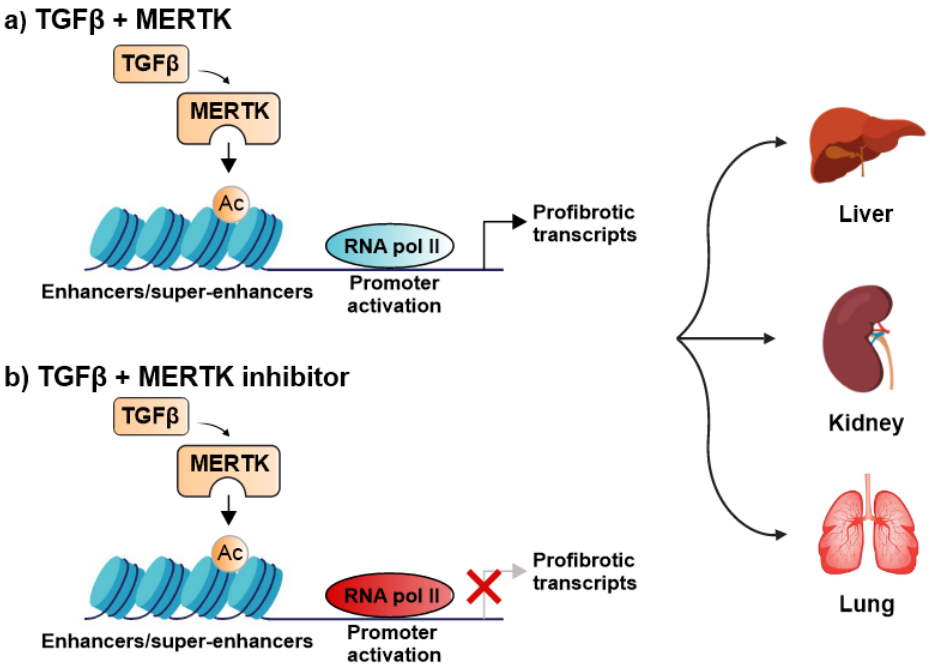

Figure 7.1 Model of MerTK mechanisms for regulating the TGF-β core fibrotic pathway across various organs

7.2 Findings Significance

In summary, I have identified MerTK as a profibrotic kinase that is upregulated in multiple models of fibrosis in mice. TGF-β stimulates an increase in fibroblast and macrophage MerTK, which, in turn, promotes profibrotic ERK/AKT and SMAD signalling. These findings not only broaden our understanding of the roles of MerTK but also reveal new regulatory molecules that regulate TGF-β activity during fibrosis. These results suggest that using small-molecule MerTK inhibitors might be a useful and selective strategy for the treatment of tissue fibrosis.

7.3 Overview of forthcoming questions and unresolved issues

Together, multiple fibrosis diseases account for approximately half of all disease deaths worldwide [176]. However, despite such huge statistics, there are still no clinically approved treatments that directly target the fibrosis process.

Although many antifibrosis drugs are in preclinical development, very few have actually entered clinical trials [177]. The reasons for the failure of targeted drugs in development include the fact that organ fibrosis is a complex biological process, there are redundancies in the wound-healing/fibrosis process and there are species differences between humans and mice, resulting in poor correlation of specific markers for assessing fibrosis severity and resolution [178].

My data suggest that MerTK is a key driver of multiorgan fibrosis and that TGF-β stimulates the increase of MerTK in fibroblasts and macrophages during sustained injury, thereby promoting fibrosis-promoting ERK/AKT and SMAD signalling. This suggests that MerTK and TGF-β signalling interact to form a feedforward loop that promotes profibrosis TGF-β signalling.

These findings suggest that small-molecule MerTK inhibitors may be a useful and selective strategy for the treatment of tissue fibrosis. However, the potential effects of MerTK inhibition on other metabolic processes are unknown before practical clinical application, and there is a lack of studies on animal models simulating obesity disease in patients with MAFLD. These are more research areas that need to be explored in the future.

7.4 Future research directions

7.4.1 Exploring the role of MERTK in other cell subpopulations in the liver

Organ fibrosis is a complex biological process involving cross-talk between multiple cell types. Liver fibrosis, for example, involves the combined action of hepatocytes, hepatic stellate cells, Kupffer cells, infiltrating macrophages and other inflammatory cells [179]. This study focused on the role of MerTK in HSCs at the cellular level because HSCs are the main sources of myoblasts responsible for the secretion of collagen in the process of liver fibrosis [180]. As the main receptor of apoptotic macrophages, MerTK is mainly expressed in M2c macrophages [181]. Therefore, analysing the different effects of MerTK on macrophages and other cell types is also important. Single-cell sequencing technology can be used to examine the changes in different cell types caused by MerTK inhibition in the samples of fibrosis models of various organs to gain a deeper understanding of the mechanism of MerTK in fibrosis.

7.4.2 Targeting MerTK as a therapeutic strategy in potential clinical trials

All these results support MerTK as a therapeutic target for multiorgan fibrosis and suggest that fibrotic diseases are similar in different organs [182]. Furthermore, it is very important if MerTK can be applied as a therapeutic strategy in a potential clinical trial, such as those on MAFLD, CKD and IPF. It will be a great achievement if we can develop a therapeutic strategy that can be applied to fibrosis in different organs.

Meanwhile, although there are some small-molecule and monoclonal antibodies against the TAM family under development, there are still limited inhibitors that specifically target MerTK [183]; therefore, developing more targeted MerTK inhibitors with fewer side effects in future clinical studies is urgent. At the same time, if markers that can accurately measure MerTK activity and drug response can be developed, such as MerTK inhibitors, they can aid in stratifying patients in clinical trials and in evaluating the effectiveness of treatment.

Chapter8: References

Reference

1. Wynn, T.A., *Common and unique mechanisms regulate fibrosis in various fibroproliferative diseases.* J Clin Invest, 2007. **117**(3): p. 524-9.
2. Friedman, S.L., et al., *Therapy for fibrotic diseases: nearing the starting line.* Sci Transl Med, 2013. **5**(167): p. 167sr1.
3. Henderson, N.C., F. Rieder, and T.A. Wynn, *Fibrosis: from mechanisms to medicines.* Nature, 2020. **587**(7835): p. 555-566.
4. Ratziu, V. and S.L. Friedman, *Why do so many NASH trials fail?* Gastroenterology, 2020.
5. Sarin, S.K., et al., *Correction to: Acute-on-chronic liver failure: consensus recommendations of the Asian Pacific association for the study of the liver (APASL): an update.* Hepatol Int, 2019. **13**(6): p. 826-828.
6. Marcellin, P. and B.K. Kutala, *Liver diseases: A major, neglected global public health problem requiring urgent actions and large-scale screening.* Liver Int, 2018. **38 Suppl 1**: p. 2-6.
7. Williams, R., et al., *Disease burden and costs from excess alcohol consumption, obesity, and viral hepatitis: fourth report of the Lancet Standing Commission on Liver Disease in the UK.* Lancet, 2018. **391**(10125): p. 1097-1107.
8. Economics, D.A., *The economic cost and health burden of liver diseases in Australia.* Sydney: Gastroenterological Society of Australia/Australian Liver Association, 2013.
9. Sarin, S.K., et al., *Liver diseases in the Asia-Pacific region: a Lancet Gastroenterology & Hepatology Commission.* Lancet Gastroenterol Hepatol, 2020. **5**(2): p. 167-228.
10. Campana, L. and J.P. Iredale, *Regression of Liver Fibrosis.* Semin Liver Dis, 2017. **37**(1): p. 1-10.
11. Yin, C., et al., *Hepatic stellate cells in liver development, regeneration, and cancer.* J Clin Invest, 2013. **123**(5): p. 1902-10.
12. Yin, C.Y., et al., *Hepatic stellate cells in liver development, regeneration, and cancer.* Journal of Clinical Investigation, 2013. **123**(5): p. 1902-1910.
13. Younossi, Z., et al., *Global burden of NAFLD and NASH: trends, predictions, risk factors and prevention.* Nature Reviews Gastroenterology & Hepatology, 2018. **15**(1): p. 11-20.
14. Hagstrom, H., et al., *Risk for Development of Severe Liver Disease in Lean Patients With Nonalcoholic Fatty Liver Disease: A Long-Term Follow-Up Study.* Hepatology Communications, 2018. **2**(1): p. 48-57.
15. Friedman, S.L., *Hepatic stellate cells: Protean, multifunctional, and enigmatic cells of the liver.* Physiological Reviews, 2008. **88**(1): p. 125-172.
16. Karlmark, K.R., et al., *Hepatic recruitment of the inflammatory Gr1+ monocyte subset upon liver injury promotes hepatic fibrosis.* Hepatology, 2009. **50**(1): p. 261-74.
17. Chen, T.K., D.H. Knicely, and M.E. Grams, *Chronic Kidney Disease Diagnosis and Management: A Review.* JAMA, 2019. **322**(13): p. 1294-1304.
18. Glassock, R.J., D.G. Warnock, and P. Delanaye, *The global burden of chronic kidney disease: estimates, variability and pitfalls.* Nat Rev Nephrol, 2017. **13**(2): p. 104-114.
19. Chen, T.K., D.H. Knicely, and M.E. Grams, *Chronic Kidney Disease Diagnosis and Management: A Review.* Jama-Journal of the American Medical Association, 2019. **322**(13): p. 1294-1304.
20. Yuan, Q., B. Tang, and C. Zhang, *Signaling pathways of chronic kidney diseases, implications for therapeutics.* Signal Transduction and Targeted Therapy, 2022. **7**(1).
21. Rockey, D.C., P.D. Bell, and J.A. Hill, *Fibrosis - A Common Pathway to Organ Injury and Failure Reply.* New England Journal of Medicine, 2015. **373**(1): p. 96-96.
22. Falke, L.L., et al., *Diverse origins of the myofibroblast -implications for kidney fibrosis.* Nature Reviews Nephrology, 2015. **11**(4): p. 233-244.
23. Ruiz-Ortega, M., et al., *Targeting the progression of chronic kidney disease.* Nature Reviews Nephrology, 2020. **16**(5): p. 269-288.

24. Martinez, F.J., et al., *Idiopathic pulmonary fibrosis.* Nature Reviews Disease Primers, 2017. **3**.
25. Mathai, S.K., et al., *Pulmonary fibrosis in the era of stratified medicine.* Thorax, 2016. **71**(12): p. 1154-1160.
26. King, T.E., A. Pardo, and M. Selman, *Idiopathic pulmonary fibrosis.* Lancet, 2011. **378**(9807): p. 1949-1961.
27. Berchtold, L., et al., *Diagnosis and assessment of renal fibrosis: the state of the art.* Swiss Medical Weekly, 2017. **147**.
28. Dulai, P.S., et al., *Increased Risk of Mortality by Fibrosis Stage in Nonalcoholic Fatty Liver Disease: Systematic Review and Meta-Analysis.* Hepatology, 2017. **65**(5): p. 1557-1565.
29. Kaur, A., S.K. Mathai, and D.A. Schwartz, *Genetics in idiopathic Pulmonary Fibrosis Pathogenesis, Prognosis, and Treatment.* Frontiers in Medicine, 2017. **4**.
30. Weiskirchen, R., S. Weiskirchen, and F. Tacke, *Organ and tissue fibrosis: Molecular signals, cellular mechanisms and translational implications.* Molecular Aspects of Medicine, 2019. **65**: p. 2-15.
31. Kumar, V., et al., *Risk of complications with use of aspirin during renal biopsy: A systematic review.* Clinical Nephrology, 2018. **89**(2): p. 67-74.
32. Patel, K., P. Bedossa, and L. Castera, *Diagnosis of Liver Fibrosis: Present and Future.* Seminars in Liver Disease, 2015. **35**(2): p. 166-183.
33. Makela, K., et al., *Analysis of the Histologic Features Associated With Interobserver Variation in Idiopathic Pulmonary Fibrosis.* American Journal of Surgical Pathology, 2018. **42**(5): p. 672-678.
34. Wynn, T.A., *Cellular and molecular mechanisms of fibrosis.* Journal of Pathology, 2008. **214**(2): p. 199-210.
35. Distler, J.H.W., et al., *Shared and distinct mechanisms of fibrosis.* Nature Reviews Rheumatology, 2019. **15**(12): p. 705-730.
36. Trensz, F., et al., *A muscle resident cell population promotes fibrosis in hindlimb skeletal muscles of mdx mice through the Wnt canonical pathway.* American Journal of Physiology-Cell Physiology, 2010. **299**(5): p. C939-C947.
37. Akhmetshina, A., et al., *Activation of canonical Wnt signalling is required for TGF-beta-mediated fibrosis.* Nature Communications, 2012. **3**.
38. Dees, C., et al., *The Wnt antagonists DKK1 and SFRP1 are downregulated by promoter hypermethylation in systemic sclerosis.* Annals of the Rheumatic Diseases, 2014. **73**(6): p. 1232-1239.
39. Reyhani, V., et al., *PDGF-BB enhances collagen gel contraction through a PI3K-PLC gamma-PKC-cofilin pathway.* Scientific Reports, 2017. **7**.
40. Klinkhammer, B.M., J. Floege, and P. Boor, *PDGF in organ fibrosis.* Molecular Aspects of Medicine, 2018. **62**: p. 44-62.
41. Driskell, R.R., et al., *Distinct fibroblast lineages determine dermal architecture in skin development and repair.* Nature, 2013. **504**(7479): p. 277-+.
42. Demoulin, J.B. and A. Essaghir, *PDGF receptor signaling networks in normal and cancer cells.* Cytokine & Growth Factor Reviews, 2014. **25**(3): p. 273-283.
43. Lee, J., et al., *Role of Smad3 in platelet-derived growth factor-C-induced liver fibrosis.* American Journal of Physiology-Cell Physiology, 2016. **310**(6): p. C436-C445.
44. Derynck, R. and E.H. Budi, *Specificity, versatility, and control of TGF-beta family signaling.* Sci Signal, 2019. **12**(570).
45. Biernacka, A., M. Dobaczewski, and N.G. Frangogiannis, *TGF-beta signaling in fibrosis.* Growth Factors, 2011. **29**(5): p. 196-202.
46. Schiller, M., D. Javelaud, and A. Mauviel, *TGF-beta-induced SMAD signaling and gene regulation: consequences for extracellular matrix remodeling and wound healing.* J Dermatol Sci, 2004. **35**(2): p. 83-92.

47. Diebold, R.J., et al., *Early-onset multifocal inflammation in the transforming growth factor beta 1-null mouse is lymphocyte mediated.* Proc Natl Acad Sci U S A, 1995. **92**(26): p. 12215-9.
48. McEntee, C.P., S. Gunaltay, and M.A. Travis, *Regulation of barrier immunity and homeostasis by integrin-mediated transforming growth factor beta activation.* Immunology, 2020. **160**(2): p. 139-148.
49. Dewidar, B., et al., *TGF-beta in Hepatic Stellate Cell Activation and Liver Fibrogenesis-Updated 2019.* Cells, 2019. **8**(11).
50. Carthy, J.M., *TGFbeta signaling and the control of myofibroblast differentiation: Implications for chronic inflammatory disorders.* J Cell Physiol, 2018. **233**(1): p. 98-106.
51. Sheng, J., W. Chen, and H.J. Zhu, *The immune suppressive function of transforming growth factor-beta (TGF-beta) in human diseases.* Growth Factors, 2015. **33**(2): p. 92-101.
52. Raman, M., W. Chen, and M.H. Cobb, *Differential regulation and properties of MAPKs.* Oncogene, 2007. **26**(22): p. 3100-12.
53. Busca, R., J. Pouyssegur, and P. Lenormand, *ERK1 and ERK2 Map Kinases: Specific Roles or Functional Redundancy?* Front Cell Dev Biol, 2016. **4**: p. 53.
54. Parola, M. and M. Pinzani, *Liver fibrosis: Pathophysiology, pathogenetic targets and clinical issues.* Mol Aspects Med, 2019. **65**: p. 37-55.
55. Pinzani, M. and F. Marra, *Cytokine receptors and signaling in hepatic stellate cells.* Semin Liver Dis, 2001. **21**(3): p. 397-416.
56. Son, G., et al., *Inhibition of phosphatidylinositol 3-kinase signaling in hepatic stellate cells blocks the progression of hepatic fibrosis.* Hepatology, 2009. **50**(5): p. 1512-23.
57. Starkel, P. and I.A. Leclercq, *Animal models for the study of hepatic fibrosis.* Best Pract Res Clin Gastroenterol, 2011. **25**(2): p. 319-33.
58. Constandinou, C., N. Henderson, and J.P. Iredale, *Modeling liver fibrosis in rodents.* Methods Mol Med, 2005. **117**: p. 237-50.
59. Omary, M.B., et al., *Not All Mice Are the Same: Standardization of Animal Research Data Presentation.* Cell Mol Gastroenterol Hepatol, 2016. **2**(4): p. 391-393.
60. Antoine, M., et al., *Upregulation of pleiotrophin expression in rat hepatic stellate cells by PDGF and hypoxia: implications for its role in experimental biliary liver fibrogenesis.* Biochem Biophys Res Commun, 2005. **337**(4): p. 1153-64.
61. Tag, C.G., et al., *Bile duct ligation in mice: induction of inflammatory liver injury and fibrosis by obstructive cholestasis.* J Vis Exp, 2015(96).
62. Martinez-Klimova, E., et al., *Unilateral Ureteral Obstruction as a Model to Investigate Fibrosis-Attenuating Treatments.* Biomolecules, 2019. **9**(4).
63. Chevalier, R.L., M.S. Forbes, and B.A. Thornhill, *Ureteral obstruction as a model of renal interstitial fibrosis and obstructive nephropathy.* Kidney Int, 2009. **75**(11): p. 1145-1152.
64. Wongmekiat, O., D. Leelarungrayub, and K. Thamprasert, *Alpha-lipoic acid attenuates renal injury in rats with obstructive nephropathy.* Biomed Res Int, 2013. **2013**: p. 138719.
65. Kido, T., et al., *Fluoride potentiates tubulointerstitial nephropathy caused by unilateral ureteral obstruction.* Toxicology, 2017. **392**: p. 106-118.
66. Chaabane, W., et al., *Renal functional decline and glomerulotubular injury are arrested but not restored by release of unilateral ureteral obstruction (UUO).* Am J Physiol Renal Physiol, 2013. **304**(4): p. F432-9.
67. Yanagisawa, H., M. Nodera, and O. Wada, *Zinc deficiency aggravates tubulointerstitial nephropathy caused by ureteral obstruction.* Biol Trace Elem Res, 1998. **65**(1): p. 1-6.
68. Che, P., et al., *A novel tree shrew model of pulmonary fibrosis.* Lab Invest, 2021. **101**(1): p. 116-124.
69. Hay, J., S. Shahzeidi, and G. Laurent, *Mechanisms of bleomycin-induced lung damage.* Arch Toxicol, 1991. **65**(2): p. 81-94.

70. Walters, D.M. and S.R. Kleeberger, *Mouse models of bleomycin-induced pulmonary fibrosis.* Curr Protoc Pharmacol, 2008. **Chapter 5**: p. Unit 5 46.
71. Romero-Gomez, M., et al., *Genes and hepatitis C: susceptibility, fibrosis progression and response to treatment.* Liver Int, 2011. **31**(4): p. 443-60.
72. Eslam, M. and J. George, *Genome-Wide Association Studies and Hepatitis C: Harvesting the Benefits of the Genomic Revolution.* Semin Liver Dis, 2015. **35**(4): p. 402-20.
73. Visscher, P.M., et al., *Five years of GWAS discovery.* Am J Hum Genet, 2012. **90**(1): p. 7-24.
74. Visscher, P.M., et al., *10 Years of GWAS Discovery: Biology, Function, and Translation.* Am J Hum Genet, 2017. **101**(1): p. 5-22.
75. Patin, E., et al., *Genome-wide association study identifies variants associated with progression of liver fibrosis from HCV infection.* Gastroenterology, 2012. **143**(5): p. 1244-1252 e12.
76. Petta, S., et al., *MERTK rs4374383 polymorphism affects the severity of fibrosis in non-alcoholic fatty liver disease.* J Hepatol, 2016. **64**(3): p. 682-90.
77. Jimenez-Sousa, M.A., et al., *The Myeloid-Epithelial-Reproductive Tyrosine Kinase (MERTK) rs4374383 Polymorphism Predicts Progression of Liver Fibrosis in Hepatitis C Virus-Infected Patients: A Longitudinal Study.* J Clin Med, 2018. **7**(12).
78. Mukherjee, S.K., A. Wilhelm, and C.G. Antoniades, *TAM receptor tyrosine kinase function and the immunopathology of liver disease.* Am J Physiol Gastrointest Liver Physiol, 2016. **310**(11): p. G899-905.
79. Smirne, C., et al., *Gas6/TAM Signaling Components as Novel Biomarkers of Liver Fibrosis.* Dis Markers, 2019. **2019**: p. 2304931.
80. Axelrod, H. and K.J. Pienta, *Axl as a mediator of cellular growth and survival.* Oncotarget, 2014. **5**(19): p. 8818-52.
81. Sasaki, T., et al., *Structural basis for Gas6-Axl signalling.* EMBO J, 2006. **25**(1): p. 80-7.
82. Hong, C.C., et al., *Receptor tyrosine kinase AXL is induced by chemotherapy drugs and overexpression of AXL confers drug resistance in acute myeloid leukemia.* Cancer Lett, 2008. **268**(2): p. 314-24.
83. Goruppi, S., E. Ruaro, and C. Schneider, *Gas6, the ligand of Axl tyrosine kinase receptor, has mitogenic and survival activities for serum starved NIH3T3 fibroblasts.* Oncogene, 1996. **12**(3): p. 471-80.
84. Anderson, H.A., et al., *Serum-derived protein S binds to phosphatidylserine and stimulates the phagocytosis of apoptotic cells.* Nat Immunol, 2003. **4**(1): p. 87-91.
85. Rothlin, C.V., et al., *TAM receptors are pleiotropic inhibitors of the innate immune response.* Cell, 2007. **131**(6): p. 1124-36.
86. Camenisch, T.D., et al., *A novel receptor tyrosine kinase, Mer, inhibits TNF-alpha production and lipopolysaccharide-induced endotoxic shock.* J Immunol, 1999. **162**(6): p. 3498-503.
87. Zizzo, G., et al., *Efficient clearance of early apoptotic cells by human macrophages requires M2c polarization and MerTK induction.* J Immunol, 2012. **189**(7): p. 3508-20.
88. Triantafyllou, E., et al., *MerTK expressing hepatic macrophages promote the resolution of inflammation in acute liver failure.* Gut, 2018. **67**(2): p. 333-347.
89. Benzakour, O., et al., *[Gas-6 and protein S: vitamin K-dependent factors and ligands for the TAM tyrosine kinase receptors family].* Med Sci (Paris), 2007. **23**(10): p. 826-33.
90. Caberoy, N.B., Y. Zhou, and W. Li, *Tubby and tubby-like protein 1 are new MerTK ligands for phagocytosis.* EMBO J, 2010. **29**(23): p. 3898-910.
91. Dong, R., et al., *Galectin-3 as a novel biomarker for disease diagnosis and a target for therapy (Review).* Int J Mol Med, 2018. **41**(2): p. 599-614.
92. Nagata, K., et al., *Identification of the product of growth arrest-specific gene 6 as a common ligand for Axl, Sky, and Mer receptor tyrosine kinases.* J Biol Chem, 1996. **271**(47): p. 30022-7.

93. Mark, M.R., et al., *Characterization of Gas6, a member of the superfamily of G domain-containing proteins, as a ligand for Rse and Axl.* J Biol Chem, 1996. **271**(16): p. 9785-9.
94. Barcena, C., et al., *Gas6/Axl pathway is activated in chronic liver disease and its targeting reduces fibrosis via hepatic stellate cell inactivation.* J Hepatol, 2015. **63**(3): p. 670-8.
95. Meijers, W.C., et al., *Galectin-3 and post-myocardial infarction cardiac remodeling.* Eur J Pharmacol, 2015. **763**(Pt A): p. 115-21.
96. Henderson, N.C., et al., *Galectin-3 regulates myofibroblast activation and hepatic fibrosis.* Proc Natl Acad Sci U S A, 2006. **103**(13): p. 5060-5.
97. Christoph, S., et al., *UNC569, a novel small-molecule mer inhibitor with efficacy against acute lymphoblastic leukemia in vitro and in vivo.* Mol Cancer Ther, 2013. **12**(11): p. 2367-77.
98. Schlegel, J., et al., *MERTK receptor tyrosine kinase is a therapeutic target in melanoma.* J Clin Invest, 2013. **123**(5): p. 2257-67.
99. Lee-Sherick, A.B., et al., *Efficacy of a Mer and Flt3 tyrosine kinase small molecule inhibitor, UNC1666, in acute myeloid leukemia.* Oncotarget, 2015. **6**(9): p. 6722-36.
100. Zhang, W., et al., *Pseudo-cyclization through intramolecular hydrogen bond enables discovery of pyridine substituted pyrimidines as new Mer kinase inhibitors.* J Med Chem, 2013. **56**(23): p. 9683-92.
101. Liu, J., et al., *Discovery of Novel Small Molecule Mer Kinase Inhibitors for the Treatment of Pediatric Acute Lymphoblastic Leukemia.* ACS Med Chem Lett, 2012. **3**(2): p. 129-134.
102. El Sharkawy, R., *MERTK receptor tyrosine kinase: A novel therapeutic target for liver fibrosis*. 2020, University of Sydney.
103. Bayoumi, A., *Mistranslation drives alterations in protein levels and the effects of a synonymous variant at the FGF21 locus*. 2020, The University of Sydney.
104. Alharthi, J., *A metabolic associated fatty liver disease risk variant in MBOAT7 regulates toll like receptor induced outcomes*. 2022, The University of Sydney.
105. Alharthi, J., et al., *A metabolic associated fatty liver disease risk variant in MBOAT7 regulates toll like receptor induced outcomes.* Nature Communications, 2022. **13**(1): p. 7430.
106. Alharthi, J., et al., *Loss of metabolic adaptation in lean MAFLD is driven by endotoxemia leading to epigenetic reprogramming.* Metabolism, 2023. **144**: p. 155583.
107. Magoč, T. and S.L. Salzberg, *FLASH: fast length adjustment of short reads to improve genome assemblies.* Bioinformatics, 2011. **27**(21): p. 2957-2963.
108. Yu, G., et al., *clusterProfiler: an R package for comparing biological themes among gene clusters.* Omics: a journal of integrative biology, 2012. **16**(5): p. 284-287.
109. Langmead, B. and S.L. Salzberg, *Fast gapped-read alignment with Bowtie 2.* Nat Methods, 2012. **9**(4): p. 357-9.
110. Zhang, Y., et al., *Model-based analysis of ChIP-Seq (MACS).* Genome Biol, 2008. **9**(9): p. R137.
111. Robinson, J.T., et al., *Integrative genomics viewer.* Nat Biotechnol, 2011. **29**(1): p. 24-6.
112. Friedman, S.L., *Transcriptional regulation of stellate cell activation.* J Gastroenterol Hepatol, 2006. **21 Suppl 3**: p. S79-83.
113. Asrani, S.K., et al., *Increasing Health Care Burden of Chronic Liver Disease Compared With Other Chronic Diseases, 2004-2013.* Gastroenterology, 2018. **155**(3): p. 719-729 e4.
114. Carey, E.J., A.H. Ali, and K.D. Lindor, *Primary biliary cirrhosis.* Lancet, 2015. **386**(10003): p. 1565-75.
115. Alharthi, J., et al., *Macrophages in metabolic associated fatty liver disease.* World Journal of Gastroenterology, 2020. **26**(16): p. 1861.
116. Friedman, S.L., et al., *Therapy for fibrotic diseases: nearing the starting line.* Science translational medicine, 2013. **5**(167): p. 167sr1-167sr1.
117. Krenkel, O., et al., *Single Cell RNA Sequencing Identifies Subsets of Hepatic Stellate Cells and Myofibroblasts in Liver Fibrosis.* Cells, 2019. **8**(5).
118. Trivedi, P., S. Wang, and S.L. Friedman, *The Power of Plasticity-Metabolic Regulation of Hepatic Stellate Cells.* Cell Metab, 2021. **33**(2): p. 242-257.

119. Eslam, M. and J. George, *Genetic and epigenetic mechanisms of NASH.* Hepatol Int, 2016. **10**(3): p. 394-406.
120. Junqueira, L.C., G. Bignolas, and R.R. Brentani, *Picrosirius staining plus polarization microscopy, a specific method for collagen detection in tissue sections.* Histochem J, 1979. **11**(4): p. 447-55.
121. Duffield, J.S., et al., *Selective depletion of macrophages reveals distinct, opposing roles during liver injury and repair.* J Clin Invest, 2005. **115**(1): p. 56-65.
122. Gordon, S., A. Pluddemann, and F. Martinez Estrada, *Macrophage heterogeneity in tissues: phenotypic diversity and functions.* Immunol Rev, 2014. **262**(1): p. 36-55.
123. Inagaki, Y. and I. Okazaki, *Emerging insights into Transforming growth factor beta Smad signal in hepatic fibrogenesis.* Gut, 2007. **56**(2): p. 284-92.
124. Liu, Y., et al., *Transforming growth factor-beta (TGF-beta)-mediated connective tissue growth factor (CTGF) expression in hepatic stellate cells requires Stat3 signaling activation.* J Biol Chem, 2013. **288**(42): p. 30708-30719.
125. Kinnman, N. and C. Housset, *Peribiliary myofibroblasts in biliary type liver fibrosis.* Front Biosci, 2002. **7**: p. d496-503.
126. Cai, B., et al., *Macrophage MerTK Promotes Liver Fibrosis in Nonalcoholic Steatohepatitis.* Cell Metab, 2020. **31**(2): p. 406-421 e7.
127. Park, J.W., et al., *Primary Biliary Cholangitis and Primary Sclerosing Cholangitis: Current Knowledge of Pathogenesis and Therapeutics.* Biomedicines, 2022. **10**(6).
128. Lang, E., et al., *Cholestasis induced liver pathology results in dysfunctional immune responses after arenavirus infection.* Sci Rep, 2018. **8**(1): p. 12179.
129. Hume, D.A., et al., *The mononuclear phagocyte system revisited.* J Leukoc Biol, 2002. **72**(4): p. 621-7.
130. Bayoumi, A., et al., *The Epigenetic Drug Discovery Landscape for Metabolic-associated Fatty Liver Disease.* Trends Genet, 2020. **36**(6): p. 429-441.
131. Eslam, M. and J. George, *Genetic Insights for Drug Development in NAFLD.* Trends Pharmacol Sci, 2019. **40**(7): p. 506-516.
132. Tashiro, J., et al., *Exploring Animal Models That Resemble Idiopathic Pulmonary Fibrosis.* Front Med (Lausanne), 2017. **4**: p. 118.
133. Jenkins, R.G., et al., *An Official American Thoracic Society Workshop Report: Use of Animal Models for the Preclinical Assessment of Potential Therapies for Pulmonary Fibrosis.* Am J Respir Cell Mol Biol, 2017. **56**(5): p. 667-679.
134. Tang, P.M., D.J. Nikolic-Paterson, and H.Y. Lan, *Macrophages: versatile players in renal inflammation and fibrosis.* Nat Rev Nephrol, 2019. **15**(3): p. 144-158.
135. Epelman, S., K.J. Lavine, and G.J. Randolph, *Origin and functions of tissue macrophages.* Immunity, 2014. **41**(1): p. 21-35.
136. Hashimoto, D., et al., *Tissue-resident macrophages self-maintain locally throughout adult life with minimal contribution from circulating monocytes.* Immunity, 2013. **38**(4): p. 792-804.
137. Barkauskas, C.E. and P.W. Noble, *Cellular mechanisms of tissue fibrosis. 7. New insights into the cellular mechanisms of pulmonary fibrosis.* Am J Physiol Cell Physiol, 2014. **306**(11): p. C987-96.
138. Glassock, R.J., D.G. Warnock, and P. Delanaye, *The global burden of chronic kidney disease: estimates, variability and pitfalls.* Nature Reviews Nephrology, 2017. **13**(2): p. 104-114.
139. Martinez, F.J., et al., *Idiopathic pulmonary fibrosis.* Nat Rev Dis Primers, 2017. **3**: p. 17074.
140. Kreuter, M., et al., *Health related quality of life in patients with idiopathic pulmonary fibrosis in clinical practice: insights-IPF registry.* Respir Res, 2017. **18**(1): p. 139.
141. van Manen, M.J., et al., *Optimizing quality of life in patients with idiopathic pulmonary fibrosis.* Ther Adv Respir Dis, 2017. **11**(3): p. 157-169.
142. Sharif, R., *Overview of idiopathic pulmonary fibrosis (IPF) and evidence-based guidelines.* Am J Manag Care, 2017. **23**(11 Suppl): p. S176-S182.

143. Diamantopoulos, A., et al., *The Burden of Illness of Idiopathic Pulmonary Fibrosis: A Comprehensive Evidence Review.* Pharmacoeconomics, 2018. **36**(7): p. 779-807.
144. Yu, Y.F., et al., *Patterns and Economic Burden of Hospitalizations and Exacerbations Among Patients Diagnosed with Idiopathic Pulmonary Fibrosis.* J Manag Care Spec Pharm, 2016. **22**(4): p. 414-23.
145. Yan, L., et al., *Submicron emulsion of cinnamaldehyde ameliorates bleomycin-induced idiopathic pulmonary fibrosis via inhibition of inflammation, oxidative stress and epithelial-mesenchymal transition.* Biomed Pharmacother, 2018. **102**: p. 765-771.
146. Mann, J., et al., *MeCP2 controls an epigenetic pathway that promotes myofibroblast transdifferentiation and fibrosis.* Gastroenterology, 2010. **138**(2): p. 705-14, 714 e1-4.
147. Mayer, S.C., et al., *Adrenergic Repression of the Epigenetic Reader MeCP2 Facilitates Cardiac Adaptation in Chronic Heart Failure.* Circ Res, 2015. **117**(7): p. 622-33.
148. Klemm, S.L., Z. Shipony, and W.J. Greenleaf, *Chromatin accessibility and the regulatory epigenome.* Nat Rev Genet, 2019. **20**(4): p. 207-220.
149. Mansisidor, A.R. and V.I. Risca, *Chromatin accessibility: methods, mechanisms, and biological insights.* Nucleus, 2022. **13**(1): p. 236-276.
150. *Proceedings of the Third Annual RECOMB Satellite Workshop on Massively Parallel Sequencing (RECOMB-seq 2013), April 11-12, 2013, Beijing, China.* BMC Bioinformatics, 2013. **14 Suppl 5**: p. S1-18.
151. Fillman, S.G., et al., *Increased inflammatory markers identified in the dorsolateral prefrontal cortex of individuals with schizophrenia.* Mol Psychiatry, 2013. **18**(2): p. 206-14.
152. Ren, S., et al., *RNA-seq analysis of prostate cancer in the Chinese population identifies recurrent gene fusions, cancer-associated long noncoding RNAs and aberrant alternative splicings.* Cell Res, 2012. **22**(5): p. 806-21.
153. Buenrostro, J.D., et al., *Transposition of native chromatin for fast and sensitive epigenomic profiling of open chromatin, DNA-binding proteins and nucleosome position.* Nat Methods, 2013. **10**(12): p. 1213-8.
154. Buenrostro, J.D., et al., *ATAC-seq: A Method for Assaying Chromatin Accessibility Genome-Wide.* Curr Protoc Mol Biol, 2015. **109**: p. 21 29 1-21 29 9.
155. Bajic, M., K.A. Maher, and R.B. Deal, *Identification of Open Chromatin Regions in Plant Genomes Using ATAC-Seq.* Methods Mol Biol, 2018. **1675**: p. 183-201.
156. Picelli, S., et al., *Tn5 transposase and tagmentation procedures for massively scaled sequencing projects.* Genome Res, 2014. **24**(12): p. 2033-40.
157. Bowers, S.L., Q. Meng, and J.D. Molkentin, *Fibroblasts orchestrate cellular crosstalk in the heart through the ECM.* Nature Cardiovascular Research, 2022. **1**(4): p. 312-321.
158. Bonnans, C., J. Chou, and Z. Werb, *Remodelling the extracellular matrix in development and disease.* Nat Rev Mol Cell Biol, 2014. **15**(12): p. 786-801.
159. Singh, N., et al., *Transcription by RNA polymerase II and the CTD-chromatin crosstalk.* Biochem Biophys Res Commun, 2022. **599**: p. 81-86.
160. Hao, Y., et al., *Integrated analysis of multimodal single-cell data.* Cell, 2021. **184**(13): p. 3573-3587 e29.
161. Shukla, S., et al., *CTCF-promoted RNA polymerase II pausing links DNA methylation to splicing.* Nature, 2011. **479**(7371): p. 74-9.
162. Core, L.J. and J.T. Lis, *Paused Pol II captures enhancer activity and acts as a potent insulator.* Genes Dev, 2009. **23**(14): p. 1606-12.
163. Ding, N., et al., *A vitamin D receptor/SMAD genomic circuit gates hepatic fibrotic response.* Cell, 2013. **153**(3): p. 601-13.
164. Wohlfahrt, T., et al., *PU.1 controls fibroblast polarization and tissue fibrosis.* Nature, 2019. **566**(7744): p. 344-349.
165. Zeitlinger, J., et al., *RNA polymerase stalling at developmental control genes in the Drosophila melanogaster embryo.* Nat Genet, 2007. **39**(12): p. 1512-6.

166. Ernst, J. and M. Kellis, *ChromHMM: automating chromatin-state discovery and characterization.* Nat Methods, 2012. **9**(3): p. 215-6.
167. Kaya-Okur, H.S., et al., *CUT&Tag for efficient epigenomic profiling of small samples and single cells.* Nat Commun, 2019. **10**(1): p. 1930.
168. Kornberg, R.D., *Eukaryotic transcriptional control.* Trends Cell Biol, 1999. **9**(12): p. M46-9.
169. El Agha, E., et al., *Two-Way Conversion between Lipogenic and Myogenic Fibroblastic Phenotypes Marks the Progression and Resolution of Lung Fibrosis.* Cell Stem Cell, 2017. **20**(4): p. 571.
170. Kisseleva, T., et al., *Myofibroblasts revert to an inactive phenotype during regression of liver fibrosis.* Proc Natl Acad Sci U S A, 2012. **109**(24): p. 9448-53.
171. Troeger, J.S., et al., *Deactivation of hepatic stellate cells during liver fibrosis resolution in mice.* Gastroenterology, 2012. **143**(4): p. 1073-83 e22.
172. Guerrero-Martínez, J.A., et al., *TGFβ promotes widespread enhancer chromatin opening and operates on genomic regulatory domains.* Nature communications, 2020. **11**(1): p. 6196.
173. Sundqvist, A., et al., *Specific interactions between Smad proteins and AP-1 components determine TGFβ-induced breast cancer cell invasion.* Oncogene, 2013. **32**(31): p. 3606-3615.
174. Hollenhorst, P.C., *RAS/ERK pathway transcriptional regulation through ETS/AP-1 binding sites.* Small GTPases, 2012. **3**(3): p. 154-158.
175. Core, L.J. and J.T. Lis, *Paused Pol II captures enhancer activity and acts as a potent insulator.* Genes & development, 2009. **23**(14): p. 1606-1612.
176. Wynn, T.A., *Cellular and molecular mechanisms of fibrosis.* J Pathol, 2008. **214**(2): p. 199-210.
177. Schuppan, D. and M. Pinzani, *Anti-fibrotic therapy: lost in translation?* J Hepatol, 2012. **56 Suppl 1**: p. S66-74.
178. Schuppan, D. and Y.O. Kim, *Evolving therapies for liver fibrosis.* J Clin Invest, 2013. **123**(5): p. 1887-901.
179. Pantano, L., et al., *Molecular characterization and cell type composition deconvolution of fibrosis in NAFLD.* Sci Rep, 2021. **11**(1): p. 18045.
180. Friedman, S.L., *Hepatic stellate cells: protean, multifunctional, and enigmatic cells of the liver.* Physiol Rev, 2008. **88**(1): p. 125-72.
181. Seitz, H.M., et al., *Macrophages and dendritic cells use different Axl/Mertk/Tyro3 receptors in clearance of apoptotic cells.* J Immunol, 2007. **178**(9): p. 5635-42.
182. Li, X., et al., *Drugs and Targets in Fibrosis.* Front Pharmacol, 2017. **8**: p. 855.
183. Chen, C.J. and Y.P. Liu, *MERTK Inhibition: Potential as a Treatment Strategy in EGFR Tyrosine Kinase Inhibitor-Resistant Non-Small Cell Lung Cancer.* Pharmaceuticals (Basel), 2021. **14**(2).